Block Copolymer Self-Assembly:

Homopolymer Additives and Multiple Length Scales

A Theoretical Study

Tetyana Romanivna Klymko

Block Copolymer Self-Assembly:
Homopolymer Additives and Multiple Length Scales

T.R. Klymko

Ph.D. thesis

University of Groningen
The Netherlands

October 2008

Zernike Institute Ph.D. thesis series 2008-19
ISSN 1570-1530
ISBN 978-90-367-3547-6
ISBN electronic 978-90-367-3548-3

RIJKSUNIVERSITEIT GRONINGEN

Block Copolymer Self-Assembly: Homopolymer Additives and Multiple Length Scales

A Theoretical Study

Proefschrift

ter verkrijging van het doctoraat in de
Wiskunde and Natuurwetenschappen
aan de Rijksuniversiteit Groningen
op gezag van de
Rector Magnificus, Dr. F.Zwarts
in het openbaar te verdedigen op
vrijdag 3 oktober 2008
om 13.15 uur

door

Tetyana Romanivna Klymko
geboren op 19 november 1978
te Gorodok, Oekraine

Promotor : Prof. Dr. G. ten Brinke
Copromotor : Dr. A.V. Subbotin

Beoordelingscommissie:

Prof. Dr. I. Ya. Erukhimovich
Prof. Dr. J.J.M. Slot
Prof. Dr. F.A.M. Leermakers

ISBN: 978-90-367-3547-6

Not everything that counts can be counted
And not everything that can be counted, counts

Albert Einshtein

CONTENTS

Overview of the Thesis

The research reported in this Thesis concerns a theoretical study of several aspects of the self-assembly in block-copolymer-based systems. The self-assembly in two specific classes of block-copolymer-based systems are considered. The first one is a lamellar self-assembled diblock copolymer/homopolymer blend where the homopolymer interacts favorably with one of the diblock components. The second class comprises linear binary and ternary multiblock copolymer systems characterized by two intrinsic length scales which self-assemble in the form of hierarchically ordered structures.

The Thesis consists of two main parts. Part I is the introductory part and includes Chapters 1-3 with general information and a literature overview. Part II comprises Chapters 4-7 and contains a theoretical study of the lamellar self-assembled state of a diblock copolymer/homopolymer blend with specific exothermic interactions, as well as theoretical investigations of linear binary and ternary multiblock copolymers with two intrinsic length scales.

In Chapter 1 the various block copolymers and block-copolymer-based systems of interest will be introduced.

Chapter 2 is devoted to a literature overview of diblock copolymer/homopolymer blends. This chapter is divided into two subchapters. In the first one diblock copolymer/homopolymer blends with *repulsive* interactions are reviewed. In the second subchapter the same is done for blends with both *repulsive and attractive* interactions.

Chapter 3 presents an experimental and theoretical overview of the self-assembly and hierarchically ordered structure formation in multiblock copolymer melts characterized by two intrinsic length scales.

In Chapter 4 lamellar self-assembled AB-diblock copolymer/C-homopolymer blends with specific exothermic AC-interactions are theoretically analyzed. The problem of the maximal amount of homopolymer that can be incorporated by the diblock copolymer is addressed. Essential observations concern the conformational effects that start to become important for weakly favorable AC-interactions. The homopolymer distribution profile inside the corresponding A-block domain and the change in lamellar period as a function of the amount of homopolymer are discussed in some detail.

Next, Chapters 5,6 and 7 are devoted to the theoretical analysis of linear multiblock copolymers with two intrinsic length scales.

Linear *ternary* C-*b*-(B-*b*-A)$_m$-*b*-B-*b*-C multiblock copolymer melts are discussed in Chapter 5. The main objective is to relate the number *m* of repeating (B-*b*-A) diblocks to the number of internal “thin” domains formed in between the “thick” C-layers in the lamellar-*in*-lamellar self-assembled state of the multiblock copolymer melt under

consideration. The mean-field calculations presented in this Chapter are done in the framework of the strong segregation approach, based on the assumed strong mutual incompatibility between the three different components of the multiblock copolymer.

Chapter 6 reports the analysis of the same ternary C-*b*-(B-*b*-A)$_m$-*b*-B-*b*-C multiblocks, but now using the Alexander-de Gennes approximation. This simplified, but qualitatively and semi-quantitatively correct description, is used to better understand the physics of the hierarchical structure formation. Furthermore, it allows a detailed investigation of the influence of the block length and the Flory –Huggins interaction parameters on the domains' formation. Computer simulation modeling results, using the dissipative particle dynamics simulation technique, are also presented to support the theoretical predictions

Finally, Chapter 7 discusses the lamellar-*in*-lamellar structure of linear *binary* multiblock copolymers of the A-*b*-(B-*b*-A)$_m$-*b*-B-*b*-A type. The purpose of this Chapter is to find again a relation between the number of diblocks *m* and the number of "internal" layers in the self-assembled state of the multiblock copolymer melt and to reveal the essential differences between the linear binary and ternary multiblock copolymer systems.

PART I

INTRODUCTION

CHAPTER 1

Diblock and Multiblock Copolymers

Classification and Examples

Diblock copolymers

A *polymer* is a macromolecule which consists of a large number N_0 of monomer units. In the literature this number is also referred to as the chain length or the degree of polimerization. The simplest schematical illustration of a homopolymer (all monomer units are chemically identical) is given in Figure 1.1.

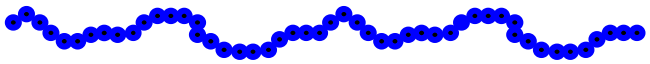

N_0 – degree of polymerization, chain length, number of monomer units

Figure 1.1. Schematical illustration of a homopolymer which consists of $N_0 >> 1$ monomer units.

Usually N_0 is a very large number which can be in a very broad range varying from hundreds for synthetic polymers to billion units for complex DNA macromolecules, for instance. Despite the fact that all polymers have their individual chemical structure, the essentially large values of the degree of polymerization allow us to ignore the chemical structure and develop a polymer description in the framework of statistical mechanics where the microscopic details are not dominant in comparison with the large number of possible polymer configurations.

Diblock copolymers are obtained by linking together two chemically different polymers, say A and B. Bringing different polymers together introduces new interactions in the system. To deal with this polymer scientists widely use the Flory-Huggins interaction parameter χ_{AB} in the case of A and B polymers, defined by

$$\chi_{AB} = \frac{z}{k_B T}\left(\varepsilon_{AB} - \frac{\varepsilon_{AA} + \varepsilon_{BB}}{2}\right) \tag{1.1}$$

where z is the number of nearest neighbour monomers, T denotes the temperature, k_B is the Boltzmann constant and ε_{AA}, ε_{BB} and ε_{AB} are the interaction energies of the A-A, B-B and A-B interactions respectively. If $\chi_{AB} > 0$ then the A- and B-component interact unfavorably. In the opposite case, if $\chi_{AB} < 0$, the different species attract each other. Note, that there is a strong tendency for χ_{AB} to be positive, i.e., in most cases the chemically different species interact repulsively. Since the thermal translational energy per macromolecule is of the order of $k_B T$, whereas the interaction energy per macromolecule is proportional to its length N_0, the product $\chi_{AB} N_0$ rather than χ_{AB} is the relevant quantity.

Diblock copolymers will have a certain composition expressed in the volume fraction of the A-component

$$f_A = \frac{N_A}{N_A + N_B} = \frac{N_A}{N} \tag{1.2}$$

or the volume fraction of the B-component

$$f_B = 1 - f_A = \frac{N_A}{N_A + N_B} = \frac{N_B}{N} \tag{1.3}$$

where N_A and N_B are the number of monomer units of A- and B-type (assumed to be of equal size) and $N = N_A + N_B$ is the total number of monomers. If $f_A = f_B$ we have a symmetric diblock. A schematical illustration of a symmetric diblock and an asymmetric diblock is presented in Figure 1.2a and 1.2b, respectively.

Polymer properties, such as glass transition temperature, viscoelasticity, mechanical strength, etc. are extremely important for many practical applications. Very often the required properties can in principle be achieved by mixing two polymers. Such mixtures are usually referred to as *polymer blends*. However, due to the generally unfavorable unlike interactions, chemically different polymers have the natural tendency to separate from each other. This separation occurs on a macroscopic scale. In diblock copolymers on the other hand, where chemically different polymers are covalently joint together, such a separation can only take place on a nanoscopic level. Here the phase separation results in the spontaneous formation of a number of different well-ordered nanostructures, depending on the block copolymer composition and temperature. This property is widely used in nanotechnology. The equilibrium structure of the ordered state is determined by the minimum of the free energy, which consists of an interfacial free energy contribution and an elastic stretching contribution. The system can lower the interfacial contribution by reducing the interface area, which in turn increases the stretching free energy. When these two competing effects are balanced, the equilibrium structure is formed.

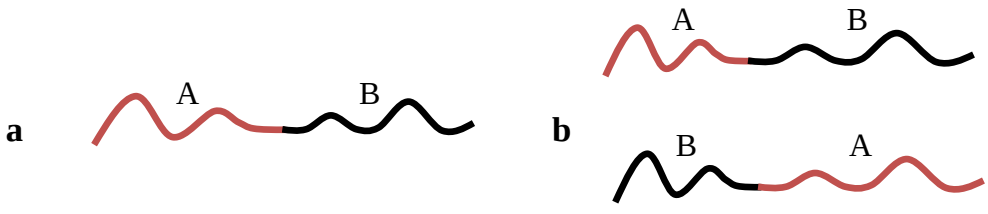

Figure 1.2. Schematic representation of a symmetric AB diblock copolymer (a) and an asymmetric AB diblock copolymer (b) with minority and majority A-component (top and bottom, respectively).

The phase behavior of a *diblock copolymer melt* as calculated by Matsen and Schick in 1994 is presented in Figure 1.3. The lamellar ($\bar{1}$), hexagonal(cylindrical) (*p*6*mm*), cubic(spherical) ($Im\bar{3}m$) and gyroid ($Ia\bar{3}d$) morphologies were found to be stable. The corresponding microstructures are schematically illustrated in Figure 1.4. We see that the diblock copolymer composition and the product χN determine the stability regions for the different morphologies.

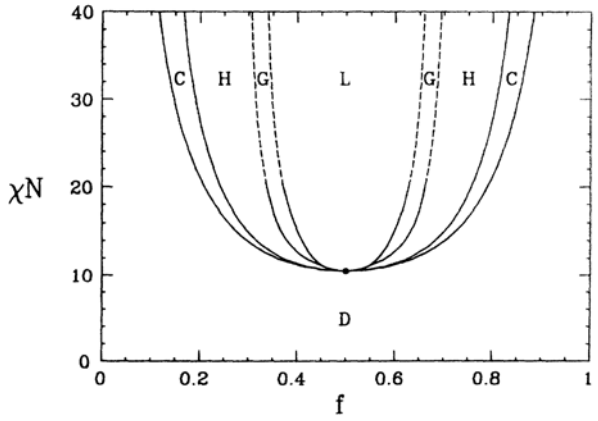

Figure 1.3. Phase diagram of diblock copolymer melt. L denotes the lamellar morphology, H - hexagonal, G - gyroid, C- spherical morphology, D – disordered state.

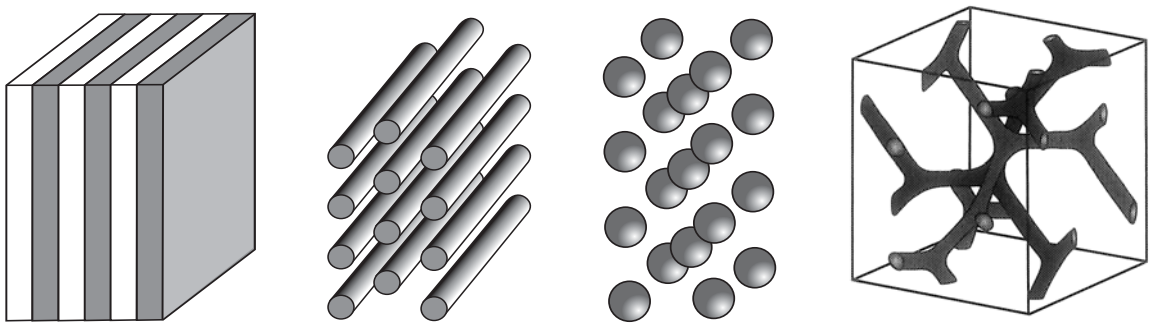

Figure 1.4. Schematic presentation of the different diblock copolymer microstructures: (a) lamellar, (b) cylindrical(hexagonal), (c) spherical, (d) gyroid.

Structure formation in diblock copolymer melts usually has only one characteristic length scale which is defined by the natural length of the polymer itself. A much richer variety of structures can be found for instance in triblock copolymers, where three chemically different species are linked together.

Depending on a degree of segregation, weak, intermediate and strong segregation regimes can be distinguished. If the temperature is close to the order-disorder temterature (T_{ODT}), the deviation of the monomer density from its average value is very small which

is referred to as the *weak segregation limit*. At this level of segregation the AB-interface is broad and the microdomains are far from pure. Decreasing the temperature, the composition deviations from the average composition become larger; the interface between A- and B-domains is, however, still relatively broad and microdomains are still not pure. This regime is referred to as the *intermediate segregation regime*. In the *strong segregation regime* the AB-interface is very sharp and pure A- and B-microdomains are formed. At this degree of segregation the product $\chi_{AB}N$ is very large, much bigger than unity.

Triblock copolymers

Triblock copolymers are obtained by linking together three polymers. Triblock copolymers can be obtained by linking only two chemically different species and thus making *binary* ABA triblock copolymers or they can be obtained using three chemically different polymers which results in *ternary* ABC triblock copolymers. Both binary and ternary triblock copolymers can be *architecturally* different: *linear* when all three polymers are sequentially linked together or as *star* triblock copolymers when the three polymers are linked together in one common point. The block lengths of the polymers can, of course, be different. Figure 1.5 illustrates different examples of triblock copolymers with equal block length.

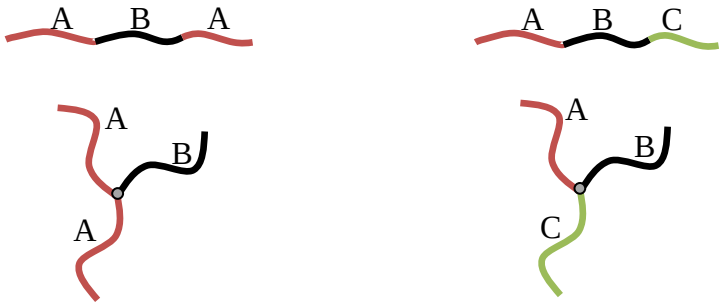

Figure 1.5. Schematic presentation of the different triblock copolymer architectures. Left: top: linear binary ABA triblock, bottom: binary ABA star triblock. Right: top: linear ternary ABC triblock, bottom: ternary ABC star triblock.

Multiblock copolymers

Multiblock copolymers can be generally presented as a sequence of blocks, see Figure 1.6 for the simplest binary multiblock copolymer with a linear architecture. When the chain length of some of the blocks (usually the end blocks) is significantly different from the other blocks, two intrinsic length scales are present. A schematic illustration of such a linear multiblock copolymer with two intrinsic lengthscales is given in Figure 1.7. The presence of two, or more, intrinsic length scales may give rise to so-called

hierarchical nanostructured materials, i.e. ordered structures are formed involving more than one length scale. An excellent example is given by the PS-*b*-(PI-*b*-PS)$_4$-*b*-PI-*b*-PS undecablock copolymer melts considered by Matsushita and co-workers (PS = polystyrene, PI = polyisoprene). Here the outer polystyrene end-blocks are considerably larger than the inner PS and PI blocks of equal length. The long characteristic length-scale is associated with the total length of the undecablock copolymer, whereas the second short length-scale is associated with the length of the internal PI-*b*-PS diblock. Another particularly nice example is the ternary P2VP-*b*-(PI-*b*-PS)$_4$-*b*-PI-*b*-P2VP undecablock copolymer system (P2VP = poly(2-vinyl pyridine). These types of copolymers will be considered in more detail in Section 3 of this thesis.

Figure 1.6. (A-*alt*-B)$_m$ linear alternating multiblock copolymer with number of repeating diblocks m = 3.

Figure 1.7. A-(B-*alt*-A)$_m$-B-A linear multiblock copolymer with two intrinsic length scales and number of repeating diblocks m = 4.

Comb-like supramolecules

Besides linear macromolecules it is, of course, also possible to form architecturally more complicated branched structures with different, rigid or flexible, side-chains. One of the simplest examples of a non-linear architecture is a star polymer, see Figure 1.8a. Other examples include so-called comb-copolymers, as presented in Figure 1.8b. When flexible side-chains are attached to a rigid backbone so-called "hairy-rods" are formed(Figure 1.8c) It is obviously also possible to combine a flexible backbone with rigid side-chains.

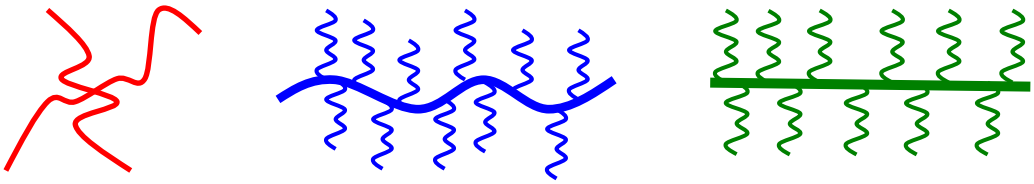

Figure 1.8. Schematic presentation of (a) star polymer, (b) comb copolymer and (c) "hairy-rod".

Moreover, the side chains can be linked to the backbone either by permanent covalent bonding or by temperature sensitive hydrogen or ionic bonding.

REFERENCES

[1] M.Doi. *Introduction to polymer physics*. Clarendon Press, Oxford, **1996**.

[2] G.R.Strobl. *The physics of polymers: concepts for understanding their structures and behavior*. Springer, Berlin, **1996**.

[3] A.Y. Grosberg and A.R. Khokhlov. *Statistical Physics of Macromolecules*. American Institute of Physics, New York, **1994**.

[4] I.W.Hamley. *The physics of block copolymers*. Oxford University Press, Oxford, **1999**.

[5] P.G. de Gennes. *Scaling concepts in polymer physics*. Cornell University Press, Ithaka, New York, **1979**.

[6] F.S.Bates, G.H.Fredrickson, *Annu. Rev. Phys. Chem*. **1990**, *41*, 525.

[7] I.W.Hamley, *J.Phys.: Condens. Matter* **2001**, *13*, R643.

[8] M.W.Matsen, *J.Phys.: Condens. Matter* **2002**, *14*, R21.

[9] V.Casteletto, I.W.Hamley, *Current Opinion in Solid State and Materials Science* **2004**, *8*, 426.

[10] G.Odian. *Principles of polymerization*. A Wiley-Interscience Publication, New York, **1991**.

[11] Y.Nagata, J.Masuda, A.Noro, D.Cho, A.Takano, Y.Matsushita, *Macromolecules* **2005**, *38*, 10220.

[12] J.Masuda, A.Takano, Y.Nagata, A.Noro, Y.Matsushita, *Phys.Rev.Lett. 2006, 97*, 098301.

CHAPTER 2

Diblock Copolymer/Homopolymer Blends

2.1. Diblock copolymer/homopolymer blends with repulsive interactions

Experimental overview

Diblock copolymer/homopolymer blends became attractive subbjects for experimental and theoretical investigations due to possible practical applications based on improved properties of different materials. Many publications are devoted to diblock-copolymer-homopolymer blends where the *homopolymer is chemically identical to one of the diblock copolymer blocks*. Depending on the concentration of the block copolymer, different morphologies, including spherical, cylindrical and lamellar are observed experimentally. It has been shown that the addition of a certain amount of homopolymer can either stabilize or destabilize already formed microdostructures depending on the amount of homopolymer. Hence, adding some homopolymer, even though it is chemically identical to one of the copolymer components, can noticeably affect the resulting equilibrium structures. Depending on the homopolymer molar mass, a diblock copolymer/homopolymer mixtures can exhibit both microphase and macrophase separation.

Recently Hashimoto and co-workers [1-3] used a combination of small-angle X-ray scattering (SAXS) and transmission electron microscopy (TEM) to investigate the ordered microdomain structures of a mixture of poly(styrene)-*b*-polyisoprene (PS-*b*-PI) diblock copolymer with polystyrene homopolymer (hS) as a function of the homopolymer molecular weight. They found that blends containing up to 20% of hPS maintain a well-ordered lamellar structure. In these blends, the thickness of the polystyrene microdomain increases with increasing hPS volume fraction, whereas the thickness the of PI microdomains decreases. The latter effect became less pronounced for higher molecular weight homopolymers. In the situation where the molecular weights of the PS block and the hS homopolymer were comparable, the thickness of the PI microdomain was not affected by increasing the amount of homopolymer. When the amount of homopolymer reached 35%, the lamellar morphology changed to hexagonally packed cylindrical microdomains. For the situation where the molecular weight of the hPS is smaller than the molecular weight of the PS block, it was concluded that the homopolymer chains dissolved in the PS domains. Longer homopolymer chains, but still with a molecular weight smaller than that of the corresponding PS block, preferred to be localized in the centre of the PS domains.

Winey et. al [4,5] studied the morphologies of AB/A and AB/B blends. The diblock copolymer used was again poly(styrene)-*b*-polyisoprene with a total molecular weigth of 48700 g/mol and a polystyrene block molecular weight of 26600 g/mol. The polystyrene homopolymer molecular weights were in the range between 2600 g/mol to 36700 g/mol. As the homopolymer concentration increased (at fixed homopolymer molecular weigth) the thickness of PS domains increased and the thickness of the PI domains decreased, just as observed by Hashimoto and co-workers. Increasing the homopolymer molecular weight at fixed concentration of homopolymer led to an increase in layer thickness of both PS and PI domains.

Russell and co-workers [6] used neutron reflectivity to obtain detailed information about the homopolymer distribution in ordered symmetric diblock copolymers. They used mixtures of polystyrene or poly(methyl methacrylate) (PMMA) homopolymers with symmetric PS-*b*-PMMA diblock copolymers. By adding perdeuterated homopolymer to unlabeled copolymer, the authors quantitatively characterized the spatial distribution of the homopolymer. They observed an almost uniform distribution of the low molecular weight homopolymer inside the corresponding domains. For molecular weights of the homopolymer that are comparable with the molecular weight of the corresponding copolymer block, the homopolymer was confined to the respective copolymer domain, with a homopolymer distribution peaked at the center of the domain.

Experiments on blends of poly(styrene)-*b*-poly(2-vinylpyridine) (PS-*b*-P2VP) block copolymer and homopolymer polystyrene, hPS, with a molecular weigth that is lower than the molecular weight of the corresponding block of the block copolymer, have been reported by Matsushita and co-workers [7-9]. They used SAXS to investigate the lamellar domain spacing in this PS-*b*-P2VP/hPS blend. Small-angle neutron scattering (SANS) was further used to investigate the conformations of the block chains in the lamellar microdomains. The authors also concluded that homopolymers with higher molecular weight are localized in the center of the corresponding lamellae while the lower molecular weight homopolymers are distributed throughout these domains. Furthermore, the authors also investigated and compared binary PS-*b*-P2VP/hPS and ternary PS-*b*-P2VP/hPS/hP2VP blends. This comparison showed that for the same molecular weight the homopolymers in binary blends are more localized than in the ternary ones.

All the above mentioned studies focused on diblock copolymers having a lamellar morphology and considered in particular the distribution of the homopolymer species and the change in lamellar spacing as a function of the amount of homopolymer added. The experimental observations on the lamellar self-assembled state showed that the spatial distribution of the homopolymer depends strongly on its relative molar mass. Generally, for low molar masses the homopolymer will be distributed uniformly throughout the layers of the corresponding block. For a molar mass of the homopolymer that is comparable to that of the corresponding block, the homopolymer will be confined to the center of the layers, i.e. segregated in the mid-plane. A significantly higher molar mass of the homopolymer, finally, results in macrophase separation.

In Ref.10, Thomas and co-workers investigated the micellar structure of a blend of poly(styrene)-*b*-polybutadiene diblock copolymer and polystyrene homopolymer using SAXS and TEM. They observed a homogeneous mixture of block copolymer and homopolymer at low diblock copolymer concentrations. When the block copolymer concentration became larger than the critical micelle concentration the formation of spherical micelles with a polybutadiene core and a polystyrene corona occurred. The micelles' coronae consist of the polystyrene block chains swollen with the homopolystyrene. Upon further increasing the block copolymer concentration, the coronae from neighboring micelles started to overlap.The authors also observed an increase in the critical micelle concentration when the molecular weight of the homopolymer decreased.

Russell and co-workers [11] investigated mixtures of PMMA homopolymers and asymmetric PMMA-*b*-PS diblock copolymers forming periodic, close-packed cylindrical PMMA microdomains with approximately 22nm in diameter. The authors observed

changes in both the diameter and the spacing of the cylindrical microdomains with the addition of PMMA homopolymer. From the AFM images they observed the decrease of the areal number density of cylinders from 7.3×10^{10} cylinders/cm^2 for pure PMMA-*b*-PS diblock copolymers to 6.6×10^{10} cylinders/cm^2 with the addition of 10% of PMMA homopolymer. The cylinder diameter of the latter mixture was about 24nm. The authors also observed the formation of about 6nm pores after the removal of the PMMA homopolymer from the mixture of PMMA-*b*-PS diblock with 10% PMMA. The pores were formed in the centre of the PMMA cylinders.

Finally we mention the study by Russell and co-workers [12] on mixtures of PMMA-*b*-PS diblocks and PMMA or PEO (poly(ethylene oxide)) homopolymers in thin film and bulk to compare the copolymer/homopolymer miscibility. They found that the PMMA homopolymer miscibility in thin films was enhanced compared with that in the bulk. PMMA homopolymer in thin films was more localized at the centre of the PMMA microdomains compared to the bulk. The same tendencies were observed in PMMA-*b*-PS/PEO blends, where PMMA interacts weakly favorable with PEO.

Theoretical overview

One of the first theoretical mean-field calculations on diblock copolymer/homopolymer blends were done by Shull and Winey [13] who used the hyperbolic tangent function given by Eq.2.1 to model the distribution $\phi_h(x)$ of the homopolymer segments. Their results were in good agreement with the experimentally observed distribution of homopolymer in the lamellar microdomains. The profile which Shull and Winey used to describe homopolymer distribution has the form

$$\phi_h(x) = \frac{1}{2}\left[\tanh\frac{\phi_A d_A + 2x}{w} + \tanh\frac{\phi_A d_A - 2x}{w}\right] \tag{2.1}$$

ϕ_A is the total volume fraction of homopolymer in the A-layer, d_A is the A-layer thickness and w characterizes the interpenetration between copolymer and homopolymer chains localized to the domain center. The analysis of Shull and Winey assumed that the homopolymer chains are fully located within the corresponding copolymer layer and that the boundaries between adjanced domains are sharp (so-called strong segregation limit). According to their analysis, the homopolymer molecular weight dependence of the copolymer profile is small for $N_h/N_c >> 1$ which fully agrees with previously described experimental observations. N_h and N_c being respectively the degree of polimerization for homopolymer and corresponding copolymer. Note, that in fact, the concepts of "wet brush" and "dry brush" were developed from these observations: in the strong segregation limit A and B blocks of lamellar AB diblock copolymers are stretched and oriented perpendicular to narrow AB-interface. At this level of segregation one can model a diblock copolymer as a brush of polymer chains, adsorbed to a non-penetrable surface. The term "wet brush" in this analogy corresponds to the situation when A(B)

homopolymer penetrates into the A(B) block domain. Likewise, the term "dry brush" reflects the situation where the homopolymer does not penetrate into the block copolymer layers but is located between the lamellar domains – the brush remains "dry".

Shull, Mayes and Russell [14] used numerical SCFT calculations to compare experimentally and numerically obtained results for homopolymer distribution profile in PS-*b*-PMMA diblock copolymer/PMMA homopolymer blends. The authors performed calculations for homopolymer molecular weights of 12 000 g/mol and 57 000 g/mol. In both cases the overall homopolymer weight fraction in the blend was about 10%. They observed that the homopolymer distribution for low molecular weight homopolymers is much broader than for high molecular weight homopolymers, which is in agreement with the theoretical predictions of Shull and Winey.

Using numerical self-consistent field theory (SCFT), Matsen [15] and Vavasour and Whitmore [16] reproduced many results of Winey et al [13]. In particular, Matsen calculated the homopolymer distribution for lamellar and hexagonal phases. He also found that while the pure diblock copolymer exhibited the spherical, cylindrical, gyroid and lamellar ordered phases, the addition of homopolymer stabilized the close-packed spherical, double-diamond and hexagonally perforated lamellar phases. It was also demonstrated than in general the minority-component microdomain can only absorb a limited amount of homopolymer before macrophase separation occurs. The phase coexistence between a diblock-rich microstructure and a homopolymer-rich disordered phase was also studied by Matsen using self-consistent field calculations. This study focused on a single slightly asymmetric diblock copolymer (f = 0.45) and was restricted to the consideration of the lamellar microstructure. It was found that the addition of high-weight homopolymer leads to macrophase separation between a diblock-rich lamellar microstructure and a homopolymer-rich disordered phase. This separation was ascribed to the attractive interactions between lamellar bilayers. In contrast, low molecular weight homopolymer can be added without resulting in macrophase separation; its addition gives rise to a repulsive interaction between the bilayers which leads to fully different behavior.

Likhtman and Semenov [17] theoretically investigated phase equilibria in block copolymer/homopolymer mixtures. They derived a general expression for the free energy and calculated it numerically for different microstructures: classical lamellar, hexagonal, body-centered cubic and also for bicontinuous double diamond and gyroid structures. Their calculations resulted in a phase diagram in the (f,φ)-plane, where f is the diblock copolymer composition and φ is the volume fraction of the homopolymer in the blend. The authors found that for all compositions and for all morphologies the free energy per block copolymer chain shows a minimum as a function of the homopolymer volume fraction at some $\varphi = \varphi_{\max}$. Thus the addition of some amount of homopolymer $\varphi < \varphi_{\max}$ always results in a free energy decrease. For $\varphi > \varphi_{\max}$ it is energetically favorable for the system to separate into two macrophases: a block copolymer phase with $\varphi = \varphi_{\max}$ and a pure homopolymer phase. Furthermore, Likhtman and Semenov predicted a region of stability for the double diamond and the gyroid phase in the composition range $f = 0.62 - 0.66$ for a homopolymer volume fraction $\varphi \approx 0.3 - 0.4$. For $\varphi < 0.3$ they found coexistence between lamellar and bicontinuous structures. In particularl they found that when the homopolymer volume fraction changed from 0 to 0.4, the structures changed as

hex → hex+BCC → BCC→ BCC+homopolymer for f = 0.8-0.9 and hex+lam → hex → hex+homopolymer for f = 0.66-0.73.

Janert and Schick [18] used mean-field theory to study binary blends of homopolymer A and symmetric diblock copolymer AB. They examined the development of lamellar, hexagonal and body-centered cubic phases starting from the weak and moving towards the intermediate segregation limit as a function of the volume fraction homopolymer in the blend.

De Pablo and co-workers [19] performed a Monte Carlo simulations study to explore the behavior of a single nanoparticle and a single homopolymer chain in the cylinders of asymmetric diblock copolymers. The authors found that homopolymers that prefer the shorter blocks of the diblock are strongly localized inside the cylinders. This result is consistent with experiments of Russell and co-workers [11] who used PMMA homopolymers added to asymmetric PS-*b*-PMMA diblock copolymers with the PMMA blocks forming cylinders. They discovered that, while short neutral homopolymers segregate at the diblock interface, longer neutral homopolymers prefer the cylinders rather than the matrix.

2.2. Diblock copolymer/homopolymer blends with attractive and repulsive interactions

Diblockcopolymer/homopolymer blends with *homopolymers that have a specific exothermic interaction with one of the blocks of the block copolymer* form a separate topic. Such blends have already been addressed in the literature, but not nearly so extensively as diblock copolymer/homopolymer blends with exclusively repulsive interactions. ***Experimentally*** copolymer/homopolymer blends with both attractive and repulsive interactions have been investigated by a small number of groups, usually involving polystyrene and poly(2,6-dimethyl-1,4-phenylene oxide) (PPO) as two of the three chemically different species.

In several studies polystyrene-based block copolymers were combined with homopolymer PPO. Paul and co-workers [20,21] used styrene-butadiene-styrene triblock copolymers in combination with PPO homopolymer to investigate the degree of solubilization of PPO by differential scanning calorimetry. They varied the molecular weight of the polystyrene block from 5300g/mol to 87000g/mol and the PPO molecular weight was varied from about 24000g/mol to 39000g/mol. A dramatic increase in the degree of homopolymer solubilization was observed compared to the situation when the homopolymer was polystyrene. This was ascribed to the additional driving force provided by the exotermic mixing of PPO and PS (the corresponding Flory-Huggins parameter $\chi_{PPO-PS} \approx -0.043$). The authors observed, that mainly the molecular weight of the polystyrene block determines to which extent PPO and PS mix, whereas the molecular weight of PPO has a very small or no influence at all on PPO-PS. No macrophase separation between PPO and the block copolymer was observed, PPO was always completely dissolved in the PS microdomains [20,21].

In Ref.22 Hashimoto and co-workers reported self-assembled pattern formation in PPO/PS-b-PI binary mixtures with low molecular weight of PPO compared to molecular

weight of the PS block. The authors discussed several possible states of the PPO/PS-b-PI mixture. Macrophase and microphase transitions which occur in the system were found as the most important factor for the final pattern formation

In a recent study Ten Brinke and co-workers [23,24] used PPO in combination with PS to introduce entanglements in the core of nanorods made from polystyrene-*block*-poly(4-vinylpyridine) (PS-*b*-P4VP) diblock copolymers and consisting of a PS core and a P4VP corona. Due to the perfect mixing properties of PPO and PS, PPO is distributed throughout the PS cylinders even if its molecular weight is larger than the molecular weight of the PS block. The authors showed that the addition of 17% PPO with a molar mass of 25700g/mol is enough to introduce sufficient entanglements in the PS cylinders thereby considerably improving the nanorods mechanical properties.

Theoretically blends of a diblock copolymer with a homopolymer that interacts favorably with one of the blocks of the diblock copolymer have been already addressed in several studies from a stabilization point of view.

Hellmann and co-workers [25] investigated A/AB and C/AB homopolymer/diblock copolymer blends using random phase approximation (RPA) calculations and compared it with experimental work using TEM . The C/AB blend was characterized by attractive C-A interactions and repulsive C-B and A-B interactions. In the case of A/BA blend the A-B interactions were repulsive. The authors main interest concerned the question of induced microphase separation: how strong should the C-A attraction be to lead to microphase separation avoiding macrophase separation. They concluded that even if the homopolymer chain length is larger than the total diblock copolymer chain length, C/AB blends exhibit microphase separation if the C and A species attract each other sufficiently strongly, i.e there is a critical value χ^{*}_{AC} such that for $\chi_{AC} < \chi^{*}_{AC}$ microphase will be observed irrespectively of the homopolymer chain length.

Zin and co-workers examined blends of poly(styrene)-*b*-polyisoprene (PS-*b*-PI) diblock copolymers and poly(vinylmethylether) (PVME) homopolymer both theoretically, using the modified Meier's theory, and experimentally by SAXS, TEM and lighth scattering techniques. Their theoretically predicted phase diagrams show that the exothermic interactions significantly increase the dissolution of homopolymer in corresponding microdomain. These predictions were in excellent agreement with the experiments on hPVME/PS-*b*-PI blends, where the added PVME homopolymer was completely dissolved in the polystyrene microdomains due to the specific interaction [26].

Borukhov and Leibler [27,28] discussed the enthalpic stabilizatin of brush-coated particles in a polymer melt and showed how favorable enthalpic interactions can change the brush from a dry to a wet brush. The favorable interactions can stabilize such a colloidal dispersion. Of course, the essential difference between homopolymer penetration inside the grafted chains of a polymer brush compared to a block copolymer layer is the possibility of the latter to adjust the interface area per block copolymer chain.

Balsara and co-workers also investigated AB/C diblock copolymer/homopolymer blends with attractive B-C interactions. The diblock copolymer they used was a poly(ethylene)-*block*-polypropylene (PE-*b*-PP) block copolymer and the homopolymer

was polyisobutylene (PIB). PE-PIB and PE-PP interactions are unfavorable, while the PIB-PP interactions are repulsive for high temperatures, but become attractive for low temperatures. Combining theoretical and experimental investigations, they observed an order-disorder transition at approximately 150^0C, and macrophase separation at about 251^0C. Between 150^0C and 251^0C the blend was homogeneously mixed [29,30].

Shull and Lefebvre in [31] considered blends of an AB-diblock copolymer and A- and C-homopolymer, where C interacts favorably with B. They focused on the situation where $\chi_{AB}N = 60$, $\chi_{AC}N = 60$ and $f_B = 0.2$. N is the diblock copolymer chain length and f_B is the diblock copolymer composition. The pure diblock copolymer system self-assembled into a BCC(body-centered cubic) structure. Swollen micelles were obtained for homopolymer C solubilized in the spherical AB copolymer micelles. For $\chi_{BC} < 0$, the copolymer chemical potential in the swollen micelle is lower than for the unswollen micelle and thus micellization is promoted by the presence of C homopolymer. The authors interest also concerned the encapsulation of nanoparticles in the centre of the swollen micelle in the case of attraction between the surface of the particles and the homopolymer.

Even though many studies have appeared already, several questions remained open. Thus we decided to study lamellar self-assembled AB-diblock copolymer/C-homopolymer blend with favorable A-C interactions in the strong segregation limit. We focused our attention on the homopolymer distribution profiles, the maximum amount of homopolymer that will dissolve in corresponding layers and the functional dependence of the lamellar period on the amount of homopolymer present. The results of this study are presented in Chapter 4 of this manuscript and have been published as Ref. 32.

REFERENCES

[1] T.Hashimoto, H.Tanaka, H.Hasegawa, *Macromolecules* **1990**, *23*, 4378.

[2] H.Tanaka, T.Hashimoto, H.Hasegawa, *Macromolecules* **1991**, *24*, 240.

[3] J.Bodycomb, D.Yamaguchi, T.Hashimoto. *Macromolecules* **2000**, *33*, 5187.

[4] K.I.Winey, E.L.Thomas, L.J.Fetters, *Macromolecules* **1991**, *24*, 6182.

[5] K.I.Winey, E.L.Thomas, L.J.Fetters. *J. Chem. Phys.* **1991**, *95*, 9367.

[6] A.M.Mayes, T.P.Russel, S.K.Satija, C.F.Majkrzak. *Macromolecules* **1992**, *25*, 6523.

[7] Y.Matsushita, N.Torikai, Y.Mogi, I.Noda, C.C.Han, *Macromolecules* **1993**, *26*, 6346.

[8] Y.Matsushita, N.Torikai, Y.Mogi, I.Noda, C.C.Han, *Macromolecules* **1994**, *27*, 4566.

[9] N.Torikai, N.Takabayashi, I.Noda, S.Koizumi, Y.Mori, Y.Matsushita, *Macromolecules* **1997**, *30*, 5698.

[10] D.J.Kinning, E.L.Thomas, L.J.Fetters, *J.Chem.Phys.* **1989**, *90*, 5806.

[11] U.Jeong, H.-C.Kim, R.L.Rodriguez, I.Y.Tsai. C.M.Stafford, J.K.Kim, C.J.Hawker, T.Russell, *Adv. Mater.* **2002**, *14*, 274.

[12] U.Jeong, D.Y.Ryu, D.H.Kho, D.H.Lee, J.K.Kim, T.P.Russell, *Macromolecules* **2003**, *36*, 3626.

[13] K.R.Shull, K.I.Winey, *Macromolecules*, **1992**, *25*, 2637.

[14] K.R.Shull, A.M.Mayes, T.P.Russell, *Macromolecules* **1993**, *26*, 3929.

[15] M.W.Matsen. *Macromolecules*, **1995**, *28*, 5765.

[16] J.D.Vavasour, M.D.Whitmore, *Macromolecules* **2001**, *34*, 3471.

[17] A.E.Likhtman, A.N.Semenov, *Macromolecules* **1997**, *30*, 7273.

[18] P.K.Janert, M.Schick, *Macromolecules* **1998**, *31***,** 1109.

[19] Q.Wang, P.Nealey, J.J.de Pablo, *J.Chem.Phys.* **2003**, *118*, 11278.

[20] P.S.Tucker, J.W.Barlow, D.R.Paul, *Macromolecules* **1988**, *21*, 1678.

[21] P.S.Tucker, J.W.Barlow, D.R.Paul, *Macromolecules,* **1988**, *21*, 2794.

[22] T.Hashimoto, K.Kimishima, H.Hasegawa, *Macromolecules* **1991**, *24*, 5704.

[23] W.van Zoelen, G.Alberda van Ekenstein, E.Polushkin, O.Ikkala and G.ten Brinke, *Soft Matter* **2005**, 1, 280.

[24] W.van Zoelen, G.O.R.Alberda van Ekenstein, O.Ikkala and G.ten Brinke, *Macromolecules* **2006**, *39*, 6574-6579.

[25] B.Lowenhaupt, A.Steurer, G.P.Hellmann, Y.Gallot, *Macromolecules* **1994**, *27*, 908.

[26] H.-K.Lee, C.-K.Kang, W.-C.Zin, *Polymer* **1996**, *37*, 287.

[27] I.Borukhov, L.Leibler, *Phys.Rev.E* **2000**, 62, R41.

[28] I.Borukhov, L.Leibler, *Macromolecules* **2002**, *35*, 5171.

[29] J.H.Lee, N.P.Balsara, A.K.Chakraborty, R.Krishnamoorti, B.Hammouda, *Macromolecules* **2002**, *35*, 7748.

[30] J.H.Lee, M.L.Ruegg, N.P.Balsara, Y.Zhu, S.P.Gido, R.Krishnamoorti, M.-H.Kim, *Mcromolecules* **2003**, *36*, 6537.

[31] M.D.Lefebvre, K.R.Shull, *Macromolecules* **2006**, *39*, 3450.

[32] T.Klymko, A.Subbotin, G.ten Brinke, *Macromolecules* **2007**, *40*, 2863.

CHAPTER 3

Multiblock Copolymers with Different Intrinsic Length Scales

3.1 Experimental overview

Different stages of complexity for multiblock copolymers can be introduced by varying their architecture (linear or comb-like, for instance) or by including more monomer types (binary, ternary multiblocks) combined with more than one characteristic length scale. Due to multi-length scale spectrum such materials possess very usefull properties such as self-healing, for example.

Hierarchically ordered block copolymers and block copolymer-based systems have been extensively investigated during the past decade. They became an attractive subject for experimental [1-23], theoretical [24-34] and computer simulation [35-40] analysis due to the possibilities to form structures with different periodicities which, in turn, can have many practical applications.

The observation of a double-periodic structure in polystyrene-*block*-poly(4-vinylpyridine) (PS-*b*-P4VP) diblock copolymers with hydrogen-bonded pentadecylphenol (PDP) side chains with the P4VP block, was first reported in Refs.1-3. The reported structure has two different periods related to the two different intrinsic length scales: the long length scale period related to the diblock copolymer character and the short length scale period due to the separation between the alkyl tails of the PDP side-chains and the hydrogen-bonded P4VP blocks.

Linear multiblock copolymers with two different length scales serve as one of the simplest examples of a multiblock architecture where the structure-*in*-structure has been observed. As reported in Ref. 4, a three-layered lamellar-*in*-lamellar self-assembled state was observed for a undecablock S-ISISISISI-S copolymer with "long" polystyrene (S) end blocks and a middle multiblock consisting of "short" polystyrene and polyisoprene (I) blocks. The self-assembled state of such multiblock resulted in a I-S-I "thin" lamellar structure in between "thick" polystyrene lamellae. The total molecular weight of the investigated copolymer was 275000 g/mol and the volume ratio between isoprene/styrene was 0.3/0.7.

Another example of a lamellar-*in*-lamellar self-assembled state has been reported in Ref.5, where the formation of a 5-layered lamellar-*in*-lamellar structure was experimentally observed for P2VP-ISISISISI-P2VP undecablock copolymers with long poly-2-vinylpyridine (denoted as P2VP) end blocks and nine short internal polyisoprene (I) and polystyrene (S) blocks, where all chemically different species are mutually incompatible. A "thin" five-layered I-S-I-S-I lamellar structure was formed by the nine short isoprene and styrene blocks within the "thick" P2VP layers [4]. The corresponding lamellae periods were 88 nm and 16 nm. The total molecular weight of the terpolymer was 339000 g/mol with a polydispersity of 1.03 and volume fractions of P, I, and S of 0.53, 0.26 and 0.21, respectively.

More recently, Matsushita and co-workers [6] investigated the same type of P2VP-ISISISISI-P2VP multiblock terpolymers with volume fractions of poly-2-vinylpyridine in between 0.08 and 0.21. Using TEM and SAXS measurements, they observed that for a volume fraction 0.08 of poly-2-vinylpyridine, the P-$(IS)_4$I-P multiblock copolymer exhibited a spheres-*in*-lamellar structure. Cylinders-*in*-lamellar were observed for the same type of terpolymer with 21% poly-2-vinylpyridine.

Matsushita and co-workers [6] also investigated another multiblock terpolymers with the structure P2VP-*b*-(I-*b*-S)$_2$-*b*-I, where the volume fractions of poly-2-vinylpyridine were respectively 0.64, 0.75 and 0.87. For these compositions the hexablock terpolymers exhibited a lamellar-in-lamellar structure, a hexagonally packed coaxial cylinders in a continuous matrix and an onion-like spherical structure in a continuous matrix.

Besides the the block copolymer-based comb-shaped supramolecular systems and the linear multiblock copolymer systems, hierarchically ordered structures have also been found in ABC-like star-shaped terpolymers, where the three different components are connected at the same junction point. In Ref.7 cylinders-*in*-lamellar, lamellae-*in*-cylinder and lamellae-*in*-sphere morphologies were found using TEM and SAXS in ISP triblocks (I-isoprene, S-styrene, P- poly-2-vinylpyridine) with volume fractions of I/S/P as 1/1.8/X, where X ranged from 4.3 to 53. On the other hand, for the triblock terpolymer $I_{1.0}S_{1.0}P_X$ with X in the range of $0.7 \le X \le 1.9$ and for the triblock terpolymer $I_{1.0}S_{1.8}P_X$ with X in the range of $0.8 \le X \le 2.9$ hierarchically ordered structures were observed.

Experimental studies of the ordering mechanism in ABC triblock terpolymers [8] was undertaken by Yamacuchi et al. who examined poly(isoprene-D_8-styrene-vinyl methyl ether) triblock terpolymers. The authos observed that the ordering process proceeded via a two-step mechanism: first one of the species segregated from the other two, and then complete microphase separation between all species occurred.

Bulk morphologies of block copolymer blends of AB/CD and ABA/CD types have been explored in Ref.9 and Ref.10, by using TEM and SAXS measurements. In the first study the authors used poly(isoprene-*block*-2-vinylpyridine) (IP) and poly(styrene-*block*-4-hydroxystyrene) (SH) with different molar ratios, 5:5 and 9:1, i.e IP55, SH91, IP55 and SH91. Using TEM and SAXS the authors observed that IP/SH blends self-assembled into complex microphase-separated structures. Two kinds of hierarchical structures were found: one is a specific lamellar structure from a symmetric IP55/SH55 blend, where one phase is mixed from P and H and form alternating lamellae, whereas I and S phases are segregated alternatingly. The other hierarchical structure has been observed from IP91/SH91 blend with equal amount of IP91 and SH91 and consists of another peculiar lamellar structure, where the P/H mixed phase forms isolated cylinders between lamellar S and I layers. In the second study, where the authors used PIP/SH samples, so-called Archimedean tiling structures were observed.

In a recent review the results of the morphological studies on triblocks and block-copolymer-based multiblocks have been discussed by Matsushita, including star-shaped terpolymers of the ABC type, block copolymer blends involving block copolymers of different types and linear multiblock copolymers [11,12].

3.2 Theoretical and computer simulation overview

Theoretically the morphological phase diagram of linear multiblock copolymers has been established by Matsen and Schick [24] in the many-block limit using the self-consistent field theory already in 1994. Bridging and looping in for self-assembled linear $(AB)_m$ multiblock copolymers has also been investigated by Matsen[25] applying both self-consistent field theory and strong segregation theory. The analysis was restricted to the lamellar phase and the fraction of blocks which make bridges across the lamellae was

determined Quite good agreement was obtained between both theories applied in the range of $\chi N < 30$, where N is the degree of polymerization of the AB diblock. The bridging fraction found was in agreement with previously calculated for ABA triblocks [26] where it was estimated that usually 40% of the copolymers form bridges for $\chi N_{TOT} = 100$ (N_{TOT} is the degree of polymerization of the ABA triblock). The fraction of bridges was an increasing function of the Flory-Huggins parameter χ between the A- and B-species, and a decreasing function of N_{TOT}.

Rasmussen and co-workers [27] using self-consistent field calculations theoretically investigated the morphology and bridging properties of $(AB)_m$ multiblock copolymers for $m \leq 6$. They found that the equilibrium period of the lamellar morphology scales as $m^{-0.8}$, in agreement with the experimental observations of Spontak and co-workers[13] on polystyrene-polyisoprene multiblock copolymers with $m \leq 4$. They predicted that more than 25% of the blocks consists of bridges in the already strongly segregated lamellar morphology. The authors also discussed how the bridging fraction affects the mechanical properties of multiblock copolymer materials.

More recently, using self-consistent field calculations, the existence of double-periodic structures has been also predicted theoretically for linear alternating A-*b*-(B-*alt*-A)$_m$ multiblock copolymers as well as for A–*b*-(A-*graft*-B)$_m$ comb copolymers where m denotes the number of repeating diblocks. Here the homopolymer end block A is significantly larger than the other blocks involved, thus creating a two-length-scale architecture. It was concluded that depending on the system parameters such as m and the volume fraction of the end A-block, a two length-scale microphase separation will take place: the A end blocks phase separate from the rest of the polymers and subsequently a "short" length scale phase separation between the A and B components within the (B-*alt*-A)$_m$ or (B-*graft*-A)$_m$ occurs [28-29].

The possibility of microphase separation at two length scales in a melt of binary multiblock copolymers with two intrinsic length scales has been explored by Kuchanov and co-workers in the weak segregation limit. Under certain conditions a pronounced change in the mesophase period was observed, a phenomenon that appears to be characteristic for these type of multiblock copolymers[30-31].

The phase behavior of A-*b*-(B-*alt*-A)$_m$-*b*-B block copolymers has also been studied extensively within the weak segregation limit[32]. The most important observations are that for $m>2$ there exists a region where the double gyroid phase remains stable in a certain temperature range up to critical point. For $m>5$ a continuous change of the length of end-blocks resulted in a change in symmetry and periodicity of the ordered phases; the periodicity length scale could increase up to ten fold. This is a most striking illustration of the two-length scale nature of the system under consideration.

We studied the lamellar-in-lamellar structures of binary A-*b*-(B-*b*-A)$_m$-*b*-B-*b*-A and ternary C-*b*-(B-*b*-A)$_m$-*b*-B-*b*-C multiblock copolymers theoretically in the strong segregation limit[33-34] focussing on the relation between the number m of repeating diblock units and the number of "thin" lamellar domains sandwiched between "thick" layers. The results of these studies form the major part of this thesis and can be found in Chapters 5-7.

A number of computer simulation results is also available for the two-length-scale copolymer molecules with linear and non-linear architecture. Hierarchical structure-in-structure morphologies in A_2-*star*-(B-*alt*-C) molecules have been investigated by Huang

and co-workers [35] using the dissipative particle dynamics simulation technique. Various types of hierarchically ordered structures were observed such as A-spheres in the matrix formed by B and C alternating layers, hexagonally packed A-cylinders in the matrix of B and C segregated layers, etc. The general observation was that the small length-scale B and C domains were parallel to the large length-scale structures. The authors also investigated A-*block*-(B-*graft*-C) copolymers using the same simulation technique.

The dissipative particle dynamics simulation technique has also been used by us [36] to support the theoretically predicted tendencies for the layers' formation in ternary C-*b*-(B-*b*-A)$_m$-*b*-B-*b*-C multiblock copolymers. Good agreement was found between the computer simulations and the theoretical predictions using the strong segregation limit. This part is presented in Chapter 6.

Finally, Gemma et al. [37] predicted hierarchical behavior for ABC star polymers using a Monte Carlo simulation method. The arm-length ratio in ABC triblock under investigation was 1:1:X. For increasing X in the range $3 \le X \le 25$ the shape of the domains formed by the A and B components changed from lamellar to cylindrical and to spherical. In this study the internal structure of the hierarchical morphologies was exclusively lamellar due to the fact that A and B components in the ABC triblock had equal volume ratios.

REFERENCES

[1] J.Ruokolainen, R.Mäkinen, M.Torkkeli, T.Mäkelä, R.Serimaa, G.ten Brinke, O.Ikkala, *Science* **1998**, *280*, 557.
[2] J.Ruokolainen, G.ten Brinke, O.Ikkala, *Adv. Mater*. **1999**, *11*, 777.
[3] O.Ikkala, G.ten Brinke, *Science* **2002**, *295*, 2407 .
[4] Y.Nagata, J.Masuda, A.Noro, D.Cho, A.Takano, Y.Matsushita, *Macromolecules* **2005**, *38*, 10220.
[5] J.Masuda, A.Takano, Y.Nagata, A.Noro, Y.Matsushita, *Phys.Rev.Lett. 2006, 97*, 098301.
[6] J.Masuda, A.Takano, J.Suzuki, Y.Nagata, A.Noro, K.Hayashida, Y.Matshushita, *Macromolecules* **2007**, *40*, 4023.
[7] K.Hayashida, N.Saito, S.Arai, A.Takano, N.Tanaka, Y.Matsushita, *Macromolecules* **2007**, *40*, 3695.
[8] K.Yamauchi, H.Hasegawa, T.Hashimoto, N.Kohler, K.Knoll, *Polymer* **2002**, *43*, 3563.
[9] T.Asari, S.Matsuo, A.Takano, Y.Matsushita, *Macromolecules* **2005,** *38,* 8811.
[10] T. Asari, S. Arai, A.Takano, Y. Matsushita, *Macromolecules* **2006,** *29,* 2232.
[11] Y.Matsushita, *Macromolecules* **2007**, *40*, 771.
[12] Y.Matsushita, *Polymer Journal* **2008**, *40*, 177.
[13] C.C Evans, F.S.Bates, M.D.Ward, *Chem. Mater.* **2000**, *12*, 236.
[14] A.F.Thünemann, S.General, *Macromolecules* **2001**, *34*, 6978.
[15] R.J.Spontak, S.D.Smith, *J,Polym.Sci. Part B: Polym.Phys*. **2001**, *39*, 947.
[16] C.Osuji, C.Y.Chao, I.Bita, C.K.Ober, E.L.Thomas, *Adv. Funct. Mater.* **2002**, *12*, 753.
[17] I.A.Ansari, V.Castelletto, T.Mykhaylyk, I.W.Hamley, Z.B.Lu, T.Itoh, C.T.Imrie, *Macromolecules* **2003**, *36*, 8898.
[18] G.O.R.Alberda van Ekenstein, E.Polushkin, H.Nijland, O.Ikkala, G.ten Brinke, *Macromolecules* **2003**, *36*, 3684.
[19] C.Y.Chao, X.Li, C.K.Ober, C.Osuji, E.L.Thomas, *Adv. Mater.* **2004**, *14*, 364.
[20] O.Ikkala, G.ten Brinke, *Chem. Com.* **2004**, 2131.
[21] C.S.Tsao, H.L.Chen, *Macromolecules* **2004**, *37*, 8984.
[22] I.W.Hamley, V.Castelletto, P.Parras, Z.B.Lu, C.T.Imrie, T.Itoh, *Soft Matter* **2005**, *1*, 355.
[23] B.Nandan, C.H.Lee, H.L.Chen, W.C.Chen, *Macromolecules* **2005**, *38*, 10117.
[24] M.W.Matsen, M.Schick, *Macromolecules* **1994**, *27*, 187.
[25] M.W.Matsen, *J.Chem.Phys*. **1995**, *102*, 3884.
[26] M.W.Matsen, M.Schick, *Macromolecules* **1994**, *27*, 7157.
[27] K.O.Rasmussen, E.M.Kober, T.Lookman, A.Saxena, *J.Polym.Sci. Part B:Poly.Phys.* **2003**, *41*, 101.
[28] R.Nap, C.Kok, G.ten Brinke, S.I.Kuchanov, *European Phys. J. E* **2001**, *4*, 515.
[29] R.Nap, N.Sushko, I.Ya.Erukhimovich, G.ten Brinke, *Macromolecules* **2006**, *39*, 6765.
[30] S.I.Kuchanov, V.E.Pichugin, G.ten Brinke, *E-Polymers* **2006**, 012.
[31] S.I.Kuchanov, V.E.Pichugin, G.ten Brinke, *Europhys. Lett.* **2006**, *76*, 959.
[32] Y.Smirnova, G.ten Brinke, I.Ya.Erukhimovich, *J.Chem. Phys.* **2006**, *124*, 054907.
[33] A.Subbotin, T.Klymko, G.ten Brinke, *Macromolecules* **2007**, *40*, 2915.
[34] T.Klymko, A.Subbotin, G.ten Brinke, submitted to *J.Chem.Phys*.
[35] C.-I.Huang, C.-M.Chen, *ChemPhysChem*, **2007,** *8*, 2588.
[36] T.Klymko, V.Markov, A.Subbotin, G. ten Brinke, *in preparation*.
[37] T.Gemma, A.Hatano, T.Dotera, *Macromolecules* **2002,** *35*, 3225.
[38] U.Micka, K.Binder, *Macromol. Theory Simul*. **1995,** *4*, 419.
[39] Y.Bahbot-Raviv, Z.G.Wang, *Phys. Rev. Lett*. **2000,** *85*, 3428.
[40] Q.Wang, P.F.Nealey, J.J.de Pablo, *Macromolecules* **2001,** *34*, 3458.

PART II

THEORETICAL ANALYSIS

CHAPTER 4

Lamellar Self-Assembled Diblock Copolymer/Homopolymer Blends Involving Specific Interactions

Abstract. The strongly segregated lamellar state of blends of a diblock copolymer with a "long" homopolymer that interacts favorably with one of the blocks of the copolymer is analysed in detail. Essential observations concern the parabolic homopolymer distribution profile, the presence of "dead" zones near the block copolymer interface where no homopolymer is present and the maximal amount of homopolymer that can be dissolved. The behavior is largely determined by the value of $\gamma/(N|\chi|^{3/2})$, where γ is the interfacial tension, N the "length" of the block copolymer and $\chi < 0$ the Flory-Huggins parameter representing the favorable interaction between the homopolymer and one of the blocks of the copolymer. If this ratio is too small no homopolymer will dissolve at all due to the unfavorable conformational effects accompanying an inhomogeneous homopolymer distribution.

4.1 Introduction

Blends of diblock copolymers with homopolymers that are chemically identical to one of the blocks have been studied extensively in the past both theoretically [1-17] and experimentally [18-29] and are reviewed in some detail in Chapter 2 of this Thesis. In many of the reviewed studies the central question concerned the solubilization and distribution of the homopolymer in the diblock copolymers domains. Apart from the situation where the homopolymer is chemically identical to one of the blocks of the diblock copolymer the case where the homopolymer interacts favorably with one of the blocks was also discussed. An outstanding example of such exothermic interactions is poly(2,6-dimethyl-1,4-phenil oxide) (PPO) in combination with polystyrene (PS). This is used for instance to introduce entanglements in the core of nanorods made from polystyrene-*block*-poly(4-vinylpyridine) (PS-*b*-P4VP) diblock copolymers and consisting of a PS core and a poly(4-vinyl pyridine) corona. Here PPO is dissolved in the PS core and possibility to introduce entanglements in this way is directly related to the low molecular weight between entanglements of PPO. In this respect the distribution of the PPO homopolymer inside the PS-domains is of considerable interest.

To address this, in this Chapter the strongly segregated lamellar state of blends of a diblock copolymer with a "long" homopolymer that interacts favorably with one of the blocks of the copolymer is analysed using the strong segregation approach. It will be shown how the pertinent parameters, such as the amount of homopolymer, the interaction strength, the block copolymer composition, etc., affect the distribution of the homopolymer inside the block copolymer layer.

4.2 The model

We consider a blend of a diblock copolymer AB and a homopolymer C, assuming from the very beginning that the homopolymer chain length N_C is longer than the total diblock copolymer length N. Hence, each block copolymer chain consists of $N = N_A + N_B$ monomer units. The volume of the different monomers is assumed to be equal and is denoted by υ. We also assume that the statistical segment length a of the A, B and C molecules is the same. The ratio $f = N_A / N$ defines the diblock copolymer composition and the ratio $\varphi = V_C / V_{total}$ represents the average homopolymer volume fraction in the diblock copolymer / homopolymer mixture, V_C being the volume occupied by homopolymer and V_{total} the volume of the diblock copolymer / homopolymer mixture. The Flory-Huggins interaction parameters χ_{AB} and χ_{BC} are taken to be positive, however, the Flory-Huggins parameter χ_{AC} is supposed to be negative implying favorable interactions between homopolymer C and the A-blocks of the diblock copolymer. The blend of polystyrene-*block*-poly (4-vinylpyridine) (PS-*b*-P4VP) and poly (2,6-dimethyl-1,4-diphenyl oxide) (PPE),

where $\chi_{PS-PPE} = -0.1$ [25-27] $\chi_{PS-P4VP} = 0.3 \div 0.35$ [28] and $\chi_{P4VP-PPE} \cong 0.6$ [29] serves as an experimental example and in fact motivated the present study.

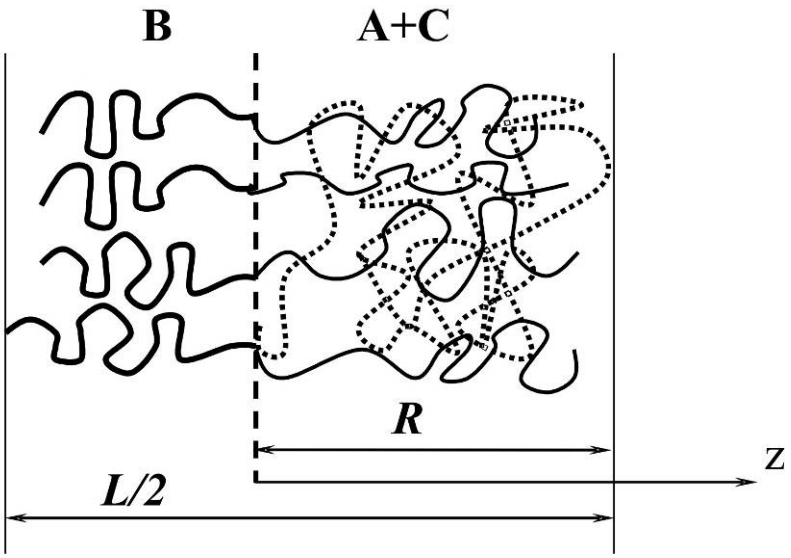

Figure 4.1. Schematic representation of AB-diblock copolymer/C-homopolymer blend in the case $\chi_{AC} < 0$. The homopolymer chains segregate exclusively into A-lamellar domains. A-chains and B-chains are depicted by thin and thick solid lines, respectively. Homopolymer chain is depicted short-dashed line. R is the thickness of half of the A-layer, i.e. the distance from the interface to the mid plane.

In the strong segregation limit the A and B blocks are stretched and directed perpendicular to the narrow AB interface [30]. At this level of segregation we can model a diblock copolymer as a polymer brush. Considering exclusively the lamellar morphology, as we will do in this paper, each lamellar domain will consist of opposite brushes [31]. Since the B-C interactions are unfavorable ($\chi_{BC} > 0$), homopolymer C will segregate exclusively in the A-domains, generally resulting in some nonuniform homopolymer distribution $\Phi(z)$ across A-lamellar domain (z is the coordinate perpendicular to the AB-interface). A schematic illustration of the model considered is given in Figure 4.1. A somewhat similar situation also involving three components was considered in Ref. 32. There the situation was considered where nanoparticles are preferably distributed in one of the lamellar domains of a diblock copolymer. Assuming from the outset a homogeneous distribution of the nanoparticles the authors derived an expression for the increase in lamellar period as a function of the nanoparticle volume fraction. Our main goal is to beyond this approach by investigating the homopolymer distribution inside the A lamellar domains and to determine the maximum amount of homopolymer that can be dissolved in the A layers. To achieve these objectives we need to obtain an expression for the free energy of the system in terms of the homopolymer distribution profile $\Phi(z)$ inside the lamellar A-domains. Hence, in contrast to Ref. 32, we will assume a free chain ends distribution inside the A-layers [31, 33-35], which results in an inhomogeneous

homopolymer distribution. The fact that the free chain ends of the A-chains are distributed non-uniformly indicates that in some cases the homopolymer may not even penetrate up to the very AB interface, but only up to a certain penetration depth. Therefore, two different regimes will be distinguished from the beginning. In the first regime the homopolymer is distributed through the whole layer, whereas in the second regime the homopolymer does not go all the way to the AB interface.

Let us start with the first regime. In this case the average homopolymer volume fraction ϕ in the A-layers is defined by:

$$\phi = \frac{1}{R}\int_0^R \Phi(z)\,dz \tag{4.1}$$

Here the equilibrium A-block layer thickness R should be determined for a given homopolymer distribution from the minimization of the total free energy of the whole system. Note, that from geometrical considerations the average homopolymer volume fraction ϕ in the A-layers and the average homopolymer volume fraction $\varphi = V_C / V_{total}$ in the whole diblock copolymer system are related via the diblock composition f :

$$\phi = \frac{\varphi}{\varphi + f(1-\varphi)} \tag{4.2}$$

4.3 Free energy calculations

The total free energy per block copolymer chain as a function of the homopolymer distribution profile consists of the free energy of the AB interface, the elastic free energy due to the stretching of the copolymer blocks and the interaction energy between the homopolymer and the A-blocks:

$$F_1 = \gamma\Sigma + \frac{\pi^2 N \upsilon^2 (1-f)}{8a^2\Sigma^2} + \frac{3\pi^2\Sigma}{8a^2N^2f^2\upsilon}\int_0^R z^2\big(1-\Phi(z)\big)\,dz - \frac{|\chi|\Sigma}{\upsilon}\int_0^R \Phi(z)\big(1-\Phi(z)\big)\,dz \tag{4.3}$$

Here the free energy is given in kT energetic units. Σ is the interfacial area per block copolymer chain, $\chi_{AC} \equiv \chi$, and $\gamma = \frac{a\sqrt{\chi_{AB}}}{\upsilon\sqrt{6}}$ is the AB-interface tension. The first term in expression (4.3) is the interfacial free energy. Note that in our treatment we restrict ourselves to the situation when $\gamma_{AB} \cong \gamma_{BC} \equiv \gamma$. In the case of $\gamma_{AB} \neq \gamma_{BC}$ the interfacial tension γ will depend on the concentration of homopolymer at the AB interface and therefore should be found self consistently. The elastic free energy is represented as a sum of two contributions representing the chain elongation in the B and A lamellar domains (second and third term in (4.3), respectively). The third term in Eq.(4.3)

represents the nonuniform chain stretching and therefore inhomogeneous distribution of the free ends of the A-chains [35]. In fact $1-\Phi(z)=\Phi_A(z)$ determines this distribution. The last term in expression (4.3) takes into account the interactions between homopolymer C and A-blocks. Two more terms, which can be considered as corrections to the free energy, are omitted in the expression (4.3). The first one is connected with the loss of conformational entropy of homopolymer C due to its nonuniform distribution inside the A-layers. This term does become important for small values of interaction parameter $|\chi|$ and the case where this term dominates will be discussed later (subsection 4.5). We also omit the ideal-gas term which is connected with the thermal motion of the homopolymer and which scales as $1/N_C$.

To obtain an analytical expression for the homopolymer distribution $\Phi(z)$ the free energy (4.3) should be minimized under the constraint (4.1). Implementation of this procedure by the Lagrange multipliers method immediately results in a parabolic form for the homopolymer concentration profile (Figure 4.2):

$$\Phi(z)=\Phi_0+\alpha z^2 \tag{4.4}$$

with

$$\Phi_0=1-\frac{\alpha R^2}{3}-\frac{fN\upsilon}{\Sigma R} \tag{4.5}$$

$$\alpha=\frac{3\pi^2}{16a^2f^2N^2|\chi|},\qquad \Sigma R=\frac{fN\upsilon}{1-\phi} \tag{4.6}$$

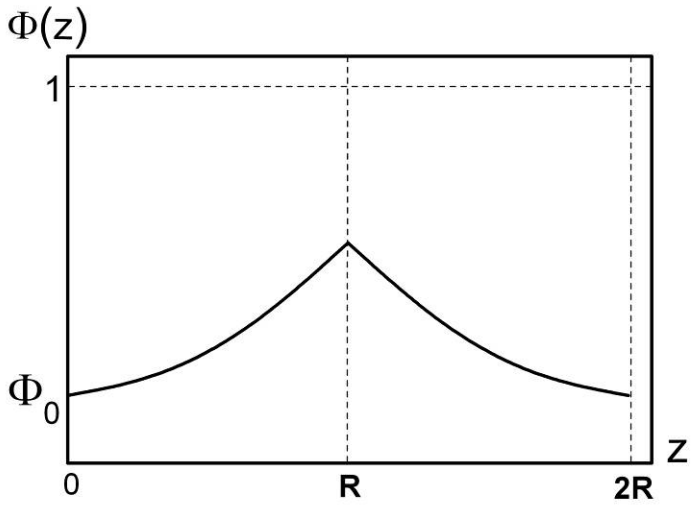

Figure 4.2. Schematic representation of typical parabolic concentration profile $\Phi(z)=\Phi_0+\alpha z^2$, $\Phi_0=\Phi_0(R,\Sigma)$, $\alpha=\alpha(\chi)$.

Thus, the addition of some amount of homopolymer to the diblock copolymer results in a homopolymer distribution (4.4) inside the A-layers. Distribution (4.4) shows a minimal amount of homopolymer, Φ_0, at interface where $z = 0$ and a maximum in the center of the lamellar domain, the so-called mid-plane, where $z = R$. Note, that the inclusion of conformational effects will smoothen this profile in the centre of the lamellar domain.

Re-writing expression (4.4) in the form

$$\Phi(z) = \alpha\left(r^2 + z^2\right) \tag{4.7}$$

and introducing the dimensionless variable $u = R/r$, we can express r and R in terms of u:

$$r = \left[\frac{3\phi}{\alpha(u^3+3)}\right]^{1/2}, \qquad R = \left[\frac{3\phi u^2}{\alpha(u^3+3)}\right]^{1/2} \tag{4.8}$$

It results in the following expression for the free energy:

$$F_1 = \gamma\Sigma + \frac{\pi^2 N\upsilon^2(1-f)}{8a^2\Sigma^2} + \frac{|\chi|\Sigma}{\upsilon}\left\{\alpha r^3\left[\frac{u^3}{3}-u\right] - \alpha^2 r^5\left[\frac{u^5}{5}-u\right]\right\} \tag{4.9}$$

Taking into account that $\Sigma R(1-\phi) = fN\upsilon$ and introducing a new parameter

$$k = \frac{\pi\gamma\upsilon}{4aN|\chi|^{3/2}} \tag{4.10}$$

which is a combination of all the different parameters occurring in the last expression for the free energy except for the diblock composition f, the final expression for the free energy is obtained in the form:

$$\frac{F_1}{F_d} = \frac{(2k)^{1/3}}{3}\frac{\phi}{1-\phi}\left\{\frac{1}{\phi^{3/2}}\left[\frac{u^2+3}{u^2}\right]^{1/2} + \frac{1}{k}\left[2(1-f)(1-\phi)^3\cdot\frac{u^2}{u^2+3} + f\cdot\frac{u^2-3}{u^2+3} - \frac{9f\phi}{5}\cdot\frac{u^4-5}{(u^2+3)^2}\right]\right\} \tag{4.11}$$

Here $F_d = \frac{3}{2}\left(\frac{\pi\gamma\upsilon}{2a}\right)^{2/3} N^{1/3}$ is the free energy of the pure diblock copolymer system. As stated in the beginning, expression (4.11) is valid only as long as the homopolymer distribution continues up to the AB-interface.

Now we turn our attention to the second regime assuming that this no longer holds. This regime appears for $\Phi_0 < 0$ (cf. Eq. 4.4). Physically it implies the presence of a "dead zone", i.e. a region near the AB-interface inside the A-layer where the homopolymer does not penetrate (Figure 4.3).

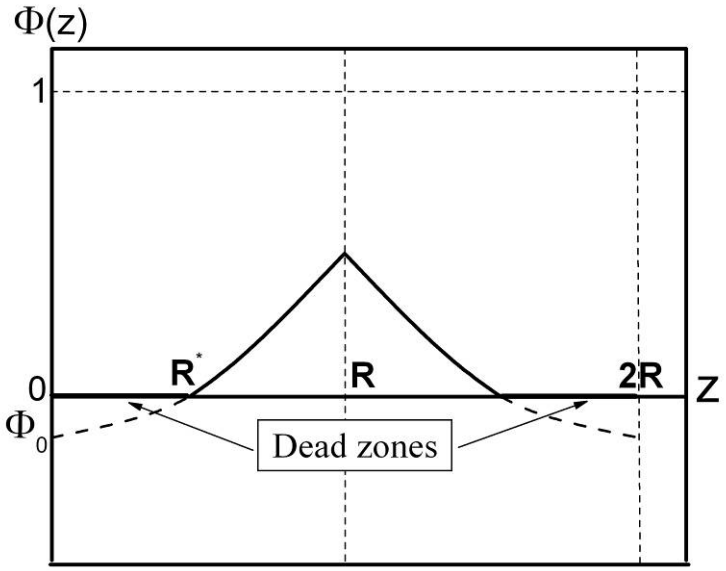

Figure 4.3. Schematic representation of typical parabolic concentration profile $\Phi(z) = \Phi_0 + \alpha z^2$ in the case when $\Phi(z=0) = \Phi_0 < 0$.

The average amount of homopolymer in the diblock copolymer / homopolymer system now satisfies

$$\phi = \frac{1}{R}\int_{R^*}^{R} \Phi(z)\, dz \qquad (4.12)$$

Increasing the average amount of homopolymer added, the "dead zone" becomes smaller and for some specific value of the average homopolymer concentration it will disappear. The condition $R^* = 0$ guarantees that the necessary amount of homopolymer has been added, after that Φ_0 starts to become positive.

Taking into account that the homopolymer is distributed only throughout the interval $[R^*, R]$, the free energy given by Eq.(4.3) transforms into

$$F_2 = \gamma\Sigma + \frac{\pi^2 N\upsilon^2(1-f)}{8a^2\Sigma^2} + \frac{3\pi^2\Sigma}{8a^2N^2f^2\upsilon}\int_0^{R^*} z^2\,dz + \frac{3\pi^2\Sigma}{8a^2N^2f^2\upsilon}\int_{R^*}^{R} z^2\big(1-\Phi(z)\big)dz - \frac{|\chi|\Sigma}{\upsilon}\int_{R^*}^{R}\Phi(z)\big(1-\Phi(z)\big)dz \tag{4.13}$$

Minimization of the free energy (4.13) with respect to $\Phi(z)$ yields again a parabolic form for the homopolymer distribution profile. This profile satisfies the requirement $\Phi(R^*) = 0$ and reads

$$\Phi(z) = \alpha\left(z^2 - R^{*2}\right) \tag{4.14}$$

with constant α determined according to Eq. (4.6).

At this point we introduce a new variable $u = R/R^*$. Combining the homopolymer distribution profile (4.14) with condition (4.12) leads to the following expression for R and R^*, similar to (4.8):

$$R = \left[\frac{3\phi u^3}{\alpha(u^3 - 3u + 2)}\right]^{1/2}, \quad R^* = \left[\frac{3\phi u}{\alpha(u^3 - 3u + 2)}\right]^{1/2} \tag{4.15}$$

In terms of u the following expression for the free energy is obtained:

$$F_2 = \gamma\Sigma + \frac{\pi^2 N\upsilon^2(1-f)}{8a^2\Sigma^2} + \frac{|\chi|\Sigma}{\upsilon}\left\{\alpha R^{*3}\left[\frac{u^3}{3} + u - \frac{2}{3}\right] - \alpha^2 R^{*5}\left[\frac{u^5}{5} - u + \frac{4}{5}\right]\right\} \tag{4.16}$$

Applying the same sequence of calculations as described above the free energy is found in the form given below:

$$\frac{F_2}{F_d}=\frac{(2k)^{1/3}}{3}\frac{\phi}{1-\phi}\left\{\frac{1}{\phi^{3/2}}\left[\frac{u^3-3u+2}{u^3}\right]^{1/2}+\right.$$
$$\left.\frac{1}{k}\left[2(1-f)(1-\phi)^3\cdot\frac{u^3}{u^3-3u+2}+f\cdot\frac{u^3+3u-2}{u^3-3u+2}-\frac{9f\phi}{5}\cdot\frac{u^6-5u^2+4u}{(u^3-3u+2)^2}\right]\right\} \tag{4.17}$$

When the condition $R^*=0$ is fulfilled the second regime transforms into the first one. For fixed values of f and k the free energies (4.11) and (4.17) are functions of the average homopolymer volume fraction ϕ and the dimensionless variable u. To see how the free energy behaves as a function of the homopolymer volume fraction, the free energy has been minimized with respect to u. It is important to note that since we have a nonuniform distribution $\Phi(z)$, in contrast to the Alexander-de Gennes model where the homopolymer is distributed uniformly, the maximum amount of homopolymer inside the lamellar domains is not determined by the location of the minimum of the free energy alone, as it is shown in Appendix A for a Alexander-de Gennes brush, but involves in addition the requirement $\Phi(R)\le 1$. This demand guarantees that the amount of homopolymer does not exceed unity in the center of the A domains, i.e in the position where the homopolymer distribution has its maximum value.

4.4 Results and Discussions

4.4.1 Free energy behavior

The equations presented are used to numerical analysis of different situations. First, the free energy is considered for a symmetric diblock copolymer for different values of $k=02,05,0.8$ and for different diblock copolymer compositions $f=0.3,0.5,0.6$ at fixed $k=0.2$. The results are presented in Figs. 4.4 and 4.5.

As shown in Figure 4.4 for a given diblock copolymer composition, the free energy is a decreasing function of the homopolymer volume fraction. This demonstrates that the penetration of the homopolymer is a favorable process up to a maximum concentration of homopolymer $\phi_{\max}$. $\phi_{\max}$ is determined by the requirement $\Phi(R)\le 1$. The maximum amount of homopolymer strongly depends on the value of the parameter $k=\pi\gamma\nu/\left(4aN|\chi|^{3/2}\right)$. The larger k is, the smaller the maximum amount of homopolymer is. Small values of k correspond either to large values of N at fixed Flory-Huggins interaction parameter $|\chi|$, or to large values of $|\chi|$ at fixed diblock

copolymer length N. The first statement shows that thicker lamellar domains can incorporate more homopolymer. The second observation implies that more favorable interactions, as expected, also allow more homopolymer to be dissolved.

The analysis of Figure 4.5 shows that changes in diblock copolymer composition also affect the maximum possible amount of homopolymer inside the lamellar domains: the larger the volume fraction of A-blocks in the diblock copolymer, the larger the amount of homopolymer that can be incorporated. A comparison between Figures 4.4 and 4.5 reveals that the maximum allowable homopolymer amount $\phi_{\max}$ is more sensitive to changes in k than to changes in the diblock copolymer composition.

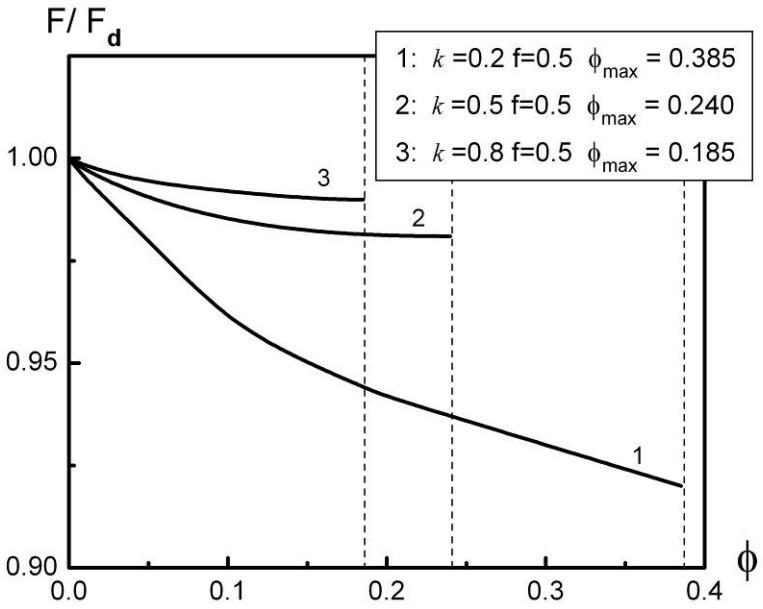

Figure 4.4. Numerically calculated free energies for different values of parameter k. Diblock composition $f = 0.5$. Dashed lines correspond to maximum allowable amount of homopolymer $\phi_{\max}$ for values of k as indicated.

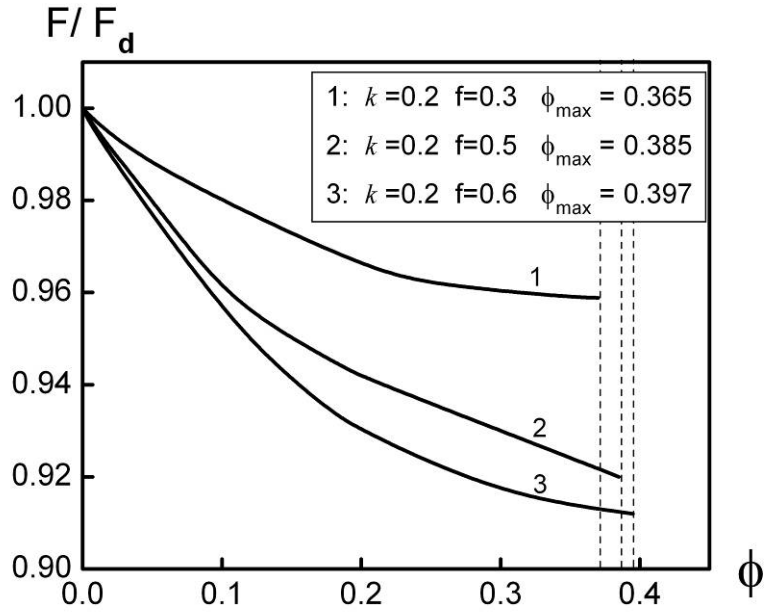

Figure 4.5. Numerically calculated free energies for different diblock compositions at $k = 0.2$. Dashed lines indicate maximum amount of homopolymer that can be dissolved for values of the diblock composition f as indicated.

4.4.2 Maximally allowable amount of homopolymer

As already mentioned, the maximally allowable homopolymer amount $\phi_{\max}$ also depends on the diblock copolymer chain length N. The numerically obtained dependence is depicted in Figure 4.6 for a symmetric diblock copolymer taking $\chi_{AB} = 0.32$.

For extremely small values of k, which is the case for very strong favorable AC-interactions or infinitely long diblock copolymers, the maximum value of $\phi_{\max}$ approaches unity. Referring to the experimental example already introduced before, in the case of a P4VP-PS/PPE blends with $\chi_{PS-PPE} = -0.1$, $\chi_{PS-P4VP} = 0.32$ and a number of monomer units $N = 1000$, we have $k = 0.006$ implying $\phi_{\max} = 0.82$. Experimentally it has indeed been observed that PPE homopolymer can be incorporated in PS domains up to a large amount. However, as mentioned before, for large amounts of homopolymer the lamellar structure will obviously no longer correspond to the equilibrium morphology.

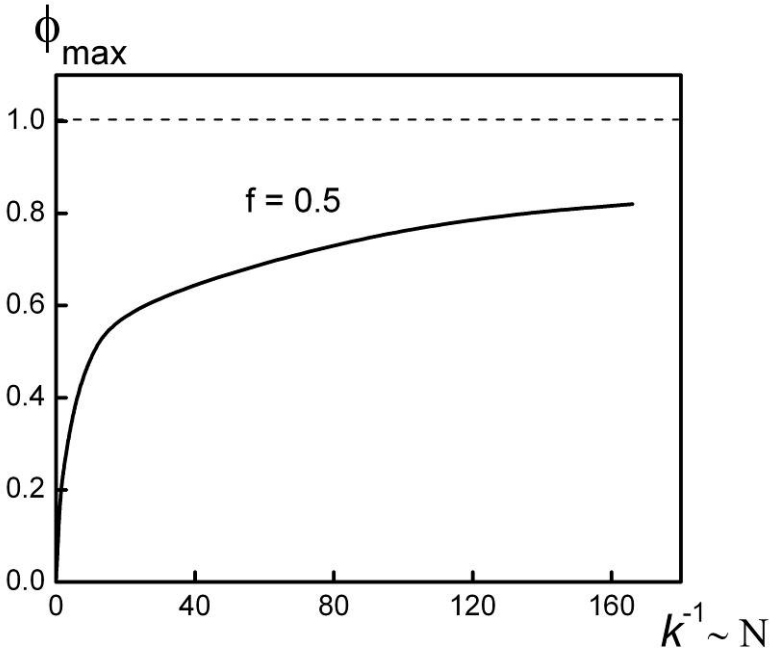

Figure 4.6. Maximum allowable amount of homopolymer as a function of diblock chain length N. For infinitely long diblock copolymer chains $\phi_{\max}$ asymptotically approaches unity.

The presence of "dead zones" is illustrated by the behavior of $R*/R$ as a function of average homopolymer concentration ϕ presented in Figure 4.7 for two different situations. Curve 1 in this figure corresponds to the case $k = 0.2$ and demonstrates that for an average homopolymer concentration $\phi' = 0.19$ switching between the two regimes occurs, i.e at $\phi' = 0.19$ the condition $R^* = 0$ is fulfilled. This means that for $k = 0.2$ for all average homopolymer concentrations satisfying $\phi > \phi' = 0.19$ we will always have some amount of homopolymer at the AB-interface. The maximum amount of homopolymer in the A-layers equals $\phi_{\max 1}$=0.385. Curve 2 in Figure 4.7 for $k = 0.5$ with $\phi_{\max 2}$=0.24 represents the opposite situation where we will never have homopolymer present at the AB-interface; in this case R^* is never zero. This happens because the average homopolymer concentration achieves it maximum allowable value $\phi_{\max 2} = 0.24$ before the switching between the two regimes takes place. In the case depicted by curve 2 in Figure 4.7 the system will always remain in the second regime. In the situation represented by curve 1 in Figure 4.7 there is a cross-over between the two regimes. The maximum amount of homopolymer in the A-layers equals $\phi_{\max 1}$=0.385. Curve 2 in Figure 4.7 for $k = 0.5$ with $\phi_{\max 2}$=0.24 represents the opposite situation where we will never have homopolymer present at the AB-interface; in this case R^* is never zero.

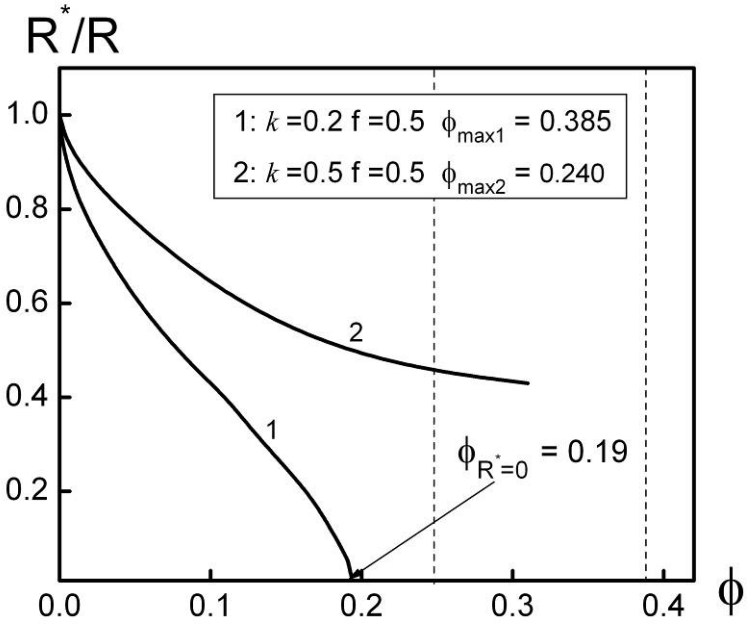

Figure 4.7. Dependence of homopolymer penetration depth on average homopolymer volume fraction for different values of parameter k .The figure represents two different situations corresponding to the possibilities of presence (curve 1) and absence (curve 2) of homopolymer at the AB-interface. Dashed lines depict maximum allowable average homopolymer concentrations for indicated values of k .

This happens because the average homopolymer concentration achieves it maximum allowable value $\phi_{\max 2} = 0.24$ before the switching between the two regimes takes place. In the case depicted by curve 2 in Figure 4.7 the system will always remain in the second regime. In the situation represented by curve 1 in Figure 4.7 there is a cross-over between the two regimes.

4.4.3 Homopolymer distribution profiles

Homopolymer distribution profiles for $k = 0.006$ and for different average homopolymer volume fractions are presented in Figure 4.8. The value $k = 0.006$ corresponds to P4VP-*b*-PS/PPE blend with $f = 0.5$, $\chi_{PS-PPE} = -0.1$, $\chi_{PS-P4VP} = 0.32$ and number of monomer units $N = 1000$. Our approach therefore predicts that starting from a volume fraction $\phi_{PPE} = 0.013$ PPE will go up to the PS/P4VP interface.

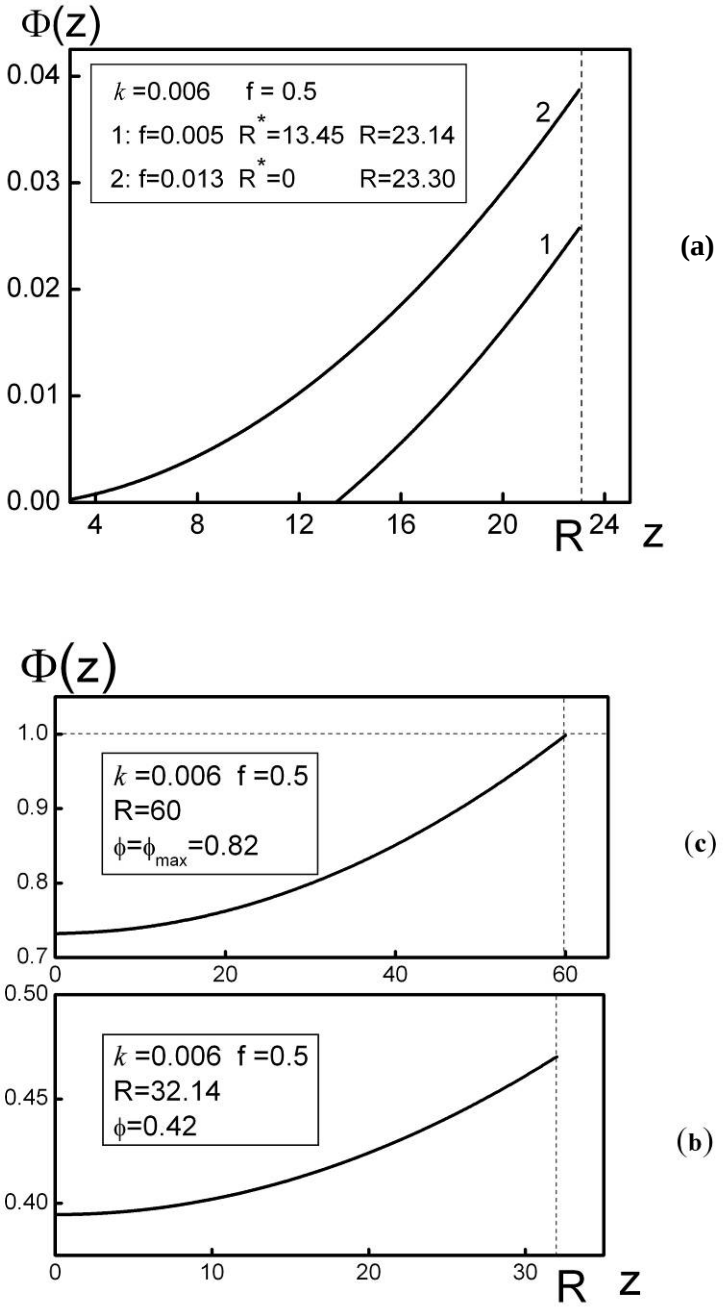

Figure 4.8 (a). Calculated homopolymer concentration profiles for different average homopolymer volume fractions ϕ for $k = 0.006$, with a maximum possible average amount of homopolymer $\phi_{\max} = 0.82$. Curve 1: the absence of homopolymer at the AB interface is illustrated for $\phi = 0.005$. Ratio $R^* / R = 0.58$. Curve 2: average homopolymer volume fraction is increased up to $\phi = 0.013$. Here the homopolymer goes very close to the AB interface and is distributed through the A-domains with a parabolic distribution profile. **(b)** Homopolymer distribution for an intermediate value of the average concentration of homopolymer, $\phi = 0.42$, with the minimum homopolymer fraction at the interface ($z = 0$) and the maximum in the centre of A-lamellar domain ($z = R$); $k = 0.006, \phi_{\max} = 0.82$ **(c)** Homopolymer distribution for $\phi = \phi_{\max} = 0.82$. In the centre of the A-layers $\Phi(R) = 1$, indicating that more homopolymer can not be incorporated; $k = 0.006, \phi_{\max} = 0.82$.

4.4.4 Lamellar period in the presence of the homopolymer

Next we consider how the lamellar period changes in the presence of the homopolymer. Without the homopolymer the long period L of pure diblock copolymers reads

$$L_d = \left(\frac{2aN}{\pi}\right)^{2/3} (\gamma\upsilon)^{1/3} \tag{4.18}$$

The long period L of the copolymer / homopolymer blend is directly related to the thickness of the A-lamellar domains. This in turn depends on the average homopolymer concentration as determined by the minimization of the free energy given by Eq.(4.11) or Eq.(4.17). In the first regime (expression (4.11) for the free energy is used) the behaviour of the long period L as a function of average homopolymer volume fraction ϕ is found to be given by the expression

$$\frac{L}{L_d} = \left(\frac{4}{k}\right)^{1/3} \phi^{1/2} (1-\phi(1-f)) \left[\frac{u^2}{u^2+3}\right]^{1/2} \tag{4.19}$$

In the second regime where the free energy is given by Eq.(4.17) the long period L satisfies

$$\frac{L}{L_d} = \left(\frac{4}{k}\right)^{1/3} \phi^{1/2} (1-\phi(1-f)) \left[\frac{u^3}{u^3-3u+2}\right]^{1/2} \tag{4.20}$$

In these equations u has a value which is determined by minimization of Eq.(4.11) and Eq.(4.17), respectively. The combination of expressions (4.19) and (4.20) gives the long period of the diblock copolymer / homopolymer blend for all homopolymer volume fractions that are allowed. Subsequent numerical calculations show the change in the lamellar period in the presence of homopolymer (Figure 4.9(a)). The situation depicted by curve 3 in this figure corresponds to the familiar experimental example of P4VP-PS/PPE with $k = 0.006$. In all cases the long period L increases as a function of the amount of homopolymer inside the lamellar domains. Figure 4.9(b) compares the results of the numerical calculations with the experimental data for the P4VP-PS/PPE blend. The parameter values for the numerical calculations were taken from the experiments in ref. 22: $f = 0.5$, $\chi_{AB} = \chi_{PS-P4VP} = 0.32$ and $N = N_{PS-P4VP} = 400$.

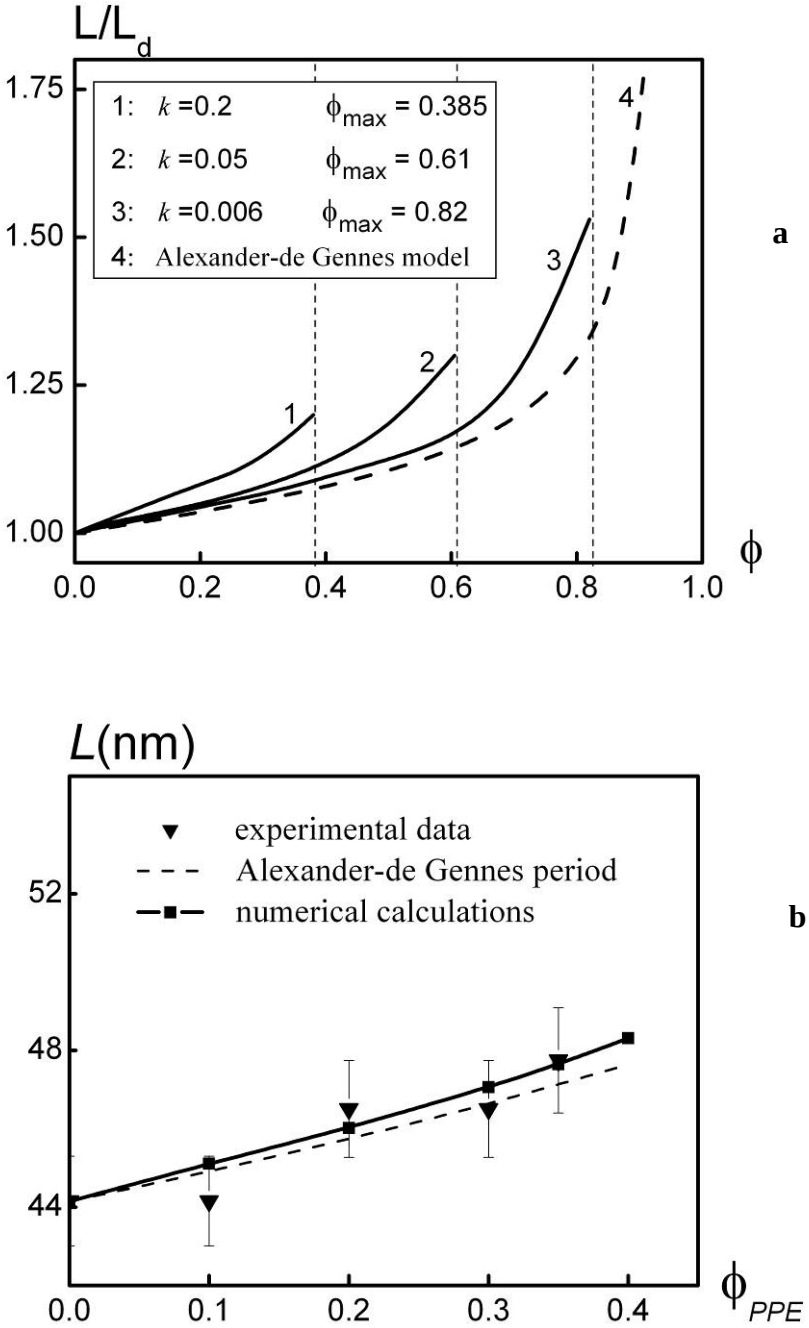

Figure 4.9. **(a)**: Changes in period L in the presence of homopolymer are depicted for symmetric diblock for different values of k. Dashed line shows long period predicted by the Alexander-de Gennes approach. **(b)** Comparison of the results of numerical calculations and experimental data for $f = 0.5$, $\chi_{AB} = 0.32$ and $N = 400$ ($k = 0.014$).

The dashed line in Figure 4.9(a) represents the behavior of the long period as predicted by the Alexander-de Gennes model assuming that all chain ends are at the mid plane and that the homopolymer is distributed uniformly throughout the layer. As one can see, curve 4 in Figure 4.9(a) demonstrates that for small values of k (large $\phi_{\max}$) the long period L asymptotically approaches the Alexander-de Gennes prediction. This is

the evidence that for large values of the diblock copolymer length N and Flory-Huggins parameter $|\chi_{AC}|$, the Alexander-de Gennes model can be considered as a limiting case of our more general model with nonuniform homopolymer distribution. Note that in the case of the Alexander-de Gennes approach, due to the uniform homopolymer distribution *ratio* L/L_d is independent of k and is given by (see also Ref.32)

$$\frac{L}{L_d}=\left(1+\frac{f\phi}{1-\phi}\right)\left(1-f+\frac{f}{(1-\phi)^2}\right)^{1/3} \tag{4.21}$$

whereas in our case because of the inhomogeneous distribution the ratio L/L_d depends on k as reflected in Eqs.(4.19) and (4.20). For the P4VP-*b*-PS/PPE blends the difference in long period between our more elaborated model and the simplified Alexander-De Gennes picture is relatively small and both descriptions describe the experimental data within experimental errors (Figure 4.9(b)).

4.4.5 Conformational effects

So far the conformational effects due to the inhomogeneous distribution of the homopolymer have been neglected. These start to become important if the interaction parameter $|\chi|$ is small. By substitution of the analytical expressions for the homopolymer distribution profiles presented in Figs.4.8(b) – 4.8(c) into expression (4.3) for the free energy we can verify whether the conformational term [30]

$$F_{conform}=\frac{a^2\Sigma}{24\upsilon}\int_0^R\frac{[\nabla\Phi(z)]^2dz}{\Phi(z)(1-\Phi(z))} \tag{4.22}$$

is actually small compared to the other terms in expression (4.3). It turns out that for the situation depicted in Figure 4.8(a), where the average homopolymer concentration is small, this is no longer the case. This forces us to consider in more detail the conformational free energy contribution for small average homopolymer volume fractions. Taking into account the loss of conformational entropy the free energy (4.1) reads

$$F=\gamma\Sigma+\frac{\pi^2N\upsilon^2(1-f)}{8a^2\Sigma^2}+\frac{3\pi^2\Sigma}{8a^2N^2f^2\upsilon}\int_0^R z^2\big(1-\Phi(z)\big)dz-\frac{|\chi|\Sigma}{\upsilon}\int_0^R\Phi(z)\big(1-\Phi(z)\big)dz+\frac{a^2\Sigma}{24\upsilon}\int_0^R\frac{[\nabla\Phi(z)]^2dz}{\Phi(z)(1-\Phi(z))} \tag{4.23}$$

Again, to get the homopolymer distribution profile the free energy (4.23) should be minimized with respect to $\Phi(z)$. In order to simplify our calculations we use the function

$$\Phi(x) = \frac{\Phi_0}{ch^2 \alpha x} \tag{4.24}$$

as a trial function for the homopolymer distribution profile. The particular feature of this function is that it makes the homopolymer distribution profile smoother compared to a parabolic profile and thus does not allow the homopolymer distribution to have a sharp break in the centre of the lamellar domain. The result of substitution of (4.24) into (4.23) is straightforward and brings us to the expression for the free energy in terms of $\tilde{x} = R/R_d$, where $R_d = f \cdot \left(\frac{2aN}{\pi}\right)^{2/3} (\gamma\upsilon)^{1/3}$ is the period of the pure diblock copolymer and $\Phi_0 = \alpha R\phi$ is determined from Eq.(4.1) for the homopolymer distribution profile (4.24). Hence, including the conformational term the free energy becomes:

$$\frac{F}{F_d} = \frac{1}{1-\phi}\left\{\frac{2}{3\tilde{x}} + f\tilde{x}^2\left[\frac{(1-f)(1-\phi)^3}{3f} + \frac{1}{3} - \phi + \frac{2\phi^2 \ln 2}{\Phi_0}\right] - \frac{2f\phi}{3(2k)^{2/3}}\left[1 - \frac{2}{3}\Phi_0\right] + \frac{2\Phi_0 \mu^{4/3}}{9\phi f\tilde{x}^2}\left[1 - \sqrt{\frac{1-\Phi_0}{\Phi_0}}\arctan\sqrt{\frac{\Phi_0}{1-\Phi_0}}\right]\right\} \tag{4.25}$$

In Eq.4.(25) k has been introduced by (4.10) and $F_d = \frac{3}{2}\left(\frac{\pi\gamma\upsilon}{2a}\right)^{2/3} N^{1/3}$ is the free energy of the pure diblock copolymer. Compared to the Eqs.(4.11) or (4.17), we have one more parameter

$$\mu = \sqrt{\frac{\pi}{2N}}\frac{a}{\upsilon\gamma} = \sqrt{\frac{3\pi}{\chi_{AB}N}} \tag{4.26}$$

which does not depend on homopolymer properties and is determined only by the diblock copolymer, its length N and the Flory-Huggins parameter χ_{AB}.

Subsequently the free energy (4.25) was minimized numerically with respect to $\tilde{x}$ and Φ_0. But before presenting the results, we first discuss the qualitative changes that may be anticipated from conformational effects. When these effects were not considered the free energy behaved as a decreasing function of the average homopolymer volume fraction for arbitrary negative values of the Flory-Huggins interaction parameter $\chi_{AC} \equiv \chi$ (see for example Figure 4.4). It implied that the

penetration of homopolymer into A-lamellar domains is favorable even for very weakly attractive AC interactions, i.e even for very small values of the Flory-Huggins interaction parameter $|\chi|$. Including conformational effects, in the case of weakly favorable AC interactions (which corresponds to the case where only a small amount of homopolymer can be incorporated in the lamellar structure) the entropic penalty due to the loss of conformational entropy becomes bigger compared to the strength of the weakly favorable interactions. Therefore, in this case the conformational effects play a determining role [36]. Consequently, there should exist a critical value $|\chi|^{critical}$ such that for all $|\chi| \le |\chi|^{critical}$ penetration of homopolymer is no longer favorable. Referring to Eq.(4.10) this means that there is some critical value $k^{critical}$ such that for all $k \ge k^{critical}$ penetration of homopolymer is unfavorable. These qualitative considerations are confirmed by the results of the numerical calculations shown in Figs. 4.10(a)-4.10(b).

As follows from the numerical calculations for $\mu = 0.1$, there is a critical value $k^{critical} = 0.89$ such that for $k < k^{critical}$ the free energy reaches a minimum as a function of the average amount of homopolymer (see Figure 4.10(a)). The position of this minimum defines the maximum amount of homopolymer able to penetrate inside the lamellar domain for given value of μ. It follows from Eq. (4.26) that the value of μ is determined by the diblock length N and the interaction parameter χ_{AB}. If the latter is constant, μ depends only on the diblock copolymer length N. Since longer diblock copolymers can incorporate more homopolymer and because μ scales as $N^{-1/2}$, one can conclude that for smaller values of μ more homopolymer can be incorporated for the same value of parameter k. This conclusion is corroborated by numerical calculations: the minimum in curve 1 in Figure 4.10(a) for $k = 0.5, \mu = 0.1$ is shifted to the right compared to the position of the minimum in curve 2 in Figure 4.10(b) for $k = 0.5, \mu = 0.2$. In other words, the minimum for $k = 0.5, \mu = 0.1$ corresponds to a larger amount of homopolymer in comparison with $k = 0.5, \mu = 0.2$. In the case where μ is constant, increasing the Flory-Huggins parameter value $|\chi|$ decreases the value of k making it smaller than $k^{critical}$. This allows to incorporate more homopolymer inside lamellar domain, as demonstrated by Figure 4.10(a) and Figure 4.10(b).

A comparison of Eqs.(4.10) and (4.26) yields the following expressions for $|\chi|N$:

$$|\chi|N = \frac{\pi}{2(2k\mu)^{2/3}} \tag{4.27}$$

The numerical calculations show that $k^{critical}$ and $|\chi|^{critical}$ behave as a function of μ and diblock copolymer chain length N as presented in Figures 4.11(a) and 4.11(b), respectively. Here, the Flory-Huggins interaction parameter χ_{AB} was taken to be 0.32. For a diblock copolymer length $N = 1000$ and $\chi_{AB} = 0.32$, critical value $k^{critical} = 0.63$

and therefore according to Eq.(4.10) $|\chi|^{critical} = 0.0044$. Hence, for all $|\chi| < |\chi|^{critical} = 0.0044$ penetration of homopolymer will not be favorable.

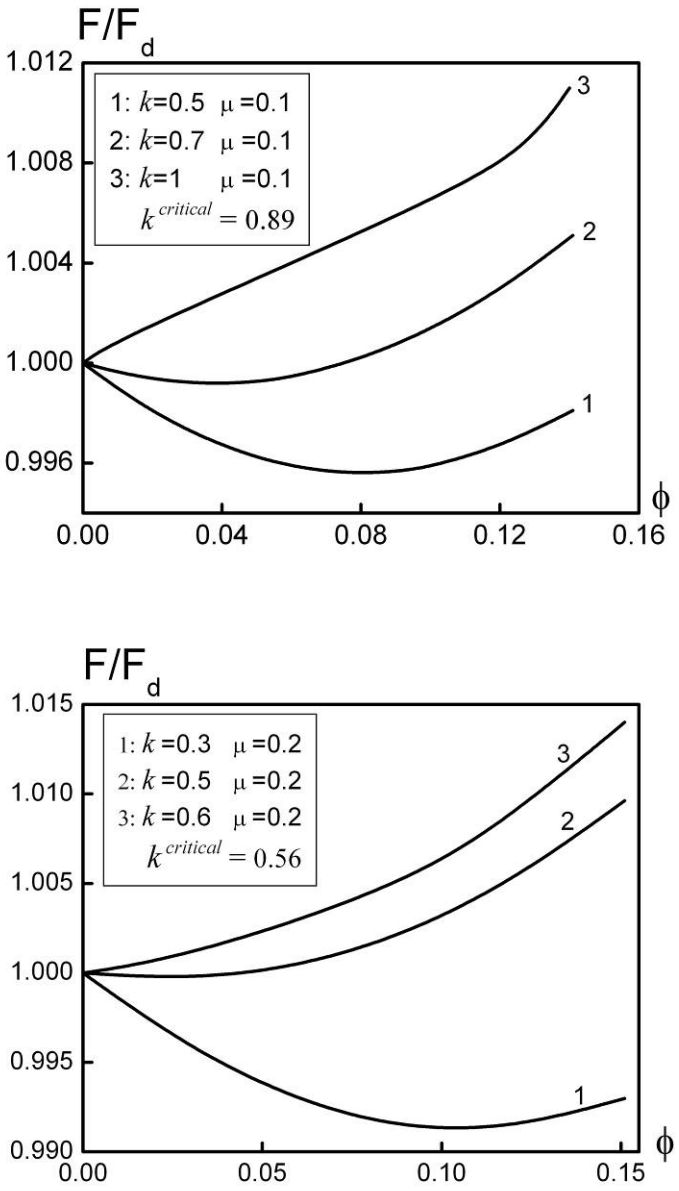

Figure 4.10. Free energy as a function of average homopolymer volume fraction for different values of parameters k and μ. **(a)** $\mu = 0.1$, $k = 0.5, 0.7, 1.0$. For $k > k^{critical} = 0.89$ the free energy is an increasing function of the average homopolymer volume fraction. **(b)** $\mu = 0.2$, $k = 0.3, 0.5, 0.6$, $k^{critical} = 0.56$.

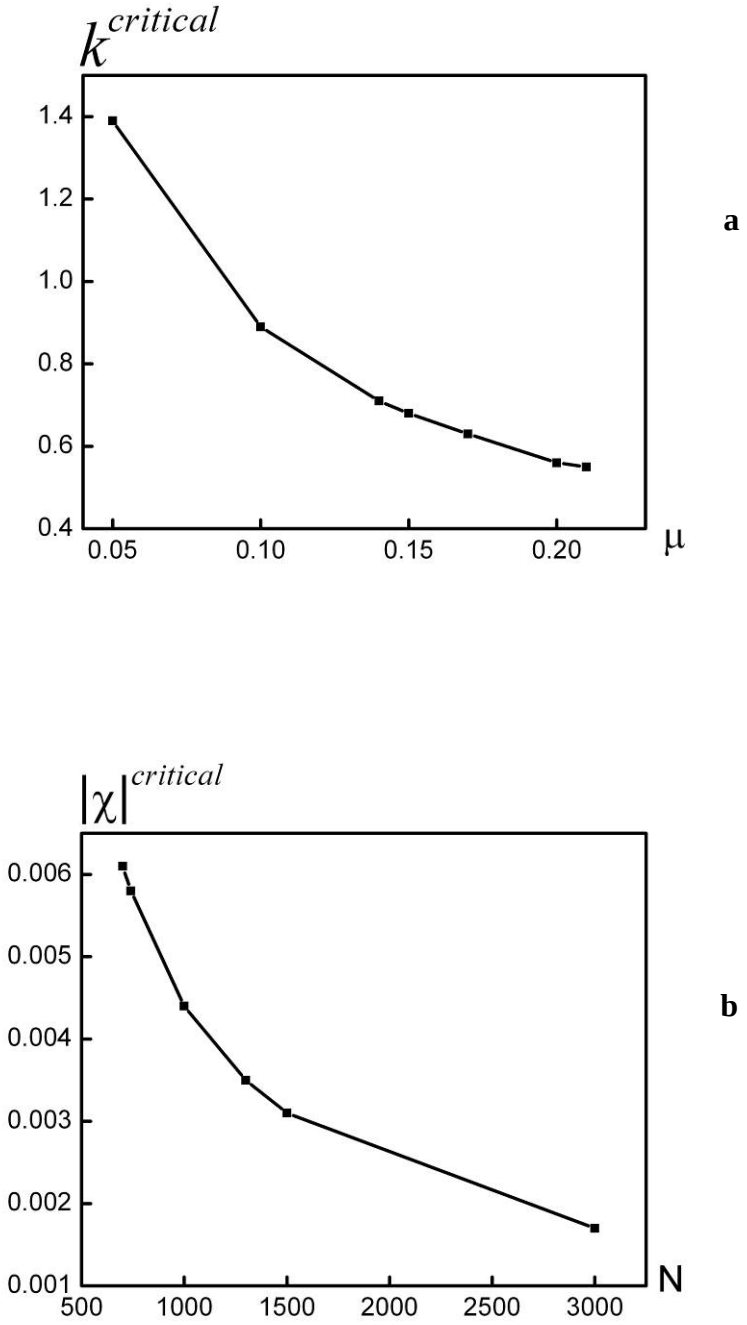

Figure 4.11. Numerically calculated dependences. **(a)** $k^{critical} = k^{critical}(\mu)$ and **(b)** $|\chi|^{critical} = |\chi|^{critical}(N)$ at fixed $\chi_{AB} = 0.32$.

4.5 Concluding remarks

In this chapter, we presented a theoretical analysis of the lamellar self-assembled state of blends of a diblock copolymer and a homopolymer where the homopolymer is assumed to interact favorably with one of the blocks of the diblock copolymer. Throughout the discussion a strong segregated lamellar morphology is assumed to be present with the homopolymer dissolving exclusively in one of the two different layers. The essential parameter governing the incorporation of the homopolymer inside the corresponding lamellar domains turned out to be $k = (\pi\gamma\upsilon)/(4aN|\chi|^{3/2})$. Here γ is the interfacial tension, N the block copolymer chain length and χ the Flory-Huggins parameter representing the favorable interactions between the homopolymer and the corresponding block. The homopolymer is assumed to have a chain length exceeding N. Furthermore, γ is assumed to be constant even if some homopolymer is present at the interface.

The value of k determines whether the dissolved homopolymer will be able to reach the interface. If k is sufficiently small this will be possible, however, for the homopolymer to be actually present at the interface the amount of homopolymer still has to exceed some critical average volume fraction. If that is the case, the homopolymer distribution is close to parabolic with its minimum at the interface and its maximum in the centre of lamellar microdomain, i.e. at the mid plane. If these requirements are not met, a "dead" zone will be present near the block copolymer interface where no homopolymer is present. Additionally, the maximal amount of homopolymer that can be incorporated may also be bounded. This property is, however, of less interest since for a large amount of homopolymer the assumption of the lamellar morphology will in general no longer hold.

These predictions are based on calculations that assume the homopolymer conformational effects due to the inhomogeneous distribution of homopolymer to be small. Such effects do, however, become important in the case of weakly favorable homopolymer-block copolymer interactions, i.e. $|\chi| << 1$. Since these conformational effects are unfavorable regarding the dissolution of the homopolymer into the lamellar domains, a critical value $|\chi|^{critical}$ exists such that for all $|\chi| \le |\chi|^{critical}$ the homopolymer will not dissolve.

Appendix. Alexander-de Gennes Approach

In this appendix, we consider the so-called Alexander-de Gennes approximation: homopolymer C with average volume fraction ϕ is *uniformly* distributed throughout the A-layers of lamellar self-assembled AB-diblock copolymers. The diblock copolymer chain ends are considered to be *fixed* at the mid plane. The set of Flory-Huggins interaction parameters satisfies the same conditions as before: $\chi_{AB} > 0$, $\chi_{BC} > 0$ and $\chi_{AC} < 0$. Due to the presence of component C in the A-layer, the thickness of this part becomes

$$R_A = \frac{fN\upsilon}{(1-\phi)\Sigma} \tag{A1}$$

where symbols f, N and υ denote the same physical quantities as before.

The thickness of the B-layer is independent of concentration of homopolymer C and reads as follows

$$R_B = \frac{(1-f)Nv}{\Sigma} \tag{A2}$$

The free energy per block copolymer chain is given by

$$F = \gamma\Sigma + \frac{3R_A^2}{2fNa^2} + \frac{3R_B^2}{2(1-f)Na^2} + \chi f N\phi \tag{A3}$$

Substitution of Eqs.(A1) and (A2) into (A3) yields the following expression:

$$F = \frac{3N\upsilon^2}{2\Sigma^2 a^2}\left((1-f) + \frac{f}{(1-\phi)^2}\right) + \gamma\Sigma + \chi f N\phi \tag{A4}$$

Subsequent minimization of Eq.(A4) with respect to Σ, i.e. $dF/d\Sigma = 0$, leads to the final expression for free energy per block copolymer chain:

$$F = \frac{3}{2}\left[\frac{3N\upsilon^2\gamma^2}{a^2}\right]^{1/3}\left((1-f) + \frac{f}{(1-\phi)^2}\right)^{1/3} + \chi f N\phi \tag{A5}$$

For $f = 0.5,$ $\chi_{AB} = 0.32$ and $N = 1000$, the free energy per block copolymer chain for different values of Flory-Huggins interaction parameter χ_{AC} behaves as a function of the average homopolymer concentration ϕ as presented in Figure A1. For all homopolymer volume fractions $\phi < \phi_{\max}$ it is energetically favorable to dissolve into the A-block lamellar domains. For $\phi \geq \phi_{\max}$ maximum only an amount $\phi_{\max}$ will dissolve into the A-lamellar domains. The rest will be macrophase separated. The more favorable the interactions between the homopolymer and the A-blocks the larger amount of homopolymer can be incorporated in A-domains, provided, of course, the lamellar structure is present.

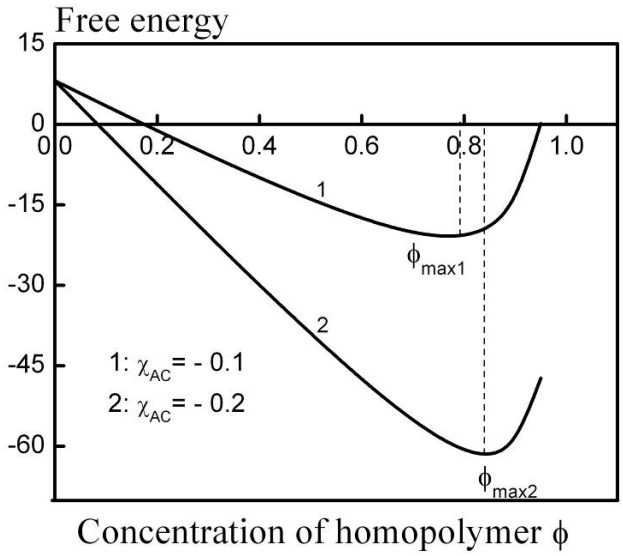

Figure A1. Calculated free energy per block copolymer chain as a function of homopolymer concentration ϕ. $f = 0.5,$ $\chi_{AB} = 0.32$, $N = 1000$.

REFERENCES

[1] I.W.Hamley. *The Physics of Block Copolymers.* **1998**, Oxford University Press, Oxford.

[2] T.Hashimoto, H.Tanaka, H.Hasegawa, *Macromolecules* **1990**, *23*, 4378.

[3] H.Tanaka, T.Hashimoto, H.Hasegawa, *Macromolecules* **1991**, *24*, 240.

[4] K.I.Winey, E.L.Thomas, L.J.Fetters, *Macromolecules* **1991**, *24*, 6182.

[5] K.Shull, A.M.Mayes, T.P.Russell, *Macromolecules* **1993**, *26*, 3929.

[6] A.M.Mayes, T.P.Russel, S.K.Satija, C.F.Majkrzak, *Macromolecules* **1992**, *25*, 6523.

[7] K.R.Shull, K.I.Winey, *Macromolecules* **1992**, *25*, 2637.

[8] D.J.Kinning, E.L.Thomas, L.J.Fetters, *J. Chem. Phys*. **1989**, *90*, 5806.

[9] K.I.Winey, E.L.Thomas, L.J.Fetters, *J. Chem. Phys.*, **1991**, *95*, 9367.

[10] J.Bodycomb, D.Yamaguchi, T.Hashimoto, *Macromolecules* **2000**, *33*, 5187.

[11] J.H.Lee, N.P.Balsara, A.K.Chakraborty, R.Krishnamoorti, B.Hammouda, *Macromolecules* **2002**, *35*, 7748.

[12] A.N.Semenov, *Macromolecules* **1993**, *26*, 2273.

[13] A.E.Likhtman, A.N.Semenov, *Macromolecules* **1997**, *30*, 7273.

[14] A.N.Semenov, *Macromolecules* **1992,** *25*, 4967.

[15] M.W.Matsen, *Macromolecules* **1995**, *28*, 5765.

[16] P.K.Janert, M.Schick, *Macromolecules* **1998**, *31***,** 1109.

[17] H.-K.Lee, C.-K.Kang, W.-C.Zin, *Polymer* **1997**, *38*, 1595.

[18] J.H.Ahn, B.-H.Sohn, W.-C.Zin, S.-T.Noh, *Macromolecules* **2001**, *34*, 4459.

[19] P.S.Tucker, J.W.Barlow, D.R.Paul, *Macromolecules* **1988**, *21*, 1678.

[20] P.S.Tucker, J.W.Barlow, D.R.Paul, *Macromolecules* **1988**, *21*, 2794.

[21] T.Hashimoto, K.Kimishima, H.Hasegawa, *Macromolecules* **1991**, *24*, 5704.

[22] W. van Zoelen, G.O.R.Alberda van Ekenstein, O.Ikkala, G. ten Brinke, *Macromolecules* **2006**, *39*, 6574-6579.

[23] O.Olabisi, L.M.Robeson, M.T.Shaw, In *Polymer-Polymer Miscibility*, Academic Press, New York, **1979**.

[24] W. van Zoelen, G.Alberda van Ekenstein, E.Polushkin, O.Ikkala, G.ten Brinke, *Soft Matter*, **2005**, *1*, 280

[25] N.E.Weeks, F.E.Karasz, W.J.MacKnight, *J. Apl. Phys.* **1977**, *48*, 4068.

[26] R.P.Kambour, J.T.Bendler, R.C.Bopp, *Macromolecules* **1983**, *16*, 753.

[27] G. ten Brinke, F.E.Karasz, W.J.MacKnight, *Macromolecules* **1983**, *16*, 1827.

[28] G.O.R.Alberda van Ekenstein, E.Polushkin, H.Nijland, O.Ikkala, G. ten Brinke, *Macromolecules* **2003**, *36*, 3684.

[29] J. de Wit, G.O.R.Alberda van Ekenstein, G.ten Brinke, *Polymer*, **2007**, *48*, 1606.

[30] A.N.Semenov, *Sov.Phys. JETP* **1985**, *61*, 733.

[31] S.T.Milner, T.A.Witten, M.E.Cates, *Macromolecules* **1988**, *21*, 2610.

[32] B.Hamdoun, D.Ausserre, V.Cabuil, S.Joly, *J. Phys. II France* **1996**, ***6***, 503.

[33] J.U.Kim, B.O'Shaughenessy, *Macromolecules* **2006**, *39*, 413.

[34] T.A.Witten, L.Leibler, P.A.Pincus, *Macromolecules* **1990**, *23*, 824.

[35] A. Subbotin, J. de Jong, G. ten Brinke. *Eur. Phys. J. E*, **2006**, *20*, 99.

[36] R.Hasewaga, Y.Aoki, M.Doi, *Macromolecules* **1996**, *29*, 6656.

CHAPTER 5

Lamellar-in-Lamellar Structure of Linear Ternary Multiblock Copolymers

Abstract. The number k of "internal" layers for the lamellar self-assembled state of a new class of multiblock copolymers C-*b*-(B-*b*-A)$_m$-*b*-B-*b*-C is determined as a function of m in the strong segregation limit. Here the outer C-blocks are assumed to be considerably longer than the $2m+1$ blocks of equal length of the (B-*b*-A)$_m$-*b*-B middle multiblock, and the self-assembled state is assumed to consist of k "thin" A- and B-layers sandwiched between "thick" C-layers. The predictions are in excellent agreement with the available experimental data.

5.1 Introduction

Hierarchically ordered block copolymer-based systems have become an active area of research recently [1-26]. In many cases diblock copolymers are involved where one of the blocks contains side chains that are either fully flexible or contain mesogenic units. Furthermore, the side chains can be covalently linked or attached via physical interactions such as, e.g., hydrogen bonding. Here the diblock copolymer introduces one of the length scales while a second one is associated with the side chains and thus with the graft-like nature of one of the blocks. Self-assembly in such such systems with hierarchical structure formation was was observed by ten Brinke and co-workes and is reported in Ref.[1,2].

Ternary P2VP-*b*-(PI-*b*-PS)$_4$-*b*-PI-*b*-P2VP linear undecablock copolymers, introduced and studied by Matsushita and co-workers [20], is an examples of block copolymers with a linear architecture where double periodic behavior has been also observed experimentally. Here P2VP denotes poly-2-vinylpyridine end blocks, PI denotes polyisoprene and PS denotes polystyrene. In the multiblock copolymers used all chemically different species are mutually incompatible. It was observed that this undecablock copolymer self-assembled in a 5-layered lamellar-*in*-lamellar structure as shown in Fig.5.1. The thick layers consist of the relatively long P2VP end blocks, and the thin layers are due to the PI-PS separation within the internal (PI-*b*-PS)$_4$-*b*-PI part of the multiblock. A general overview of multiblock copolymers with two intrinsic length scales is presented in Chapter 3 of this Thesis.

In this Chapter we consider the simplest representative of this class of systems consisting of a C-*b*-(B-*b*-A)$_m$-*b*-B-*b*-C multiblock copolymers. We consider the situation where A- and B-layers are formed in between C-layers. Furthermore, strong segregation with respect to all chemically different species involved will be assumed. This situation corresponds to the experimental P2VP-*b*-[(PI-*b*-PS)$_4$-*b*-PI]-*b*-P2VP multiblock copolymer system investigated by Matsushita and co-workers [20] .

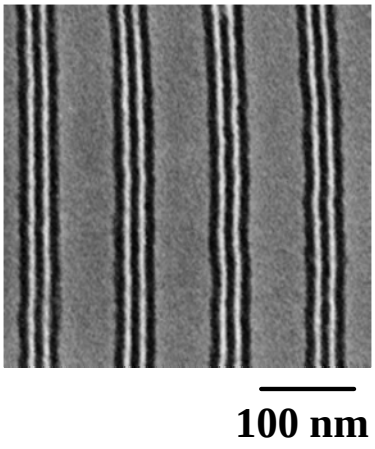

Figure 5.1. Lamellar-*in*-lamellar self-assembled state of P2VP-*b*-[(PI-*b*-PS)$_4$-*b*-PI]-*b*-P2VP multiblock copolymer system (courtesy Prof. Yushu Matsushita).

The central problem addressed in this Chapter concerns the number k of internal A- and B-layers for lamellar-*in*-lamellar self-assembled C-*b*-(B-*b*-A)$_m$-*b*-B-*b*-C multiblock copolymers as a function of the pertinent parameters, notably m.

5.2 The model

The number k of internal A- and B-layers for self-assembled C-*b*-(B-*b*-A)$_m$-*b*-B-*b*-C multiblock copolymers as a function of the pertinent parameters, notably m, equals k = 3,5,7… and the precise value should be obtained from a free energy minimization. To address this we will make the simplifying assumption that the statistical segment length and the volume per segment are identical for all species involved. They will be denoted as a and υ. It is also assumed that the C-blocks contain N segments, whereas the A- and B-block each consist of the same number of n segments with $n<<N$. The Flory-Huggins parameters, χ_{AB} and χ_{BC} are sufficiently positive implying strong unfavourable interactions between the different species and thus the formation of pure domains. It allows us to apply the strong segregation theory.

Let $2m+1$ short blocks from the internal part of the multiblock form a k - layered structure. Generally, the global multiblock conformation can be either a bridge, which starts from one C-layer and ends in the next C-layer, or a loop which starts and ends in the same C*A*-layer. Both the multiblock bridge and the multiblock loop consists of a sequence of local loops and bridges, and *A*-tails as illustrated in Fig.5.2.

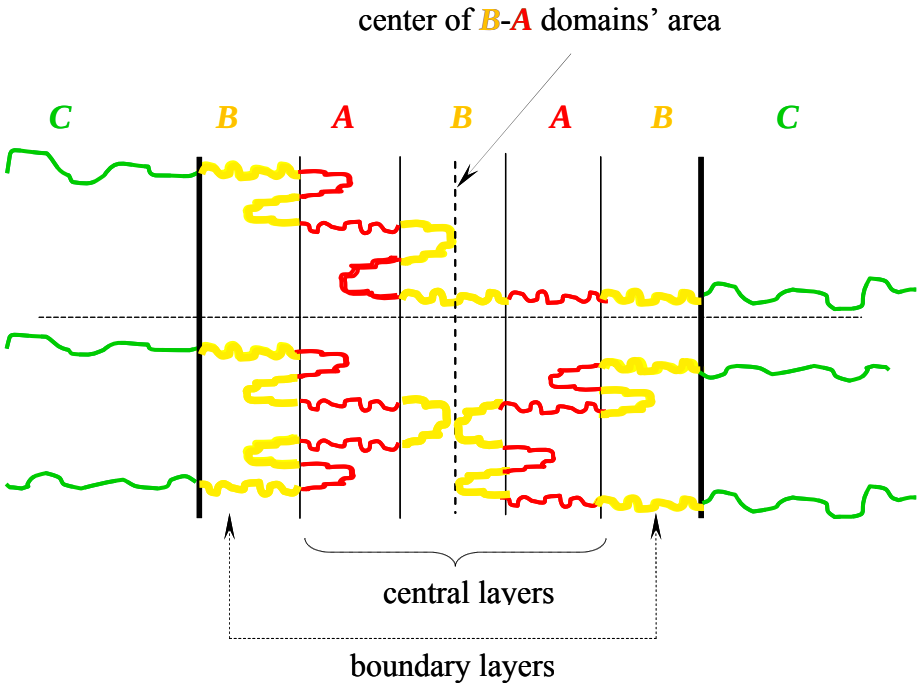

Figure 5.2. Schematic representation of a global bridge and a loop C-*b*-(B-*b*-A)$_m$-*b*-B-*b*-C (m = 4) multiblock copolymer conformation.

If x is the fraction of multiblock bridges and 1-x the fraction of multiblock loops, then the average energy per copolymer chain is given by

$$F = xF_{bridge} + (1-x)F_{loop} + x\ln x + (1-x)\ln(1-x) \tag{5.1}$$

where F_{bridge} is the bridge free energy and F_{loop} is the loop energy. Using a mean-field picture and assuming that the average number of local loops and bridges in the global loop conformation is approximately equal to the average number of local loops and bridges in the global bridge conformation, in as a first approximation we will assume that $F_{bridge} = F_{loop}$ and $x = ½$. Hence,

$$F = F_{bridge} - \ln 2 \tag{5.2}$$

Here and below in the chapter the free energy will be given in k_BT energetic units.

Next we concentrate on the multiblock bridge conformation which consists of a sequence of local loops and bridges. Due to the assumed strong incompatibility between the *A*- and *C*-blocks we expect that the multiblock forms only one bridge in the first *B*-layer located in between the *A*- and *C*-layer. The number of bridges in the central *B* and *C* layers depends on two factors, namely on the degree of stretching of the multiblock and the thermal fluctuations. For strong multiblock stretching the thermal fluctuations are small and only one bridge per domain is formed. We will focus on this case because this also seems to be the situation realised in recent experiments [20].

5.3 Free energy calculations

The total free energy per multiblock copolymer includes AB and BC interfacial free energies F_{AB} and F_{BC}, the elastic free energy F_C of the outer C-domains, the elastic free energy F_{B1} of the two boundary B-domains, the elastic free energy F_{B2} and F_A of the central B- and A-layers and the conformational free energy of the multiblock copolymer chain:

$$F_{bridge} = 2F_{BC} + (k-1)F_{AB} + F_C + 2F_{B1} + \frac{k-3}{2}F_{B2} + \frac{k-1}{2}F_A + F_{conf} \tag{5.3}$$

The interfacial free energies depend on the corresponding interfacial tension and average area per multiblock copolymer Σ,

$$F_{AB} = \gamma_{AB}\Sigma, \quad F_{BC} = \gamma_{BC}\Sigma \tag{5.4}$$

where $\gamma_{AB} = \frac{a}{\upsilon}\sqrt{\frac{\chi_{AB}}{6}}$, $\gamma_{BC} = \frac{a}{\upsilon}\sqrt{\frac{\chi_{BC}}{6}}$ and χ_{AB}, χ_{BC} are the Flory-Huggins parameters.

The elastic free energy of the C-layer is given by [23]

$$F_A = \frac{\pi^2 N v^2}{4a^2\Sigma^2} \tag{5.5}$$

In order to consider conformational contribution to the free energy, the multiblock chain in its middle part is considered as a chain of (2*m*-1) blocks, both bridges and loops, which form (*k*-2) parts which we will call blobs. Each blob contains on average (2*m*-1)/(*k*-2) blocks including one bridge and loops. The chain of blobs is stretched in one direction, therefore the probability of this conformation is $(1/2)^{k-2}$. It corresponds to a conformational free energy (in units $k_B T$)

$$F_{conf} \approx (k\text{-}2)\ln 2 \tag{5.6}$$

Because the A and B blocks are characterized by the same molecular parameters, the elastic stretching energies of these blocks are equal, i.e. $F_A = F_{B2}$. Schematically the structure of an internal A-domain is shown in Figure 5.3. For the calculation of the elastic free energy of the A-layer we use the method that has been reported in Refs. 24-25. An A-layer consists of one bridge and loops (Fig. 5.3). A loop is treated as two linear chains.

Let q denote the average number of loops from each side of the AB interface

$$q = \frac{1}{2}\frac{2m+1-k}{k-1} \tag{5.7}$$

We introduce α as the fraction of the bridge that is inside the loop region. To satisfy the incompressibility condition we suppose that in the remaining *2H* region the bridging chains are stretched uniformly, whereas they are non-uniformly stretched in the region where both loops and bridges are present.

The elastic free energy of the A-layers is given by

$$F_A = \frac{3H^2}{a^2 n(1-\alpha)} + \frac{3}{a^2}\int_0^R E_1(z)dz + \frac{6q}{a^2}\int_0^R d\xi\, f(\xi)\int_0^\xi E_2(z,\xi)dz \tag{5.8}$$

The first term in (5.8) describes uniform stretching of the bridging chain and the second and the third terms describe the non-uniform stretching of bridge and loops belonging to one multiblock chain, respectively. $E_1(z)$ is the local tension of that part of the bridge which is non-uniformly stretched, z is the coordinate, $E_2(z)$ is the local tension of the

loop whose end (the point of turn) is located at $\xi \le R$ and $f(\xi)$ is the corresponding end-distribution function, q denotes the average number of loops in A-layer.

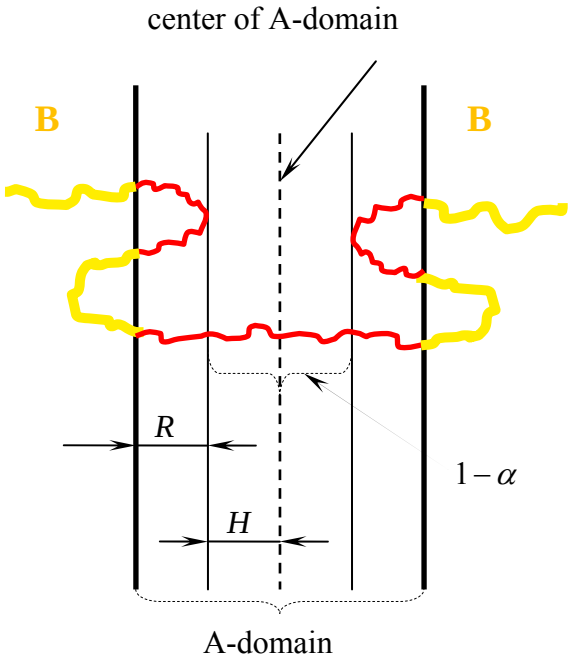

Figure 5.3. Schematic representation of a multiblock copolymer conformation in the A-layer. *R* denotes the thickness of the loop region, *2H* is the thickness of the middle part of the A-layer where only bridging chain segments are present, 1-α is the fraction of the bridging segments that are in the *2H* region.

There are the following constraints for the bridging and looping chains in the A-domain. First, the conservation law of monomers for bridges and loops must be fulfilled which corresponds to eqs. (5.9) and (5.10), respectively:

$$\int_0^R \frac{dz}{E_1(z)} = \frac{\alpha n}{2} \tag{5.9}$$

$$\int_0^\xi \frac{dz}{E_2(z)} = \frac{n}{2} \tag{5.10}$$

Next, we have the incompressibility condition which guarantees constant melt density inside the domain:

$$\frac{1}{E_1(z)} + 2q\int_z^R \frac{f(\xi)\,d\xi}{E_2(z,\xi)} = \frac{\Sigma}{\upsilon} \tag{5.11}$$

Minimization of the free energy (5.8) under the constraints (5.9)-(5.11) defines the equilibrium state of the A-domain and yields the local stretching functions as

$$E_1(z) = \frac{\pi}{n}\sqrt{\frac{R^2}{\sin^2 \pi\alpha/2} - z^2} \tag{5.12}$$

$$E_2(z) = \frac{\pi}{n}\sqrt{\xi^2 - z^2} \tag{5.13}$$

Substitution of (5.12) and (5.13) into (5.8) leads to the final expression for the free energy of the A-domain:

$$F_A = F_{B2} = \frac{n\upsilon^2 f_1(\alpha)}{a^2\Sigma^2} \tag{5.14}$$

with $f_1(\alpha) = \frac{1}{\pi}\tan^3\frac{\pi\alpha}{2} + \frac{3}{\pi}\tan\frac{\pi\alpha}{2} + \frac{3(1-\alpha)}{2}$.

The total thickness of the A-layer is

$$2(R+H) = 2\left(\frac{n\upsilon}{\pi\Sigma}\tan\frac{\pi\alpha}{2} + \frac{n\upsilon(1-\alpha)}{2\Sigma}\right) \tag{5.15}$$

In a similar way we consider the boundary B-layer which is in contact with outer C-layer. The structure of this layers is schematically represented in Fig. 5.4.

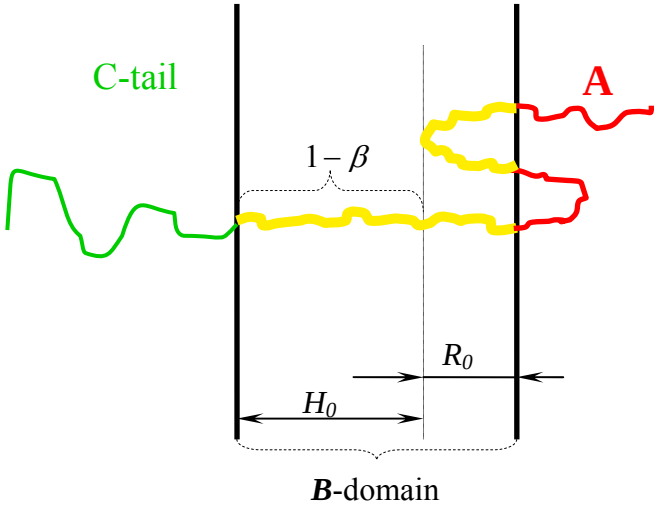

Figure 5.4. Schematic representation of multiblock copolymer conformation in the B-layer contacted to the outer C-layer. R_0 denotes the thickness of the loop region, H_0 is the thickness of the middle part of the B-domain where only segments belonging to the bridging chain are present, 1-β being the fraction of the bridge segments in the H_0 region.

If we introduce β as a fraction of the bridge which is stretched homogeneously in the B-layer, then the final expression for the free energy of the boundary B-domain reads in a form similar to (5.14):

$$F_{B1} = \frac{n\upsilon^2 f_2(\beta)}{a^2\Sigma^2} \tag{5.16}$$

with $f_2(\beta) = \frac{1}{\pi}\tan^3 \pi\beta + \frac{3}{\pi}\tan \pi\beta + 3(1-\beta)$.

The thickness of the loop region in the boundary B-domain

$$R_0 = \frac{n\upsilon}{\pi\Sigma}\tan \pi\beta \tag{5.17}$$

and the thickness of the middle part where only segments belonging to the bridging chain are present, is

$$H_0 = \frac{n\upsilon(1-\beta)}{\Sigma} \tag{5.18}$$

The average free energy per multiblock copolymer is thus

$$F = (k-3)\ln 2 + 2\gamma_{BC}\Sigma\left(1 + \frac{k-1}{2}\frac{\gamma_{AB}}{\gamma_{BC}}\right) + \frac{\pi^2 N\upsilon^2}{4a^2\Sigma^2} g(k,\alpha,\beta) \tag{5.19}$$

where

$$g(k,\alpha,\beta) = 1 + \frac{4}{\pi^2}\frac{n}{N}\left[(k-2) f_1(\alpha) + 2 f_2(\beta)\right] \tag{5.20}$$

Using Eq.5.15, the probability that a short block is a bridge in the middle B- and A-domains equals

$$p = \frac{H}{(1-\alpha)(R+H)} = \frac{\pi}{\pi(1-\alpha) + 2\tan\frac{\pi\alpha}{2}} \tag{5.21}$$

and similarly after consideration of Eqs.5.17 and 5.18, in the boundary B-domain the probability of a bridge is

$$p' = \frac{\pi}{\pi(1-\beta) + \tan\pi\beta} \tag{5.22}$$

Taking into account the assumption that one bridge per domain is formed, from the geometrical constraints we obtain the equations to find α and β:

$$\frac{2m}{k-1} = 1 - \alpha + \frac{2}{\pi}\tan\left(\frac{\pi\alpha}{2}\right) \tag{5.23}$$

$$\frac{1}{2}\frac{2m+1-k}{k-1} = \frac{1}{\pi}\tan(\pi\beta) - \beta \tag{5.24}$$

Next, to find the equilibrium interface area we minimize the free energy (5.19) with respect to Σ, which brings to the final expression for the free energy as a function of the number k of internal domains for given values of m, n/N, χ_{AB}, χ_{BC}:

$$F(k) = (k-3)\ln 2 + 3\left(\frac{\pi^2}{24}\chi_{BC}N\right)^{1/3}\left(1+\frac{k-1}{2}\sqrt{\frac{\chi_{AB}}{\chi_{BC}}}\right)g^{1/3}(k,\alpha,\beta) \qquad (5.25)$$

In the limit of large m minimization of the last expression with respect to k gives as its asymptotic behavior

$$k \propto \begin{cases} 2m\left(\frac{n}{N}\right)^{1/3}, & 1 < m < \left(\frac{\chi_{BC}N^2}{n}\right)^{1/3} \\ \left(\frac{\pi}{2}\right)^{1/3}\left(\frac{m}{\ln 2}\right)^{1/2}\left(\frac{\chi_{BC}n}{6}\right)^{1/6}, & m > \left(\frac{\chi_{BC}N^2}{n}\right)^{1/3} \end{cases} \qquad (5.26)$$

In the more realistic case of relatively small m the free energy should be considered as a function of odd values of k = 3, 5, 7,…. The equilibrium value of k corresponds to the minimal value of $F(k)$.

5.4 Results and discussions

Explicit calculations have been performed for the situation that corresponds to the experimental system P2VP-*b*-[(PI-*b*-PS)$_m$-*b*-PI]-*b*-P2VP with m = 4 and for different values of m = 3, 5, 6 and 7. For the experimental system we have [20,26] $\chi_{BC}N = 340$, $\chi_{AB}N = 85$ and n/N = 0.2. The equilibrium values obtained for the number of internal layers k as a function of m are k = 5, 5, 7, 7 and 9 respectively for m = 3,4,5,6,7. In Table 5.1 these are compared with the values given in Ref. 20 using combinatorial arguments only. The value of k = 5 found for m = 4 is exactly what has been observed experimentally. The corresponding plots of F(k) are given in Figs. 5.5a-d.

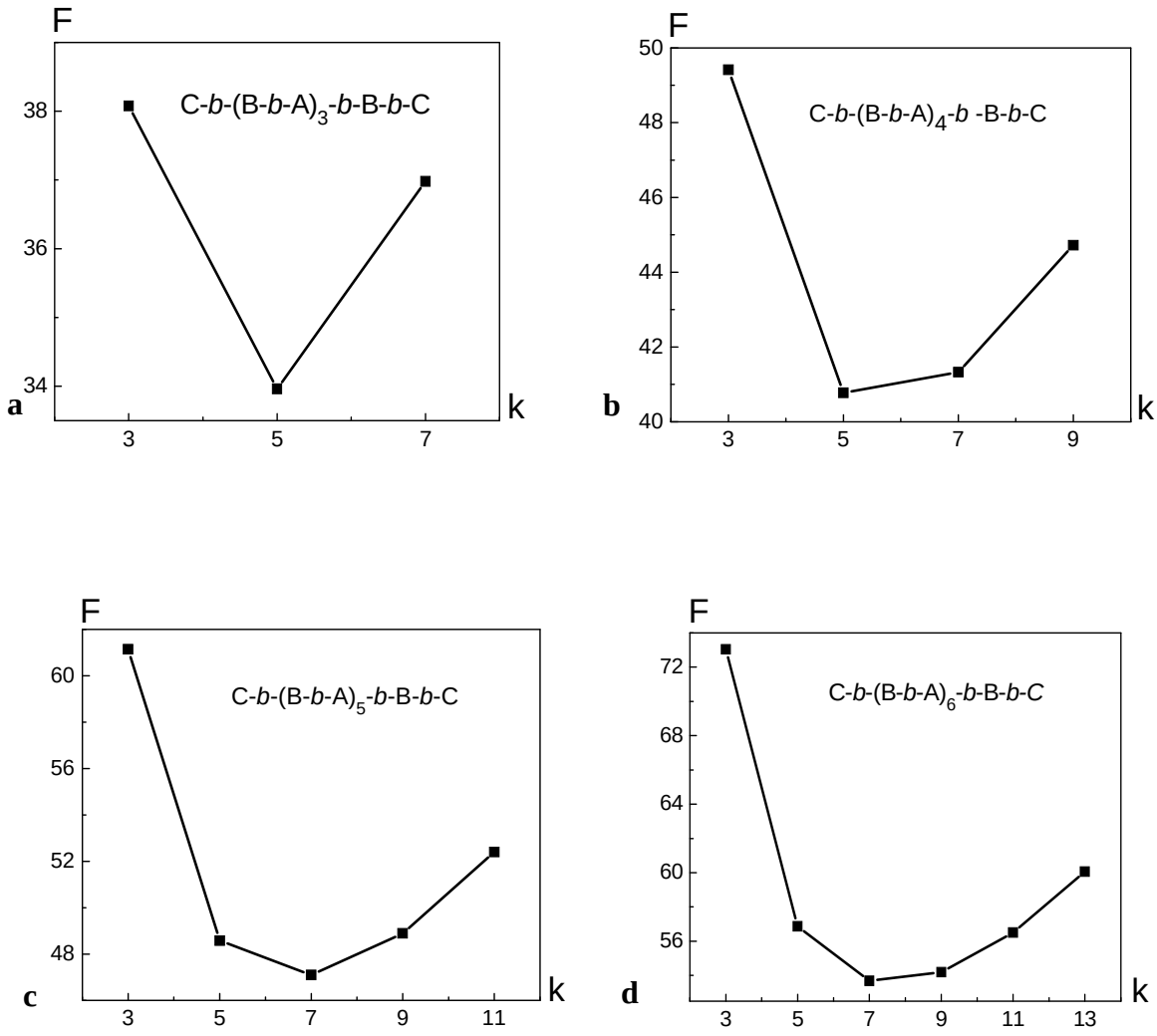

Figure 5.5. Free energy F of the C-*b*-(B-b-A)$_m$-*b*-B-*b*-C multiblock copolymer as a function of the number k of internal layers for $\chi_{BC}N = 340$, $\chi_{AB}N = 85$, n/N = 0.2. (a) m = 3, (b) m = 4, (c) m = 5, (d) m = 6.

The values of k at the minima of $F(k)$ are given in Table 5.1.

Table 5.1. Number of internal layers *k*

Predictions of Ref.20		**Predictions of present model**	
m	*k*	*m*	*k*
2	3	2	3
3	5	3	5
4	5	4	5
5	5	5	7
6	5	6	7
7	7	7	9

5.5 Concluding remarks

In summary, we see that, besides combinatorial contributions, i.e, different ways of creating specific sequences of loops and bridges, the number of internal layers is determined to a large extent by the balance between the elastic stretching of the individual blocks and the interfacial area. Combinatorial effects become more pronounced for larger values of *m*.

REFERENCES

[1] J.Ruokolainen, R.Mäkinen, M.Torkkeli, T.Mäkelä, R.Serimaa, G.ten Brinke, O.Ikkala, *Science* **1998**, *280*, 557.
[2] J.Ruokolainen, G.ten Brinke, O.Ikkala, *Adv. Mater.* **1999**, *11*, 777.
[3] C.C.Evans, F.S.Bates, M.D.Ward, *Chem. Mater.* **2000**, *12*, 236.
[4] A.F.Thünemann, S.General, *Macromolecules* **2001**, *34*, 6978.
[5]R. Nap, C.Kok, G.ten Brinke, S.Kuchanov, *European Phys. J. E*, **2001**, *4*, 515.
[6] C.Osuji, C.-Y.Chao, I.Bita, C.K.Ober, E.L.Thomas, *Adv. Funct. Mater.* **2002**, *12*, 753.
[8] O.Ikkala, G.ten Brinke, *Science* **2002**, *295*, 2407.
[9] I.A.Ansari, V.Castelletto, T.Mykhaylyk, I.W.Hamley, Z.B.Lu, T.Itoh, C.T.Imrie, *Macromolecules* **2003**, *36*, 8898.
[10] G.O.R.Alberda van Ekenstein, E.Polushkin, H.Nijland, O.Ikkala, G.ten Brinke, *Macromolecules* **2003**, *36*, 3684.
[11] C.-Y.Chao, X.Li, C.K.Ober, C.Osuji, E.L.Thomas, *Adv. Mater.* **2004**, *14*, 364.
[12] O.Ikkala, G.ten Brinke, *Chem. Com.* **2004**, 2131.
[13] C.-S.Tsao, H.-L.Chen, *Macromolecules* **2004**, *37*, 8984.
[14] I.W.Hamley, V.Castelletto, P.Parras, Z.B.Lu, C.T.Imrie, T.Itoh, *Soft Matter* **2005**, *1*, 355.
[15] B.Nandan, C.-H.Lee, H.-L.Chen, W.-C.Chen, *Macromolecules* **2005**, *38*, 10117.
[16] Y.Nagata, J.Masuda, A.Noro, D.Cho, A.Takano, Y.Matsushita, *Macromolecules* **2005**, *38*, 10220.
[17] Y.Smirnova, G.ten Brinke, I.Ya.Erukhimovich, *J.Chem.Phys.* **2006**, *124*, 0544907
[18] R.Nap, N.Sushko, I.Ya.Erukhimovich, G.ten Brinke, *Macromolecules* **2006**, *39*, 6765.
[19] S.I.Kuchanov, V.E.Pichugin, G.ten Brinke, *E-Polymers* **2006**, *012.*
[20] J.Masuda, A.Takano, Y.Nagata, A.Noro, Y.Matsushita, *Phys. Rev. Lett.* **2006**, *97*, 098301.
[21] S.I.Kuchanov, V.E.Pichugin, G.ten Brinke, *Europhys. Lett.* **2006**, *76*, 959.
[22]S.Valkama, T.Ruotsolainen, A.Nykänen, A.Laiho, H.Kosonen, G.ten Brinke, O.Ikkala, J.Ruokolainen, *Macromolecules* **2006,** *39*, 9327.
[23] A.N.Semenov, *Sov. Phys. JETP* **1985**, *61*, 733.
[24] E.B.Zhulina, A.Halperin, *Macromolecules* **1992**, *25*, 5730.
[25] A.N.Semenov, A.V.Subbotin, *Sov. Phys. JETP* **1992**, *74*, 660.
[26] R.L.Lescanec, L.J.Fetters, E.L.Thomas, *Macromolecules* **1998**, *31*, 1680.

CHAPTER 6

Lamellar-in-Lamellar Self-Assembly in Linear Ternary Multiblock Copolymers: Alexander-de Gennes Approach and Dissipative Particle Dynamics Simulations

Abstract. A simple theoretical analysis of the lamellar-*in*-lamellar self-assembled state of ternary C-*b*-(B-*b*-A)$_m$-*b*-B-*b*-C multiblock copolymer melts in the strong segregation limit is presented using the Alexander-de Gennes approximation. For a given value of *m*, the influence of the chain length of the various blocks and the Flory-Huggins χ_{AB} and χ_{BC} interaction parameters on the number *k* of internal domains is discussed in detail. The theoretical results are corroborated by computer simulations using the dissipative particle dynamics technique.

6.1 Introduction

In this Chapter we consider once more C-*b*-(B-*b*-A)$_m$-*b*-B-*b*-C multiblock copolymers. Such systems are the simplest representatives of hierarchically ordered block copolymer-based systems. Due to the possibility to form structures that combine different length scales this class of systems has been the subject of many experimental [1-15] and theoretical [16-22] investigations.

Compared to the previous chapter, we will introduce a far more simple theoretical modeling of the lamellar-*in*-lamellar self-assembled state using the so-called Alexander-de Gennes approach. We show that this simplified approach provides results that are virtually identical to those obtained by the far more elaborated treatment. It allows us to analyze and discuss the domain formation in C-*b*-(B-*b*-A)$_m$-*b*-B-*b*-C multiblock copolymers in much more detail as a function of the chain length of the blocks and the Flory-Huggins χ_{AB} and χ_{BC} interaction parameters. To corroborate the theoretical predictions, we performed computer simulations using the well-known dissipative particle dynamics technique [23-31].

6.2 The model

Considering the ternary C-*b*-(B-*b*-A)$_m$-*b*-B-*b*-C multiblock copolymer melt in the Alexander-de Gennes approximation implies that we assume all $2m+1$ middle A- and B-blocks as well as the outer C-blocks to be stretched uniformly inside their respective layers. We assume that the $2m+1$ short middle blocks self-assemble into *k* internal layers confined between relatively "thick" C outer layers.

In general, a global multiblock conformation can be either a bridge or a loop as illustrated in Figure 6.1. Both global bridges and global loops consist in turn of local loops and bridges. Due to assumed strong incompatibility between the three chemically different species, the first and the last B-block of the middle multiblock will be present in the form of a local bridge conformation in the first and the last boundary B-layers (Figure 6.1).

Let x be the fraction of global bridges and $1-x$ the fraction of global loops. The average free energy per multiblock copolymer chain is then given by

$$F = xF_{bridge} + (1-x)F_{loop} + x\ln x + (1-x)\ln(1-x) \qquad (6.1)$$

where F_{bridge} and F_{loop} are the free energies of a global bridge and a global loop conformation. The last two terms in (6.1) represent the entropy of mixing between global loops and bridges. We will simply assume as a first approximation that $x \cong 1/2$, $F_{bridge} \cong F_{loop}$ and thus $F \cong F_{bridge} - \ln 2$. Hence, from now on we will restrict ourselves to

a global bridge conformation and discuss its free energy in the Alexander-de Gennes approximation.

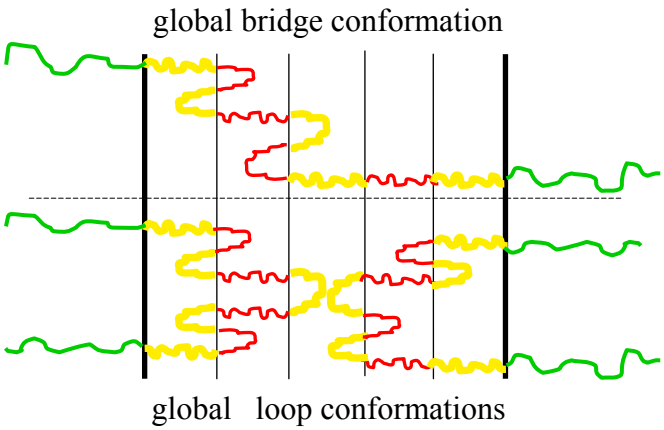

Figure 6.1. Schematic representation of a global bridge (top) and a global loop (bottom) conformation for a C-*b*-(B-*b*-A)$_4$-*b*-B-*b*-C multiblock copolymer. A, B and C blocks are denoted by red, yellow and green colors, respectively.

6.3 Theoretical analysis

Let n denote the degree of polymerization of the internal A- and B-blocks alike and N denote the degree of polymerization of the outer C-blocks, with $N >> n$. The statistical segment length and monomer volume are denoted as a and υ, respectively, and are assumed to be equal for all chemically different components. The thickness of the internal layers and the outer layer are denoted as h and H (Figure 6.2). Furthermore Σ is used to denote the interfacial area per multiblock copolymer chain. The Flory-Huggins interaction parameters are χ_{AB}, χ_{BC} and χ_{AC} and are taken positive implying unfavorable interactions between all the chemically different species.

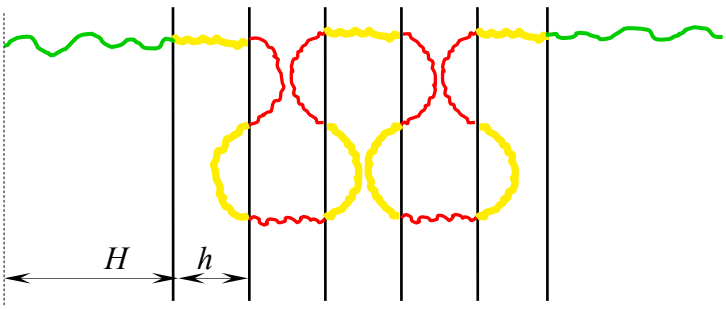

Figure 6.2. Schematic representation of a global bridge conformation of a C-*b*-(B-*b*-A)$_m$-*b*-B-*b*-C copolymer for m = 6. h and H denote the thickness of the internal layers and half of the outer layers, respectively.

Incompressibility implies

$$N\upsilon = H\Sigma \tag{6.2}$$

$$(2m+1)n\upsilon = kh\Sigma \tag{6.3}$$

The total free energy per multiblock copolymer bridge can be written as

$$F_{bridge} = 2F_{BC} + (k-1)F_{AB} + mF_{0A} + (m+1)F_{0B} + 2F_C + F_{conf} \tag{6.4}$$

Here F_{AB} and F_{BC} are the interfacial free energies related to the interfacial tensions and the average interfacial area Σ per multiblock copolymer by

$$F_{AB} = \gamma_{AB}\Sigma \qquad F_{BC} = \gamma_{BC}\Sigma \tag{6.5}$$

with interfacial tensions given by $\gamma_{AB} = \frac{a}{\upsilon}\sqrt{\frac{\chi_{AB}}{6}}$ and $\gamma_{BC} = \frac{a}{\upsilon}\sqrt{\frac{\chi_{BC}}{6}}$.

The elastic free energies of uniformly stretched short A- and B-blocks F_{0A} and F_{0B} are the same and are given by

$$F_0 = F_{0A} = F_{0B} = \frac{3h^2}{2na^2} \tag{6.6}$$

Likewise, the elastic free energy F_{0C} for the outer C-blocks is given by

$$F_C = \frac{3H^2}{2Na^2} \tag{6.7}$$

The conformational contribution F_{conf} takes into account the number of different possibilities to create multiblock conformations and, as in our previous work [21], will be considered in a simplified way by representing the middle multiblock by a chain of $k-2$ blobs propagating in one direction. The corresponding probability is $\left(\frac{1}{2}\right)^{k-2}$ resulting in an increase in free energy (in k_BT energetic units) given by

$$F_{conf} = (k-2)\ln 2 \tag{6.8}$$

Taking into account Eqs. (6.2), (6.3) and Eqs. (6.5)-(6.8), the free energy expression (6.1) transforms into

$$F = \gamma^{*}\Sigma + \frac{Q}{\Sigma^{2}} + (k-3)\ln 2, \tag{6.9}$$

with $\gamma^{*} = 2\gamma_{BC} + (k-1)\gamma_{AB}$ and $Q = \frac{3(2m+1)^{3} n\upsilon^{2}}{2k^{2}a^{2}} + \frac{3N\upsilon^{2}}{a^{2}}$.

Minimization of the free energy (6.9) with respect to Σ yields the equilibrium interface area

$$\Sigma_{0} = \left(\frac{2Q}{\gamma^{*}}\right)^{1/3} \tag{6.10}$$

which results in the final expression for the total free energy:

$$F = \frac{3}{2}\left(\gamma^{*}\right)^{2/3}\left(2Q\right)^{1/3} + (k-3)\ln 2 \tag{6.11}$$

6.4 Results and discussions

We consider first the only system investigated experimentally so far, i.e., P2VP-*b*-(PI-*b*-PS)$_4$-*b*-PI-*b*-P2VP. It corresponds to $\chi_{BC} = 0.4$, $\chi_{AB} = 0.1$, $\chi_{BC}N = 340$, $\chi_{AB}n = 17$, $m = 4$ and $n/N = 0.2$. The free energy (eq. 6.11) as a function of the number of internal layers k is presented in Figure 6.3a. The minimum occurs for $k = 5$, precisely as found experimentally [4]. Results for different values m = 3, 5 and 6 are presented in Figure 6.3b, c and d. The values of k found are 5, 5 and 7. Note, that for m = 5 the free energies for k = 5 and k = 7 are very close. These results are in good agreement with the ones obtained from a much more elaborated mean-field calculation using the same set of parameters, where the minima for m = 3, 4, 5 and 6 occurred for k = 5, 5, 7 and 7 [21].

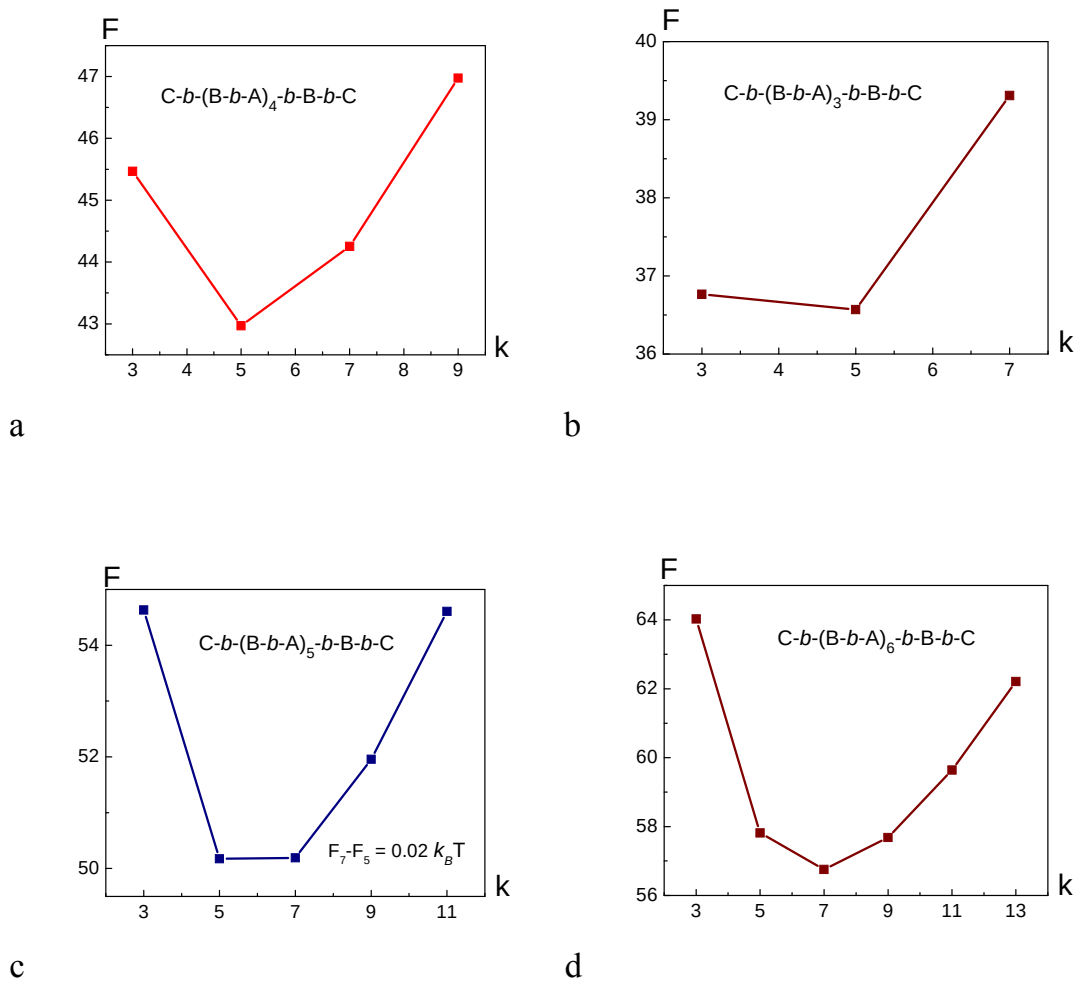

Figure 6.3. Free energy F of lamellar-*in*-lamellar self-assembled C-*b*-(B-*b*-A)$_m$-*b*-B-*b*-C multiblock copolymer melt as a function of the number k of internal layers for $\chi_{BC}N = 340$, $\chi_{AB}n = 17$, $n/N = 0.2$. (a) $m = 4$, (b) $m = 3$, (c) $m = 5$, (d) $m = 6$.

6.4.1 Influence of interaction strength

In order to investigate the effect of interfacial tension, numerical calculations were performed for different values of the Flory-Huggins χ_{BC}-parameter for $m = 3, 4, 5$ and 6, $\chi_{AB} = 0.1$ and fixed length of the internal blocks $n = 200$. Throughout the rest of this section the length N of the outer blocks is assumed to satisfy $(2m+1)n = 2N$, thus assuring an equilibrium lamellar structure. The results are summarized in Table 6.1. Figure 6.4a-d shows the free energy as function of k for m = 4 and Flory-Huggins

parameter values $\chi_{BC} = 0.1, 0.4, 1.5$ and 5, where the minima are found at k = 3, 5, 7 and 9, respectively.

Table 6.1. Equilibrium number of internal domains k_{opt} as a function of χ_{BC} for $\chi_{AB} = 0.1$ and n = 200.

	χ_{BC}				
k_{opt}	$m = 3$ $N = 700$	$m = 4$ $N = 900$	$m = 5$ $N = 1100$	$m = 6$ $N = 1300$	$m = 7$ $N = 1500$
3	0.1 – 0.25	0.1	0.1	< 0.1	
5	0.3 – 1.7	0.15 – 0.75	0.15 – 0.4	0.1 – 0.25	0.1 – 0.2
7	≥ 1.75	0.8 – 3.3	0.45 – 1.65	0.3 – 0.95	0.25 – 0.6
9		≥ 3.35	1.7 – 5.55	1.0 – 3.04	0.65 – 1.85
11			≥ 5.6	3.06 – 8.3	1.9 – 4.9
13				> 8.35	4.95 – 11.75
15					≥ 11.8

Larger χ_{BC} values force a reduction in the BC interfacial area which in turn forces the internal short blocks to become more stretched. To reliefe this stretching the system starts to create more AB interfaces, i.e. larger values of k. Of course, in reality the values of the Flory-Huggins interaction parameters hardly ever exceed unity. The calculations for larger values are nevertheless useful to track and understand the tendencies in the layer formation in ternary C-*b*-(B-*b*-A)$_m$-*b*-B-*b*-C multiblock copolymers.

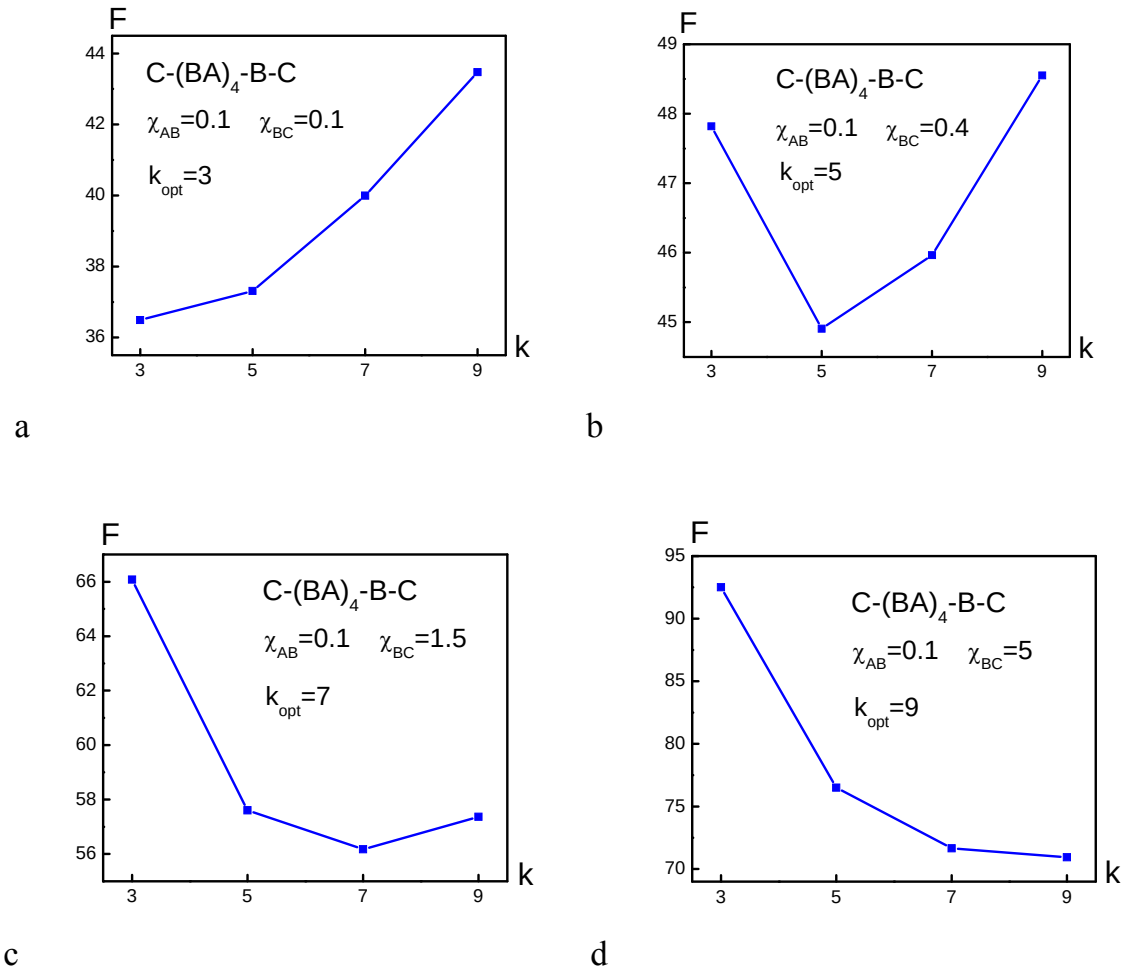

Figure 6.4. Free energy F of lamellar-*in*-lamellar self-assembled C-*b*-(B-*b*-A)$_4$-*b*-B-*b*-C multiblock copolymer melt as a function of the number k of internal layers for $n = 200$, $N = 900$, $\chi_{AB} = 0.1$ and (a) $\chi_{BC} = 0.1$, (b) $\chi_{BC} = 0.4$, (c) $\chi_{BC} = 1.5$, (d) $\chi_{BC} = 5$.

6.4.2 Chain length influence

To see how these results depend on the elastic stretching of the blocks, the length of the internal blocks was decreased to $n = 100$ with the outer block length N still satisfying $(2m+1)n = 2N$. We first consider fixed $\chi_{AB} = 0.1$. The equilibrium number of internal domains k_{opt} as a function of m and χ_{BC} are given in Table 6.2. A comparison with Table 6.1 shows that the decreased length of the blocks, implying "stiffer" springs, indeed requires larger values of χ_{BC} to obtain the same number of internal layers.

Table 6.2. Equilibrium number of domains k_{opt} as a function of χ_{BC} for $n = 100$ and $\chi_{AB} = 0.1$.

	χ_{BC}				
k_{opt}	$m = 3$ $N = 350$	$m = 4$ $N = 450$	$m = 5$ $N = 550$	$m = 6$ $N = 650$	$m = 7$ $N = 750$
3	0.05 – 0.25	0.05 – 0.15	0.05 - 0.1	0.05 – 0.08	0.05 – 0.07
5	0.3 – 2.05	0.2 – 0.9	0.15 – 0.5	0.09 – 0.3	0.08 – 0.2
7	≥ 2.1	0.95 – 4.1	0.55 – 2.0	0.35 – 1.15	0.25 – 0.75
9		≥ 4.15	2.05 – 6.85	1.2 – 3.7	0.8 – 2.25
11			≥ 6.9	3.75 – 10.35	2.3 – 6.05
13				≥ 10.4	6.1 – 14.6
15					≥ 14.65

Numerical calculations were also performed for a constant $\chi_{BC} = 0.1$ as a function of χ_{AB} with internal block lengths of $n = 200$ and $n = 100$. The results are collected in Table 6.3 and 6.4. Figure 6.5 presents free energy graphs as a function of *k* for *m* = 4, *n* = 200, $N = 900$, $\chi_{BC} = 0.1$ and $\chi_{AB} = 0.05$ (a), $\chi_{AB} = 0.15$ (b).

Table 6.3. Equilibrium number of domains k_{opt} as a function of χ_{AB} for $n = 200$ and $\chi_{BC} = 0.1$.

		k_{opt}				
χ_{AB}	$2n \cdot \chi_{AB}$	$m = 3$ $N = 700$	$m = 4$ $N = 900$	$m = 5$ $N = 1100$	$m = 6$ $N = 1300$	$m = 7$ $N = 1500$
0.05	20	3	5	5	5	5
0.1	40	3	3	3	5	5
0.15	60	3	3	3	3	5
0.2	80	3	3	3	3	3
0.25	100	3	3	3	3	3

Table 6.4. Equilibrium number of domains k_{opt} as a function of χ_{AB} for $n = 100$ and $\chi_{BC} = 0.1$.

		k_{opt}				
χ_{AB}	$2n \cdot \chi_{AB}$	$m = 3$ $N = 350$	$m = 4$ $N = 450$	$m = 5$ $N = 550$	$m = 6$ $N = 650$	$m = 7$ $N = 750$
0.1	20	3	3	3	5	5
0.15	30	3	3	3	3	3
0.2	40	3	3	3	3	3
0.25	50	3	3	3	3	3

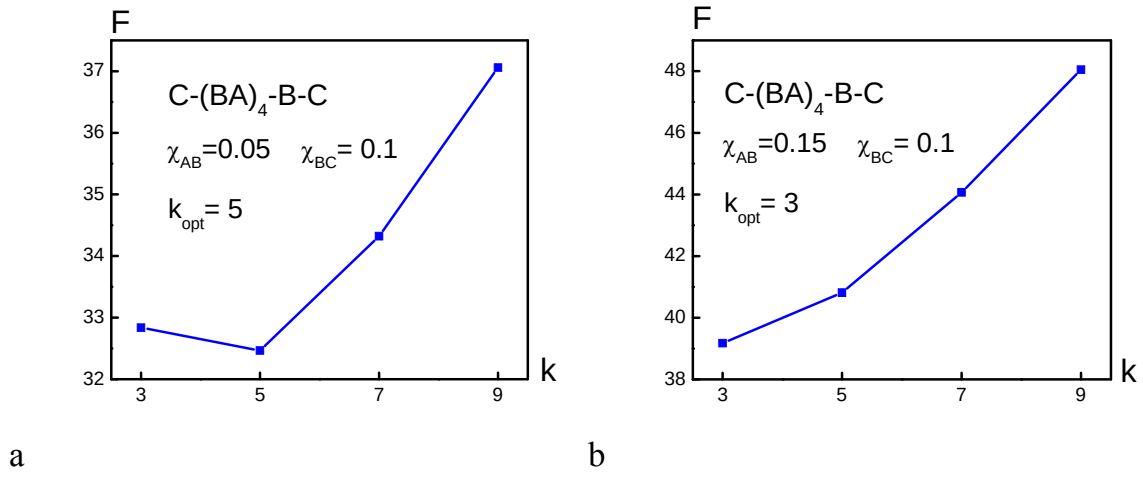

Figure 6.5. Free energy F of lamellar-*in*-lamellar self-assembled C-*b*-(B-*b*-A)$_4$-*b*-B-*b*-C multiblock copolymer melt as a function of the number k of internal layers for n = 200, N = 900, $\chi_{BC} = 0.1$ at (a) $\chi_{AB} = 0.05$, (b) $\chi_{AB} = 0.15$.

For the given value of $\chi_{BC} = 0.1$, nearly always the minimal number of k = 3 internal layers are found. Only when χ_{AB} is sufficiently small a transition to a 5-layered structure (more A/B interface) is observed. Of course, $2n\chi_{AB}$ has to be considerably larger than 10 to really have a strongly segregated lamellar-*in*-lamellar self-assembled state. The interfacial contribution to the free energy is given by $F_{interface} = 2F_{BC} + (k-1)F_{AB}$, which can be simply rewritten as $F_{interface} = \frac{(2m+1)n\upsilon}{h}\left[\gamma_{AB} + \frac{2\gamma_{BC} - \gamma_{AB}}{k}\right]$ where Eqs.6.3 and 6.5 have been used. From this expression it follows straightforward that when $\chi_{AB} > 4\chi_{BC}$ ($(\gamma_{AB} > 2\gamma_{BC})$ a 3-layered has a lower interfacial free energy than a 5-layered one. The results presented in the various tables, however, show that in reality a 3-layered structure is already formed at considerably smaller values of χ_{AB}, thus demonstrating in particular the importance of the conformational $(k-3)\ln 2$ contribution (see eq. 6.9) favouring small values of k.

The tendencies observed are corroborated by the results of computer simulations obtained by using dissipative particle dynamics simulation technique. The results are described in the next section, whereas the computational details are presented in the Appendix.

6.5 Dissipative particle dynamic dimulations of C-b-(B-b-A)$_m$-b-B-b-C multiblock copolymers

In the dissipative particle dynamics simulation technique a large series of monomers are collected into a few bead-and-spring particles in order to simulate the molecular behavior on a longer time- and length-scale [23-31]. The first situation simulated resembled the experimentally studied ternary P2VP-*b*-(PI-*b*-PS)$_4$-*b*-PI-*b*-P2VP linear undecablock copolymer system, i.e. $m = 4$ [5]. Figure 6.6 shows the corresponding self-assembled state observed for C_4-$(B_1A_1)_4B_1$-C_4 with the energy parameters representing the soft repulsion (see eq. A2) equal to $a_{BA} = 85$, $a_{BC} = 320$. Using equation A10 in the appendix for the relation between these energy parameters and the familiar Flory-Huggins parameters this corresponds to $N\chi_{BC} \cong 338$ and $n\chi_{AB} \cong 17.2$. Figure 6.6 demonstrates that a self-assembled lamellar state is formed with 5 "thin" internal layers as observed experimentally [4] and calculated theoretically (Figure 6.3a and ref. 21). The same result is obtained for internal blocks that are twice as long C_4-$(B_2A_2)_4$ B_2-C_4 (the subscripts of A, B and C denote the number of beads taken for the calculations).

Subsequently, we address the issue of the dependence of the number of internal layers on the interfacial tension. Tables 6.1-6.3 suggest that for this purpose it may be best to take $m = 5$ because then reasonable variations in the values of the Flory-Huggins parameters are theoretically predicted to induce transitions between different number of internal layers. That this is also the case in the simulations is shown in Figure 6.7, where 3 snapshots of the same system C_4-$(B_1A_1)_5$ B_1-C_4 are presented for different energy parameters a_{AB}, a_{BC}.

Figure 6.7 demonstrates that when the A-B interaction becomes less unavourable and the B-C interaction becomes more unfavorable, indeed transitions are observed from 3 to 5 to 7 internal layers. There is the obvious tendency to decrease the BC interface with a corresponding increase in the AB interface. For the system with $m = 4$, C_4-$(B_1A_1)_4$ B_1-C_4, 3 and 5 internal layers were observed varying the energy parameters.

To illustrate the dependence of the number of internal layers on the length of the internal blocks two systems C_3-$(B_1A_1)_3$ B_1-C_3 and C_3-$(B_2A_2)_3$ B_2-C_3 were simulated using the same energy parameter values. Figure 6.8 shows that in the former case 3 internal layers are formed and 5 in the latter.

Similar simulations have been performed for *m* equal to 4, 5 and 6 for the same $a_{AB} = 75$, $a_{BC} = 120$ taking $n = 1$ and $n = 2$. The number of internal layers found were 5, 5 and 7 for $m = 4$, 5 and 6, respectively, independently of *n*.

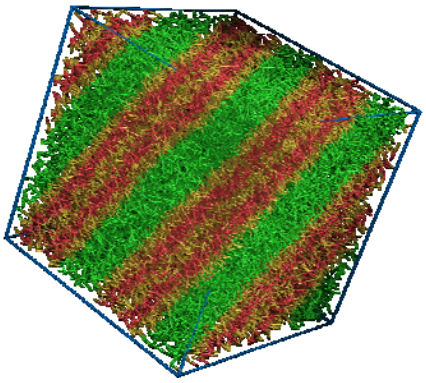

Figure 6.6. Snapshot of C_4-$(B_1A_1)_4B_1$-C_4 for a_{BA} = 85, a_{BC} = 320.

a. **b.** **c.**

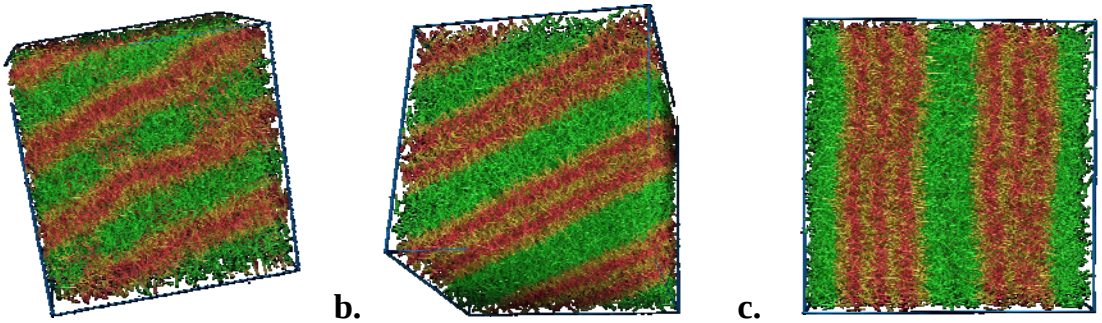

Figure 6.7. Snapshots of self-assembled C_4-$(B_1A_1)_5$ B_1-C_4 multiblock copolymer melt for: (a) a_{AB} = 250, a_{BC} = 50; (b) a_{AB} = 75, a_{BC} = 120; (c) a_{AB} = 65, a_{BC} = 300

a. **b**.

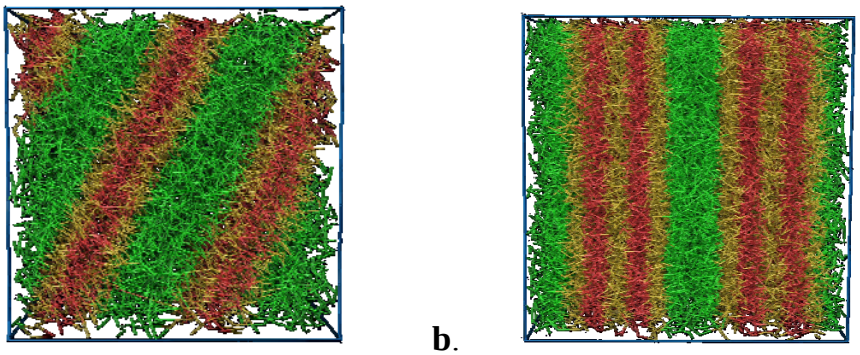

Figure 6.8. Snapshots of (a) C_3-$(B_1A_1)_3$ B_1-C_3 and (b) C_3-$(B_2A_2)_3$ B_2-C_3 for a_{AB} = 75 and a_{BC} = 120.

6.6 Summary

In this Chapter, we presented a simple theoretical analysis of the strongly segregated lamellar-*in*-lamellar self-assembled state of ternary C-*b*-(B-*b*-A)$_m$-*b*-B-*b*-C multiblock copolymers using the Alexander-de Gennes approach. This simplified description allowed us to discuss in detail the influence of the pertinent parameters on the number of internal layers *k* formed. The main observation concerns the sensitivity of *k* on the interfacial tension between the outer C-layers and the adjacent internal B-layers. The theoretically observed general tendencies were corroborated by the results of computer modeling using dissipative particle dynamics technique.

Appendix. Computational details

The dissipative particle dynamics (DPD) simulation method was introduced by Hoogerbrugge and Koelman [23] and first successfully applied by Groot and Madden [24] to AB diblock copolymer melts. The time evolution for a set of interacting particles is found by solving Newton's equations of motion. The force acting on the *i*-th particle $\vec{f}_i$ due to particle *j* is the sum of a conservative force $\vec{F}_{ij}^{C}$, a dissipative force $\vec{F}_{ij}^{D}$, and a random force $\vec{F}_{ij}^{R}$

$$\vec{f}_i = \sum_{j \neq i} \left(\vec{F}_{ij}^{C} + \vec{F}_{ij}^{D} + \vec{F}_{ij}^{R} \right) \tag{A1}$$

where the sum is over all other particles within a certain cut-off radius r_C. Since r_C is the only length scale it is used as the unit of length and thus set equal to 1. The conservative force $\vec{F}_{ij}^{C}$ is a soft repulsive force given by

$$\vec{F}_{ij}^{C} = \begin{cases} a_{ij}(1 - \dfrac{r_{ij}}{r_c})\vec{e}_{ij}, r_{ij} < r_c \\ 0, r_{ij} \geq r_c \end{cases} \tag{A2}$$

where a_{ij} is the repulsive interaction parameter between particles *i* and *j*, $\vec{r}_{ij} = \vec{r}_i - \vec{r}_j$, $\vec{e}_{ij} = \dfrac{\vec{r}_{ij}}{|\vec{r}_{ij}|}$, $r_{ij} = |\vec{r}_{ij}|$. The dissipative force $\vec{F}_{ij}^{D}$ is a hydrodynamic drag force and is defined by

$$\vec{F}_{ij}^{D} = \begin{cases} -\gamma \omega^{D}(r_{ij})(\vec{e}_{ij} \cdot \vec{v}_{ij})\vec{e}_{ij}, r_{ij} < r_c \\ 0, r_{ij} \geq r_c \end{cases} \tag{A3}$$

where γ is a friction parameter, ω^D is a *r*-dependent weight function. The random force $\vec{F}_{ij}^{D}$ describes thermal noise

$$\vec{F}_{ij}^{R} = \begin{cases} \sigma\omega^{R}(r_{ij})\dfrac{\theta_{ij}}{\sqrt{\Delta t}}\vec{e}_{ij}, r_{ij} < r_C \\ 0, r_{ij} \geq r_C \end{cases} \tag{A4}$$

where σ is the noise amplitude, ω^R is a weight function, and θ_{ij} is a random variable with normal distribution, Δt is a time step. The dissipative force slows down the particles by removing the kinetic energy from them and this effect is balanced by the random force due to thermal fluctuations. Friction γ and noise σ are related by [25]:

$$\sigma^2 = 2\gamma k_B T \tag{A5}$$

The associated weight functions satisfy the fluctuation-dissipation theorem if the following relation is satisfied [26]

$$\omega^D = \left(\omega^R(r)\right)^2 \tag{A6}$$

The standard choice for ω^D is

$$\omega^D = \begin{cases} (r_C - r_{ij})^2, r_{ij} < r_C \\ 0, r_{ij} \geq r_C \end{cases} \tag{A7}$$

The spring force $\vec{F}_i^{S}$ that acts on bead *i* due to its connection with beads *j* satisfies

$$\vec{F}_i^{S} = \sum_j C\vec{r}_{ij} \tag{A8}$$

where C is a harmonic type spring constant, which is chosen to be equal to 4 (in terms of k_BT) [25].

A modified version of the velocity-Verlet algorithm is used to solve Newton's equations of motion [27]

$$\begin{aligned} r_i(t+\Delta t) &= r_i(t) + v_i(t)\Delta t + 0.5 f_i(t)\Delta t^2 \\ \tilde{v}_i(t+\Delta t) &= v_i(t) + \lambda f_i(t)\Delta t \\ f_i(t+\Delta t) &= f_i[r_i(t+\Delta t), \tilde{v}_i(t+\Delta t)] \\ v_i(t+\Delta t) &= v_i(t) + 0.5\Delta t[f_i(t) + f_i(t+\Delta t)] \end{aligned} \tag{A9}$$

Groot and Warren [25] presented a detailed investigation of the effect of λ on the steady state temperature and showed that for a particle density $\rho=3$ and noise $\sigma=3$, the optimum value is given by λ =0.65 for which the temperature control can be maintained even at large time-steps of Δt =0.06. For our calculations we took accordingly λ = 0.65, Δt = 0.06, ρ = 3 and σ = 3.

The DPD simulations are performed in a cubic box of L^3 grids with periodic boundary conditions. Since the particle density ρ is set equal to 3, the total number of simulated DPD beads equal $3L^3$. As reported in Refs. 28-30, the morphology obtained by DPD simulations may depend on the finite size of the simulation box. In our simulations we have periodic structures with large periods and to exclude finite size effects we have to take the simulation box sufficiently large. The number of DPD beads per chain is in

the range 9-17. The size of the simulation box volume used was taken in the range $V = 10^3 - 30^3$, in such a way that for each case considered L exceded the length of the chains. All simulations were started from random positions.

Following the work of Groot and Warren [25], the repulsive parameters between the same types of particles is taken as $a_{ii} = 25$. For different types of particles a_{ij} can be chosen from the relation between the energy parameter a_{ij} and the Flory–Huggins interaction parameter χ_{ij}

$$a_{ij} = a_{ii} + 3.497\chi_{ij} \quad \text{(A10)}$$

REFERENCES

[1] J. Ruokolainen, R. Mäkinen, M. Torkkeli, T. Mäkelä, R. Serimaa, G. ten Brinke, O. Ikkala, *Science* **1998**, *280*, 557.
[2] O. Ikkala, G. ten Brinke, *Science* **2002,** *295*, 2407 .
[3] J. Ruokolainen, G. ten Brinke, O. Ikkala, *Adv. Mater.* **1999**, *11*, 777.
[4] J. Masuda, A. Takano, Y. Nagata, A. Noro, Y. Matsushita, *Phys. Rev. Lett***. 2006,** *97*, 098301.
[5] Y. Nagata, J. Masuda, A. Noro, D. Cho, A. Takano, Y. Matsushita, *Macromolecules* **2005**, *38*, 10220.
[6] C.C. Evans, F.S. Bates, M.D. Ward, *Chem. Mater*. **2000,** *12*, 236.
[7] A.F. Thünemann, S. General, *Macromolecules* **2001,** *34*, 6978.
[8] C. Osuji, C.Y. Chao, I. Bita, C.K. Ober, E.L. Thomas, *Adv. Funct. Mater.* **2002,** *12*, 753.
[9] I.A. Ansari, V. Castelletto, T. Mykhaylyk, I.W. Hamley, Z.B. Lu, T. Itoh, C.T. Imrie, *Macromolecules* **2003,** *36*, 8898.
[10] G.O.R. Alberda van Ekenstein, E. Polushkin, H. Nijland, O. Ikkala, G. ten Brinke, *Macromolecules* **2003,** *36*, 3684.
[11] C.Y. Chao, X. Li, C.K. Ober, C. Osuji, E.L. Thomas, *Adv. Mater*. **2004,** *14*, 364.
[12] O. Ikkala, G. ten Brinke, *Chem. Com*. **2004**, 2131.
[13] C.S. Tsao, H.L. Chen, *Macromolecules* **2004**, *37*, 8984.
[14] I.W. Hamley, V. Castelletto, P. Parras, Z.B. Lu, C.T. Imrie, T. Itoh, *Soft Matter* **2005,** *1*, 355.
[15] B. Nandan, C.H. Lee, H.L. Chen, W.C. Chen, *Macromolecules* **2005,** *38*, 10117.
[16] R. Nap, C. Kok, G. ten Brinke, S.I. Kuchanov, *European Phys. J. E* **2001,** *4*, 515.
[17] R. Nap, N. Sushko, I.Ya. Erukhimovich, G. ten Brinke, *Macromolecules* **2006,** *39*, 6765.
[18] Y. Smirnova, G. ten Brinke, I.Ya. Erukhimovich, *J. Chem. Phys*. **2006**, *124*, 054907.
[19] S. I. Kuchanov, V.E. Pichugin, G. ten Brinke, *E-Polymers* **2006**, 012.
[20] S.I. Kuchanov, V.E. Pichugin, G. ten Brinke, *Europhys. Lett*. **2006,** *76*, 959.
[21] A. Subbotin, T. Klymko, G. ten Brinke, *Macromolecules* **2007,** *40*, 2915.
[22] T. Klymko, A. Subbotin, G. ten Brinke, *J. Chem. Phys.* submitted.
[23] P.J.Hoogerbrugge, J.M.V.A. Koelman, *Europhys. Lett.* **1992,** *19*, 155.
[24] R.D. Groot, T.J. Madden, *J.Chem. Phys*. **1998,** *108*, 8713.
[25] R.D. Groot, P.B. Warren, *J.Chem. Phys*. **1997,** *107*, 4423.
[26] P. Espanol, P.B.Warren, *Europhys.Lett*. **1995,** *30*, 191.
[27] M.P.Allen, D.J. Tildesley, *Computer Simulation of Liquids*, **1987**, Clarendon, Oxford.
[28] U.Micka, K.Binder, *Macromol. Theory Simul*. **1995,** *4*, 419.
[29] Y. Bahbot-Raviv, Z.G. Wang, *Phys. Rev. Lett*. **2000,** *85*, 3428.
[30] Q. Wang, P.F.Nealey, J.J. de Pablo, *Macromolecules* **2001,** *34*, 3458.
[31] C.-I. Huang, C.-M. Chen, *ChemPhysChem*, **2007,** *8*, 2588.

CHAPTER 7

Lamellar-in-Lamellar Structure of Linear Binary Multiblock Copolymers

Abstract. A theoretical description of the lamellar-*in*-lamellar self-assembly of binary A-*b*-(B-*b*-A)$_m$-*b*-B-*b*-A multiblock copolymers in the strong segregation limit is presented. The essential difference between this binary multiblock system and the previously considered C-*b*-(B-*b*-A)$_m$-*b*-B-*b*-C ternary multiblock copolymer system is discussed. Considering the situation with long end-blocks, the free energy of the lamellar-in-lamellar self-assembled state is analyzed as a function of the number *k* of "thin" internal lamellar domains for different numbers *m* of repeating (B-*b*-A) units and different values of the Flory-Huggins χ_{AB} interaction parameter. The theoretical predictions are in excellent agreement with the available experimental data.

7.1 Introduction

In Chapters 5 and 6 we discussed the lamellar-*in*-lamellar self-assembly of ternary C-*b*-(B-*b*-A)$_m$-*b*-B-*b*-C multiblock copolymers using an elaborated mean-field analysis and a much more simplified treatment employing the Alexander-de Gennes approximation, respectively. This type of ternary linear multiblock copolymers belongs to the class of systems that self-assemble in the form of hierarchically ordered structures with different periodicities. Self-assembly in such kind of systems has been extensively investigated during the last decades both experimentally [1-15] and theoretically [16-27]. Strong segregation theory, weak segregation theory and and numerical self-consistent field calculations are the main theoretical tools to study conformational and phase behavior of complex multiblock copolymer systems [16-18,26].

In this Chapter we restrict ourselves to the theoretical analysis of the simplest class of multiblock copolymer systems with self-assembly involving two length scales. These consists of two chemically different species linked together to form A-*b*-(B-*b*-A)$_m$-*b*-B-*b*-A multiblock copolymers with a linear architecture. The different length scales are introduced by taking the A end blocks to be considerably longer than the internal A and B blocks. For simplicity the length of the "internal" A and B blocks are assumed to be equal. The scope of our theoretical investigation is again to relate the number m of repeating (B-*b*-A) units to the number k of "thin" lamellar layers in the self-assembled lamellar-in-lamellar state.

In the ternary C-*b*-(B-*b*-A)$_m$-*b*-B-*b*-C multiblock copolymer system, due to the assumed strong incompatibility between all three species involved, the middle blocks are never located in the outer region and, hence, the volume of the internal part formed by the $2m+1$ blocks is the same independent of the number k of internal "thin" layers formed. On the other hand, in the binary system for $k=1$, only the "short" B-blocks form the middle "thin" layer, whereas the "short" A-blocks of the multi middle block are all in the outer "thick" A-domains. As k increases the number of "short" A-blocks forming loops inside the layers formed by the "long" A-blocks gradually decreases. Once all "short" A-blocks are part of the internal "thin" lamellar layers, the volume of the internal part has doubled. This essential difference between the ternary and the binary multiblock copolymer systems is schematically illustrated in Figure 7.1a and 7.1b.

An important feature of the system considered here is the presence of two types of A blocks, "short" and "long" ones, that are not equivalent. It implies that the binary multiblock copolymer melt is characterized by two different concentration profiles for the segments belonging to the "short" respectively "long" A blocks. It results in an additional loss of conformational entropy connected to this concentration gradient. To arrive at predictions that agree with the experimental results, a proper consideration of this effect turned out to be essential.

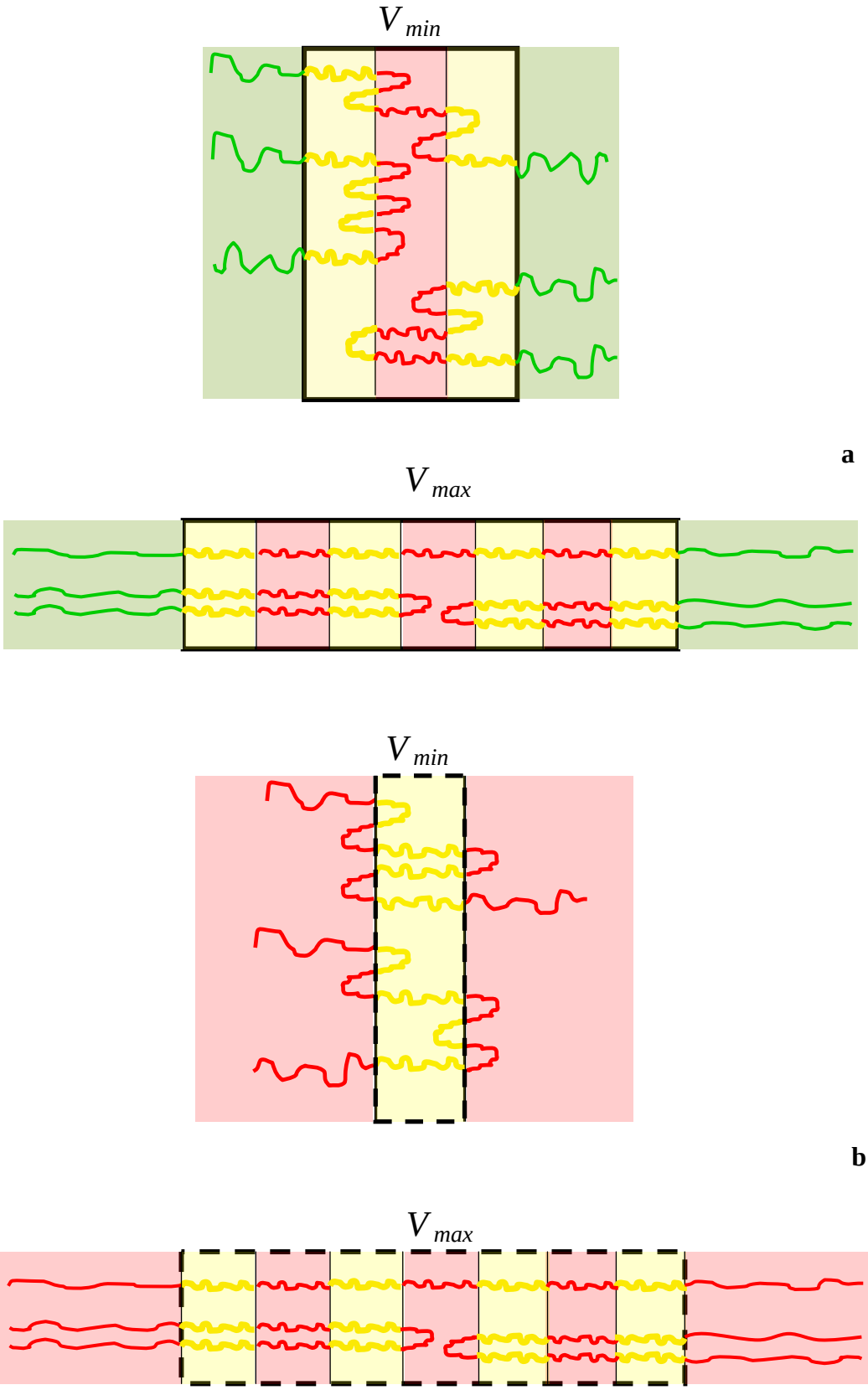

Figure. 7.1. Schematic illustration: minimal and maximal number of internal layers for (a) ternary C-*b*-(B-*b*-A)$_m$-*b*-B-*b*-C and (b) binary A-*b*-(B-*b*-A)$_m$-*b*-B-*b*-A system. (a) $V_{min} = V_{max}$; (b) $V_{min} \cong V_{max} / 2$. A, B and C blocks are depicted by red, yellow and green colors, respectively.

7.2 The model

In this section we will develop a theoretical description of the A-*b*-(B-*b*-A)$_m$-*b*-B-*b*-A multiblock copolymer lamellar-*in*-lamellar self-assembled state. Our objective is to find the dependence between the number *m* of repeating (B-b-A) units and the number *k* of the internal *k*-layered structure. We will derive the free energy expression of this A-*b*-(B-*b*-A)$_m$-*b*-B-*b*-A multiblock copolymer self-assembled state depending on the number *k* of internal domains. The minimum of the free energy as a function of *k* will determine the equilibrium *k*-layered structure.

We assume that the statistical segment length *a* and the monomer volume υ are the same for both components. It is also assumed that the degree of polymerization *N* of the A end blocks is much larger than the degree of polymerization *n* of the "short" A- and B-blocks of the internal multiblock, $N >> n$. The Flory-Huggins parameter χ_{AB} is sufficiently positive, i.e. $n\chi_{AB} >> 1$, implying the formation of pure A- and B-domains. This allows us to apply the strong segregation theory.

As in the case of ternary multiblocks discussed in Chapters 5and 6, in general a multiblock chain as part of the lamellar-*in*-lamellar self-assembled state can assume two different global conformations: either it forms a bridge where the end blocks are located in different layers or it forms a loop where the two end blocks are located in the same layer. Figure 7.1b illustrates these two possibilities. Here, since we use the same assumptions about global bridge and loop conformations as in the previous Chapter 5, the average free energy per binary multiblock copolymer can be expressed via average free energy of multiblock bridge conformation and according to Eqs.5.1 and 5.2 of Chapter 5 is written as

$$F = F_{bridge} - \ln 2 \tag{7.1}$$

The free energy will be given in k_BT energetic units.

A sketch of a possible A-*b*-(B-*b*-A)$_m$-*b*-B-*b*-A multiblock bridge conformation is given in Figure 7.2 for the case when *m* = 5. From here on we will only consider global bridge conformations.

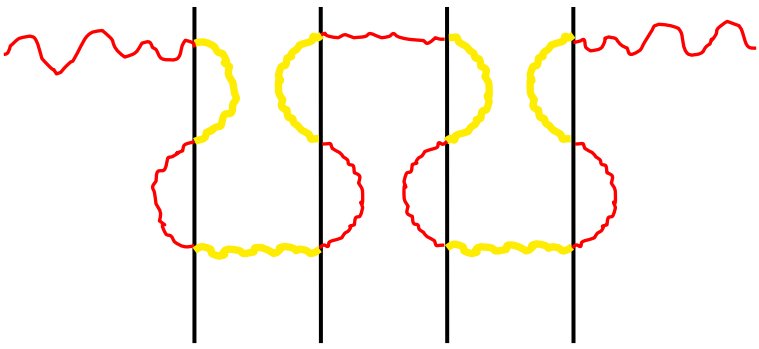

Figure 7.2. Schematic representation of a global bridge A-*b*-(B-*b*-A)$_m$-*b*-B-*b*-A (*m* = 5) multiblock copolymer conformation.

7.3 Free energy calculations

The total free energy per multiblock copolymer bridge consists of the AB interfacial free energy F_{AB}, the conformational free energy F_{conf} which appears owing to the fact that the internal multiblock chain forms a global bridge, the elastic free energy F_A of the "long" A end blocks, the elastic free energies F_B and F_{A1} of the "short" internal blocks in the central B- and A-layers respectively, and a gradient term F_∇ due to the concentration gradient of A segments belonging to the "short" and "long" blocks in the "thick" outer A-layers:

$$F_{bridge} = (k+1)F_{AB} + F_{conf} + 2F_A + \frac{k+1}{2}F_B + \frac{k-1}{2}F_{A1} + 2F_\nabla \tag{7.2}$$

Note, that there is an additional contribution to the free energy due to the nonhomogeneous distribution of the segments belonging to loops in the internal domains. However, the corresponding terms are relatively small and will be omitted.

The interfacial free energy F_{AB} can be expressed in terms of the interfacial tension γ and the average area Σ per multiblock copolymer and is given by

$$F_{AB} = \frac{a}{\upsilon}\sqrt{\frac{\chi_{AB}}{6}}\Sigma \tag{7.3}$$

where we used $\gamma = \frac{a}{\upsilon}\sqrt{\frac{\chi_{AB}}{6}}$.

As in the previous chapters 5 and 6, in order to find the combinatorial contribution F_{conf} we assume that the internal multiblock chain forms only one local bridge per internal domain and the local loops are distributed homogeneously along the multiblock trajectory. Using this simplification the multiblock part can be represented as a chain of k blobs consisting of one bridge and loops and stretched in one direction. The probability of such conformation is $\left(\frac{1}{2}\right)^k$ which corresponds to a free energy in k_BT energetic units

$$F_{conf} = k \ln 2 \tag{7.4}$$

Next we turn our attention to the free energy of one internal domain.

7.3.1 Free energy of internal domain

The structure of "short" internal A1- and B-domains for binary multiblock copolymers is the same as a structure of internal A- and B2-domains for ternary multiblocks discussed in Chapter 5. Schematically this structure is presented in Figure 5.3 of Chapter 5. Therefore all ideas, assumptions and calculations to find the expression for the free energy of one internal domain for binary multiblocks remain the same as in

Chapter 5 and here we can simply use the already obtained Eq.5.13 for the elastic free energy of the A-domains:

$$F_{A1} = F_B = \frac{n\upsilon^2 f_1(\alpha)}{a^2\Sigma^2} \tag{7.5}$$

with $f_1(\alpha) = \frac{1}{\pi}\tan^3\frac{\pi\alpha}{2} + \frac{3}{\pi}\tan\frac{\pi\alpha}{2} + \frac{3(1-\alpha)}{2}$.

The only difference in the binary system due to the possibility of presence of short A-blocks in the outer A-domain is to find the relation for α which has the same meaning as in Chapter 5. Assuming again that the multiblock forms only one bridge per domain, we obtain in the same way:

$$\frac{2m+2}{k+1} = 1-\alpha+\frac{2}{\pi}\tan\left(\frac{\pi\alpha}{2}\right) \tag{7.6}$$

7.3.2 Free energy of outer domains

Now we focus our attention on the outer A-domain. Schematically the structure of this domain is represented in Fig.7.3.

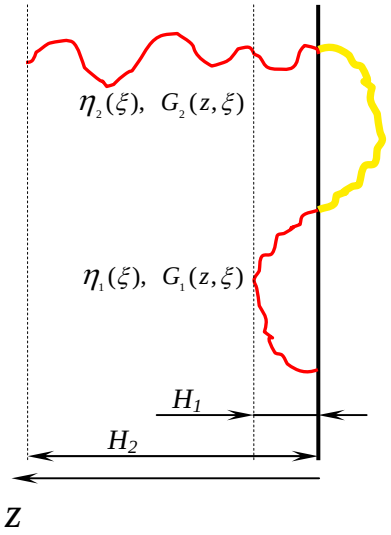

Figure 7.3. Schematic representation of the outer part of an A-*b*-(B-*b*-A)$_m$-*b*-B-*b*-A multiblock copolymer conformation. H_1 denotes the thickness of the loop region, H_2 denotes the height of long A-tail. $\eta_1(\xi)$ and $\eta_2(\xi)$ are the loop and A-tail end distribution functions, respectively. Note, that $\eta_1(\xi)$ is non-zero only in the H_1 region, whereas $\eta_2(\xi)$ in the same region has zero value. $G_1(z,\xi)$ and $G_2(z,\xi)$ are the functions of local stretching of loop and tail, respectively.

To calculate the free energy F_A we apply the method which has been presented in Ref.22.

$$F_A = F_{tail} + qF_{loop} \tag{7.7}$$

where q denotes the average number of loops from each side of the AB interface:

$$q = \frac{1}{2}\frac{2m+1-k}{k+1} \tag{7.8}$$

The free energies F_{loop} of the loop and F_{tail} of the A-tail are given by

$$F_{loop} = \frac{3}{2a^2}\int_0^{H_2} d\xi\, \eta_1(\xi)\int_0^{\xi} G_1(z,\xi)\, dz \tag{7.9}$$

$$F_{tail} = \frac{3}{2a^2}\int_{H_1}^{H_2} d\xi\, \eta_2(\xi)\int_0^{\xi} G_2(z,\xi)\, dz \tag{7.10}$$

In order to satisfy the incompressibility condition in the outer region, the A-tail is stretched differently in the H_1 and $(H_2 - H_1)$ regions:

$$G_2(z,\xi) = \begin{cases} G_{21}(z,\xi) & z < H_1 \\ G_{22}(z,\xi) & H_1 < z < H_2 \end{cases} \tag{7.11}$$

The incompressibility conditions thus become

$$\int_{H_1}^{H_2} \frac{\eta_2(\xi)d\xi}{G_{21}(z,\xi)} + 2q\int_z^{H_1} \frac{\eta_1(\xi)\,d\xi}{G_1(z,\xi)} = \frac{\Sigma}{\upsilon} \tag{7.12}$$

$$\int_z^{H_2} \frac{\eta_2(\xi)d\xi}{G_{22}(z,\xi)} = \frac{\Sigma}{\upsilon} \tag{7.13}$$

Besides, there are two more constraints to keep the number of monomer units constant:

$$\int_0^{\xi} \frac{dz}{G_1(z,\xi)} = \frac{n}{2} \tag{7.14}$$

$$\int_0^{H_1} \frac{dz}{G_{21}(z,\xi)} + \int_{H_1}^{\xi} \frac{dz}{G_{22}(z,\xi)} = N \tag{7.15}$$

To find the function of the local stretching, the free energy (7.7) has to be minimized with respect to $G_1(z,\xi)$ and $G_2(z,\xi)$ under the constraints (7.12)-(7.15). Implementation of this procedure by the Lagrange multipliers method immediately yields the next form for the local stretching functions for the A-loops and A-tail, respectively:

$$G_1(z,\xi) = \frac{\pi}{n}\sqrt{\xi^2 - z^2} \tag{7.16}$$

$$G_2(z,\xi) = \begin{cases} G_{21}(z,\xi) = \dfrac{\pi}{n}\sqrt{u^2(\xi) - z^2} & z < H_1 \\ G_{22}(z,\xi) = \dfrac{\pi}{n}\sqrt{u^2(\xi) - u^2(z)} & H_1 < z < H_2 \end{cases} \tag{7.17}$$

with

$$u(x) = \frac{x - \lambda\sqrt{x^2 - (1-\lambda^2)H_1^2}}{1-\lambda^2}, \quad \lambda = \frac{2N}{n} - 1 \tag{7.18}$$

Substitution of Eqs.7.16-7.17 into Eq.7.7 leads to the expression for the free energy of the outer A-domain in terms of $y = H_1 / H_2$:

$$F_A = \frac{\pi^2 \Sigma H_2^3}{2a^2 n^2 (1-\lambda^2)^2}\left[1 + \lambda^2 - 3\lambda\sqrt{1 - y^2 + \lambda^2 y^2} + \lambda(1 - y^2 + \lambda^2 y^2)^{3/2}\right] \tag{7.19}$$

In order to find y we use the incompressibility condition given by Eq.7.12, which yields

$$\sqrt{1 - y^2 + \lambda^2 y^2} - 1 = \frac{(\lambda - 1)qn}{qn + N} \tag{7.20}$$

7.3.3 Conformational effects

Now let's turn our attention to the analysis of the last gradient term F_{∇} in Eq.7.2. The concentration profile of the segments belonging to loops in the region H_1 of the outer A-layer is given by [22]

$$\Phi(z) = \frac{1}{2} + \frac{1}{\pi}\arcsin\frac{2H_1^2 - u^2(H_2) - z^2}{u^2(H_2) - z^2} \tag{7.21}$$

This profile results in an additional contribution F_{∇} to the total free energy [21]

$$F_{\nabla} = \frac{a^2\Sigma}{24\upsilon}\int_0^{H_1}\frac{[\nabla\Phi(z)]^2}{\Phi(z)\big(1-\Phi(z)\big)} \tag{7.22}$$

This energy diverges at $z = H_1$ because the profile given by Eq.7.21 at $z = H_1$ behaves as

$$\Phi(z) = \frac{2\sqrt{2H_1(H_1 - z)}}{\pi\sqrt{u^2(H_2) - H_1^2}} \tag{7.23}$$

To avoid this singularity we have to know the real concentration profile $\tilde{\Phi}(z)$ of loops' segments in the vicinity of $z = H_1$. This profile can be expressed in terms of the order parameter $\psi(z)$ satisfying the Schrödinger type equation [27]

$$\frac{a^2}{6}\frac{d^2\psi(z)}{dz^2} + \big(E - \mu(z)\big)\psi(z) = 0 \tag{7.24}$$

as $\tilde{\Phi}(z) = \psi^2(z)$. Here $\mu(z)$ is the molecular field acting on the segments of loops. It can be obtained from Eq.(7.16) and in the vicinity of $z = H_1$ has the form

$$\mu(z) \approx \frac{3\pi^2 H_1}{a^2 n^2}\big(H_1 - z\big) \tag{7.25}$$

Parameter E denotes the "energy" of a loop. After using Eq.(7.25), solution of Eq.7.24 can be written in terms of the Airy function $Ai(x)$ [28],

$$\tilde{\Phi}(z) = C \cdot Ai^2\left[B(z - h_0(E))\right] \tag{7.26}$$

where $B = \left(\frac{18\pi^2 H_1}{a^4 n^2}\right)^{1/3}$. $h_0 = h_0(E)$ determines the position of profile (7.26) along the z axis. After joining both profiles Eqs. (7.23) and (7.26) (the procedure is described in detail in Appendix) we arrive at the free energy F_∇:

$$F_\nabla \approx 0.076 \frac{a^2 \Sigma}{\upsilon} \sqrt{\frac{BH_1}{u^2(H_2) - H_1^2}} \tag{7.27}$$

7.3.4 Total free energy per multiblock copolymer chain

Taking into account Eqs. 7.1, 7.3, 7.4, 7.5, 7.19 and 7.27 we can write down the final expression for the free energy per multiblock copolymer chain:

$$F = (k+1)\sqrt{\frac{\chi_{AB}}{6}}\left(\frac{a\Sigma}{\upsilon}\right) + g_1(k,y)\left(\frac{a\Sigma}{\upsilon}\right)^{4/3} + g_2(k,\alpha,y)\left(\frac{a\Sigma}{\upsilon}\right)^2 + (k-1)\ln 2 \tag{7.28}$$

where

$$g_1(k,y) = 0.36 \frac{y^{2/3}(\lambda^2 - 1)}{1 - \lambda\sqrt{1 - y^2 + \lambda^2 y^2}} \left(Nn + \frac{n^2}{2}\frac{2m + 1 - k}{k+1}\right)^{-1/3}$$

and

$$g_2(k,\alpha,y) = \frac{\pi^2 N^3}{n^2(\lambda^2 - 1)^2}\left(1 + \frac{n}{2N}\frac{2m+1-k}{k+1}\right)^3 \left[1 + \lambda^2 - 3\lambda\sqrt{1 - y^2 + \lambda^2 y^2} + \lambda(1 - y^2 + \lambda^2 y^2)^{3/2}\right]$$
$$+ \frac{3}{2} Nnk\left[1 - \alpha + \frac{2}{\pi}\mathrm{tg}\frac{\pi\alpha}{2} + \frac{2}{3\pi}\mathrm{tg}^3\frac{\pi\alpha}{2}\right]$$

The free energy (7.28) is a function of the variables α, y, Σ, k and parameters λ, m, χ_{AB}. To determine α and y Eqs.7.6 and 7.20 are used. The minimization of the total free energy with respect to the interface area Σ per copolymer chain gives its equilibrium value. As a result we obtain the free energy of the A-*b*-(B-*b*-A)$_m$-*b*-B-*b*-A copolymer chain as a function of the number k of internal layers for given values of m, λ, χ_{AB}. For

different numbers of m the equilibrium number of k is determined by the minimal value of the corresponding free energy.

The results of the numerical calculations are presented and discussed in the next section.

7.4 Results and discussions

Numerical calculations have been performed first for the experimental situation corresponding to the PS-*b*-[(PI-*b*-PS)$_4$-*b*-PI]-*b*-PS multiblock copolymers. From the experimental data we have that $\chi_{AB}n = 24.3$, $n/N = 0.26$, $\chi_{AB} = 0.1$ [5]. In this case the free energy behaves as shown in Fig.7.4a. We see that the minimal value of the free energy corresponds to a number of internal domains $k = 3$, in excellent agreement with experiment [5]. Similar calculations have been done for different values of $m = 3,5,6,7$. The corresponding equilibrium number of internal layers are $k = 3,3,5,5$. The respective plots of the free energy as a function of k are presented in Figure 7.4b-d. The values of k at the minima of $F(k)$ for the binary system and for similar ternary systems with P2VP end blocks [26] are given in Table 7.1. Note, that for the binary multiblock copolymer with $m = 5$ the free energies of the three-layered and five-layered structure are very close to each other, as indicated in Fig.7.4c.

Table 7.1. Number of internal layers k for binary and ternary* systems.

A-*b*-(B-*b*-A)$_m$-*b*-B-*b*-A		C-*b*-(B-*b*-A)$_m$-*b*-B-*b*-C	
m	*k*	*m*	*k*
3	3	3	5
4	**3**	**4**	**5**
5	3	5	7
6	5	6	7

* The values for the ternary systems are taken from Ref.26.

We see that compared to the ternary system, the number of internal layers in the binary system is obviously reduced due to the possibility of having loops in the outer domains. This causes a concentration gradient in these domains with a corresponding loss of conformation entropy. This contribution turns out to be quite essential. Neglecting this gradient term gives $k = 1$ as the optimal number of internal domains for all values of m, in conflict with the available experimental data. Taking the gradient contribution into account (quantitatively this contribution scales as $\Sigma^{4/3}$, where Σ is interfacial area), we effectively create an additional interface area which becomes essential for the layers' formation.

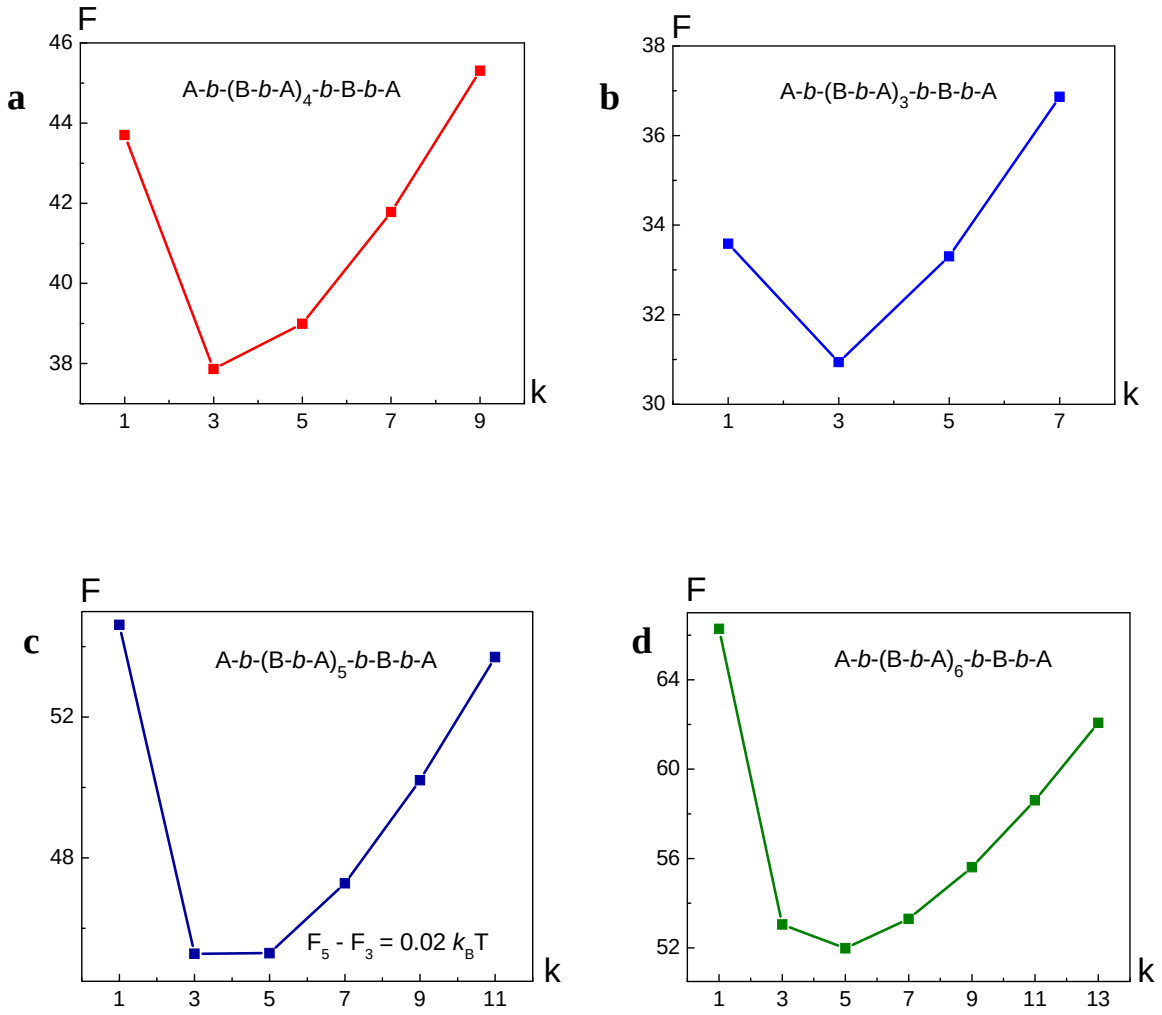

Figure 7.4. Free energy F of the A-*b*-(B-*b*-A)$_m$-*b*-B-*b*-A multiblock copolymer as a function of the number k of internal layers for $\chi_{AB}n = 24.3$, $n/N = 0.26$. (a) m = 4, (b) m = 3, (c) m = 5, (d) m = 6.

7.4.1 Analysis for selected systems

To investigate the effects of the elastic stretching and the interfacial tension we subsequently performed calculations for different values of *n/N* and different values of χ_{AB}. We start with considering different values of n/N with the length of internal blocks fixed and Flory-Huggins interaction parameter $\chi_{AB} = 0.1$. The number of lamellar domains for $m = 3,4,5,6$ and $n/N = 0.05;\ 0.1;\ 0.2;\ 0.26;\ 0.5$ are given in Table 7.2. The corresponding free energies for $m = 3$ and $m = 6$ are represented in Figure 7.5a-b. The squared symbols depict the minimum of the free energies and thus the optimal number of lamellar domains, under the assumption that this lamellar morphology remains indeed

the equilibrium morphology. Bold case in Table 7.2 reflects the experimental case described in Ref.5.

Similar calculations have been performed for $\chi_{AB} = 0.4$ with $m = 3,4,5,6$ and $n/N = 0.05; 0.1; 0.2; 0.26; 0.5$ and fixed length of the internal blocks. The minima of the corresponding free energies appear at the values of k presented in Table 3. The free energies for $m = 3$ and $m = 6$ are represented in Figure 7.6a-b.

Comparison of Table 7.2 and Table 7.3 shows that for $\chi_{AB} = 0.1$ there are more possibilities to get a 5-layered structure, whereas for $\chi_{AB} = 0.4$ there are more possibilities to get only one internal domain. In both cases the 3-layered structure is dominant. From a comparison of Table 7.2 and Table 7.3 for a fixed ratio of *n/N* we observe the tendency for a decreasing optimal number of domains for increasing Flory-Huggins parameter values, i.e then AB-interactions become more unfavorable. This is related to the fact already discussed in the introduction, that short A-chains from the middle part of the multiblock start to go to the outer A-domain when χ_{AB} increases. Note that the behavior of ternary C-*b*-(B-*b*-A)$_m$-*b*-B-*b*-C multiblock copolymers will be exactly the opposite: since none of the middle A- and B-blocks can be in the outer C-part, increasing χ_{BC} will create more internal domains.

Table 7.2. Number of layers for A-*b*-(B-*b*-A)$_m$-*b*-B-*b*-A multiblock copolymer at $\chi_{AB} = 0.1$

n/N	$m = 3$	$m = 4$	$m = 5$	$m = 6$
0.05	1	3	3	3
0.1	3	3	3	3
0.2	3	3	3	5
0.26	3	**3**	3	5
0.5	3	3	5	5

Table 7.3. Number of layers for A-*b*-(B-*b*-A)$_m$-*b*-B-*b*-A multiblock copolymer at $\chi_{AB} = 0.4$

n/N	$m = 3$	$m = 4$	$m = 5$	$m = 6$
0.05	1	1	3	3
0.1	1	3	3	3
0.2	3	3	3	3
0.26	3	3	3	3
0.5	3	3	3	5

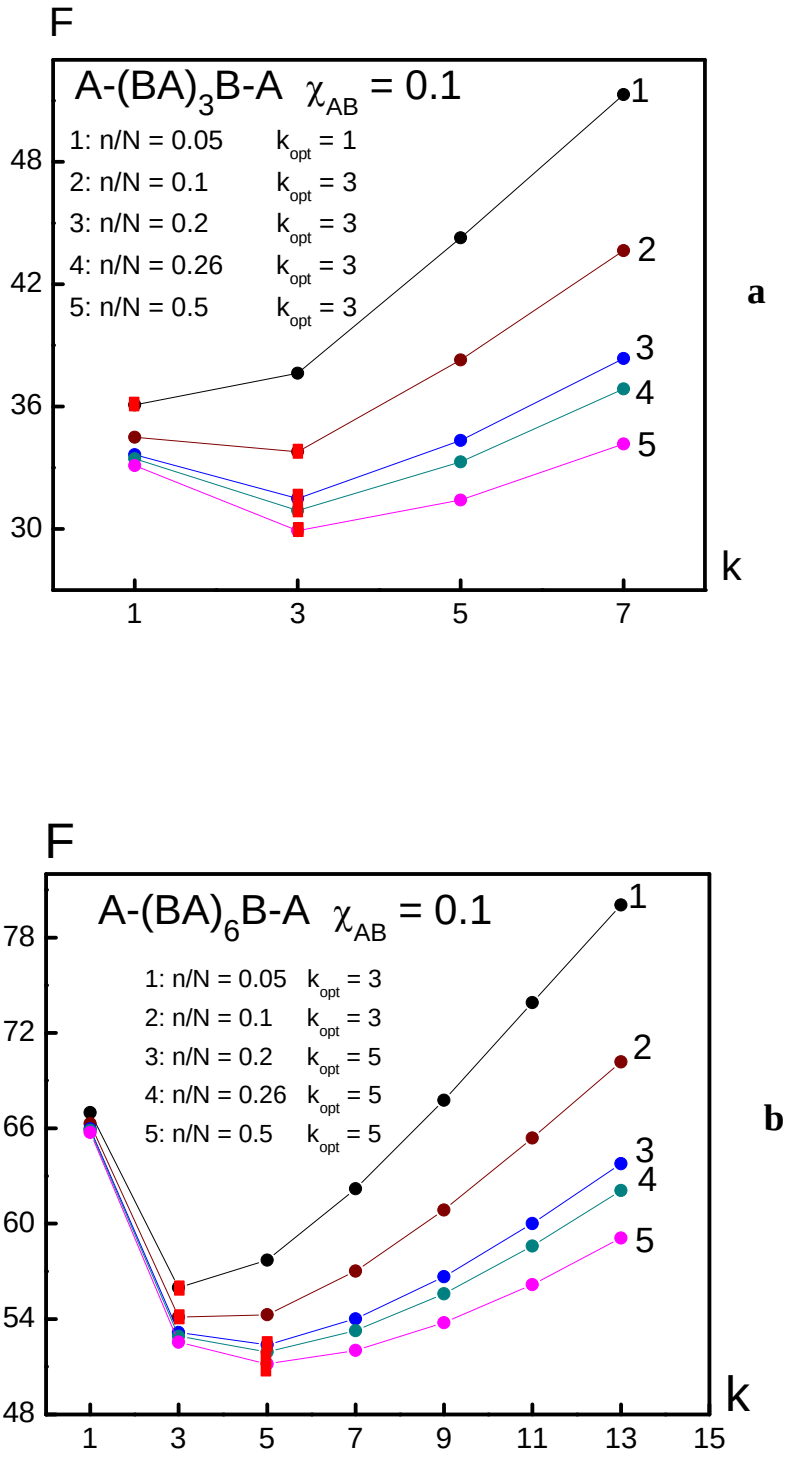

Figure 7.5. Free energy F of the A-*b*-(B-*b*-A)$_m$-*b*-B-*b*-A multiblock copolymer as a function of the number k of internal layers for $\chi_{AB}n = 24.3$ for different values of n/N for: (a) $m = 3$, (b) $m = 6$.

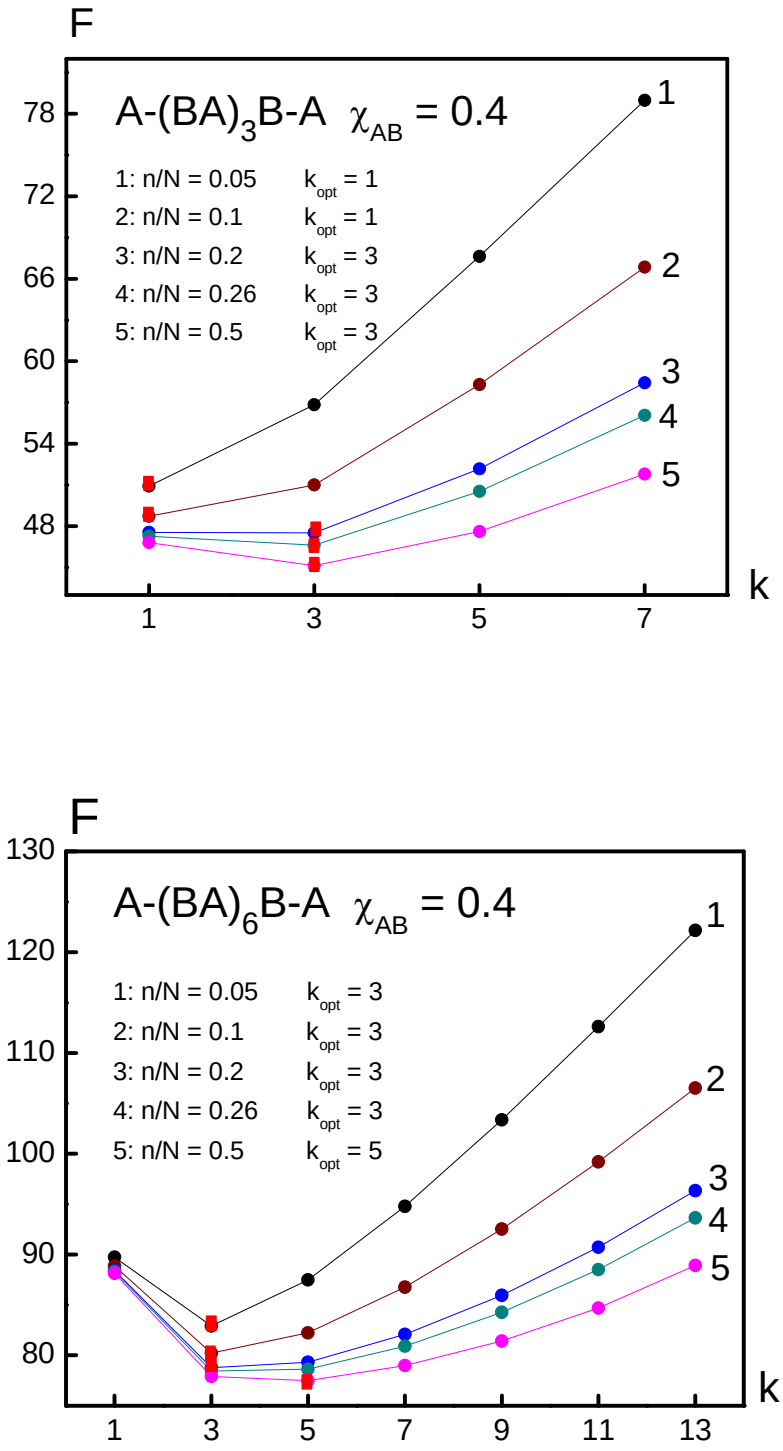

Figure 7.6. Free energy F of the A-*b*-(B-*b*-A)$_m$-*b*-B-*b*-A multiblock copolymer as a function of the number k of internal layers for $\chi_{AB}n = 97.2$ for different values of n/N for: (a) m = 3, (b) m = 6.

7.5 Concluding remarks

In this Chapter, we presented a theoretical analysis of binary A-*b*-(B-*b*-A)$_m$-*b*-B-*b*-A multiblock copolymer melts. Considering the lamellar-*in*-lamellar self-assembled state we addressed the question of the number k of internal layers as a function of the number m of repeating middle (B-*b*-A) units. Applied to a specific case, we showed that the result of our numerical calculations was in excellent agreement with the available experimental data.

We demonstrated that to a large extent the domain formation is determined by the interplay between interfacial forces and elastic stretching of the individual blocks. The combinatorial contribution corresponding to the number of different possibilities to create global loops or bridges was taken into account in an approximate manner.

Compared to a ternary system where all middle blocks are located in between the outer "long" end blocks, the binary system is considerably more complicated. The important new element in the analysis of the binary system concerns the conformational contribution associated with the concentration gradient in the outer A-domain due to the presence of "short" middle A-blocks. This gives an additional interfacial area depending contribution that is essential for the internal domain formation. Without this term the minimum of the free energy invariably occurs at $k = 1$ internal thin layers.

Of course, similar conformational effects are present in the internal domains of both the binary and ternary multiblock copolymer systems. However, these contributions are small compared to that of the outer domains in the binary multiblock copolymer system where we are dealing with "long" A end blocks together with loops formed by "short"A middle blocks.

Appendix A. Calculations of the conformational free energy

In the vicinity of $z = H_1$ the profile $\Phi(z)$ of segments belonging to loops in the outer A-region obtained using the strong stretching limit has the form (7.23)

$$\Phi(z) = \frac{2\sqrt{2H_1(H_1 - z)}}{\pi\sqrt{u^2(H_2) - H_1^2}}$$

On the other hand the form of this profile $\tilde{\Phi}(z)$ follows from the solution of the Schrödinger type equation (7.24) in the molecular field $\mu(z)$ given by Eq.(7.26)

$$\tilde{\Phi}(z) = C \cdot Ai^2\left[B(z - h_0(E))\right]$$

Schematically the behavior of the functions $\Phi(z)$ and $\tilde{\Phi}(z)$ is presented in Fig. A1.

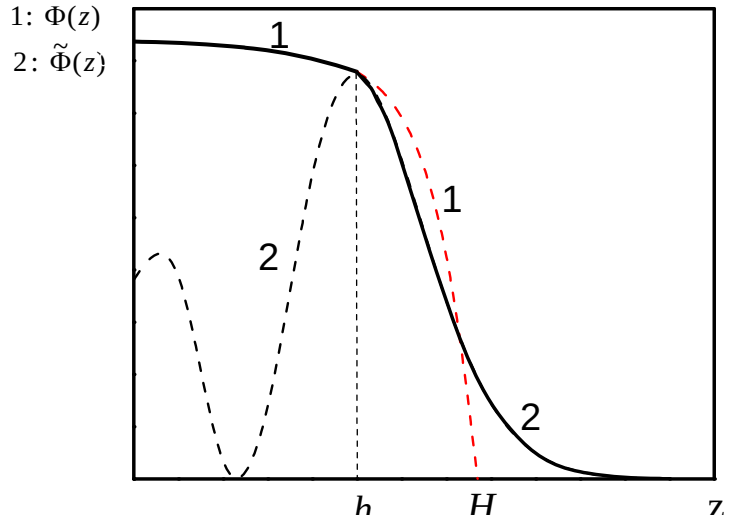

Figure A1. Schematic presentation of $\Phi(z)$ (line 1) and $\tilde{\Phi}(z)$ (line 2). The solid line corresponds to the joint profile that is used for the calculation of the conformational free energy.

At $z = h_1$ profile 1 transforms into profile 2:

$$\Phi(h_1) = \tilde{\Phi}(h_1) \qquad \text{(A1)}$$

Moreover, in order to have a smooth profile, the derivatives of $\Phi(z)$ and $\tilde{\Phi}(z)$ at $z = h_1$ have to be equal also

$$\Phi'(h_1) = \tilde{\Phi}'(h_1) \qquad \text{(A2)}$$

The conservation of monomer units implies

$$\int_{h_1}^{H_1} \Phi(z)dz = \int_{h_1}^{\infty} \tilde{\Phi}(z)dz \qquad \text{(A3)}$$

Equations (A1)-(A3) allow us to find h_0, h_1 and C. Substitution of Eqs. (7.23) and (7.26) into (A1)-(A3) and further simplifications lead to

$$\int_{-t_B}^{\infty} Ai^2(x)dx + \frac{1}{6}\frac{Ai^3(-t_B)}{Ai'(-t_B)} = 0 \tag{A4}$$

where $t_B = B(h_0 - h_1)$. The numerical solution of Eq. (A4) yields

$$h_0 - h_1 = 0.806/B \tag{A5}$$

Further using Eqs.(A1) and (A2) one gets

$$H_1 - h_1 = 1.267/B \tag{A6}$$

$$C = \frac{3.6886H_1}{\sqrt{BH_1[u^2(H_2) - H_1^2]}} \tag{A7}$$

The conformational free energy is given by

$$F = F_{\nabla}^1 + F_{\nabla}^1 = \frac{a^2\Sigma}{24\upsilon}\int_0^{h_1}\frac{[\nabla\Phi(z)]^2}{\Phi(z)(1-\Phi(z))}dz + \frac{a^2\Sigma}{24\upsilon}\int_{h_1}^{\infty}\frac{[\nabla\tilde{\Phi}(z)]^2}{\tilde{\Phi}(z)(1-\tilde{\Phi}(z))}dz \tag{A8}$$

Taking into account Eqs.(A5) and (A7) we obtain

$$F_{\nabla}^1 = \frac{a^2\Sigma}{24\upsilon}\int_0^{h_1}\frac{[\nabla\Phi(z)]^2}{\Phi(z)(1-\Phi(z))}dz \approx 0.017\frac{a^2\Sigma}{\upsilon}\sqrt{\frac{BH_1}{u^2(H_2) - H_1^2}} \tag{A9}$$

Once $h_0 - h_1 = 0.806/B$ is known, the general form of profile (7.26) can be specified as

$$\tilde{\Phi}(y) = C \cdot Ai^2(By - 0.806) \tag{A10}$$

where $y = z - h_1$ and the constant C is determined according to Eq.(A7). Using this, the second part of the conformational free energy equals

$$F_{\nabla}^{2} = \frac{a^2\Sigma}{24\upsilon}\int_0^{\infty}\frac{[\nabla\tilde{\Phi}(y)]^2}{\tilde{\Phi}(y)\left(1-\tilde{\Phi}(y)\right)}dy \approx 0.059\frac{a^2\Sigma}{\upsilon}\sqrt{\frac{BH_1}{u^2(H_2)-H_1^2}} \qquad \text{(A11)}$$

The total conformational energy is thus given by

$$F_{\nabla} = F_{\nabla}^{1} + F_{\nabla}^{2} \approx 0.076\frac{a^2\Sigma}{\upsilon}\sqrt{\frac{BH_1}{u^2(H_2)-H_1^2}} \qquad \text{(A12)}$$

REFERENCES

[1] J.Ruokolainen, R.Mäkinen, M.Torkkeli, T.Mäkelä, R.Serimaa, G.ten Brinke, O.Ikkala, *Science* **1998**, ***280***, 557.
[2] O.Ikkala, G.ten Brinke, *Science* **2002**, *295***,** 2407.
[3] J.Ruokolainen, G.ten Brinke, O.Ikkala, *Adv. Mater*. **1999**, *11*, 777.
[4] J.Masuda, A.Takano, Y.Nagata, A.Noro, Y.Matsushita, *Phys.Rev.Lett.* **2006**, *97*, 098301.
[5] Y.Nagata, J.Masuda, A.Noro, D.Cho, A.Takano, Y.Matsushita, *Macromolecules* **2005**, *38*, 10220.
[6] C.C.Evans, F.S.Bates, M.D.Ward, *Chem. Mater*. **2000**, *12*, 236.
[7] A.F.Thünemann, S.General, *Macromolecules* **2001**, *34*, 6978.
[8] C.Osuji, C.Y.Chao, I.Bita, C.K.Ober, E.L.Thomas, *Adv.Funct.Mater*. **2001**, *12*, 753.
[9] I.A.Ansari, V.Castelletto, T.Mykhaylyk, I.W.Hamley, Z.B.Lu, T.Itoh, C.T.Imrie, *Macromolecules* **2003**, *36*, 8898.
[10] G.O.R.Alberda van Ekenstein, E.Polushkin, H.Nijland, O.Ikkala, G.ten Brinke, *Macromolecules* **2003,** *36*, 3684.
[11] C.Y.Chao, X.Li, C.K.Ober, C.Osuji, E.L.Thomas, *Adv. Mater.* **2004**, *14*, 364.
[12] O.Ikkala, G.ten Brinke, *Chem. Com.* **2004**, 131.
[13] C.S.Tsao, H.L.Chen, *Macromolecules* **2004**, *37*, 8984.
[14] I.W.Hamley, V.Castelletto, P.Parras, Z.B.Lu, C.T.Imrie, T.Itoh, *Soft Matter* **2005**, *1*, 355.
[15] B.Nandan, C.H.Lee, H.L.Chen, W.C.Chen, *Macromolecules* **2005**, *38*, 10117.
[16] R.Nap, C.Kok, G.ten Brinke, S.I.Kuchanov, *European Phys. J. E* **2001**, *4*, 515.
[17] R.Nap, N.Sushko, I.Ya.Erukhimovich, G.ten Brinke, *Macromolecules* **2006**, *39*, 6765.
[18] Y.Smirnova, G.ten Brinke, I.Ya.Erukhimovich, *J. Chem. Phys.* **2006,** *124*, 054907.
[19] S. I.Kuchanov, V.E.Pichugin, G.ten Brinke, *E-Polymers* **2006**, 012.
[20] S.I.Kuchanov, V.E.Pichugin, G.ten Brinke, *Europhys. Lett.* **2006**, *76*, 959.
[21] A.N.Semenov, Sov. Phys. *JETP* **1985**, *61*, 733.
[22] T. M.Birshtein, Yu.V.Liatskaya, E.B.Zhulina, *Polymer* **1990**, *31*, 2185.
[23] E.B.Zhulina, T.M.Birshtein, *Polymer* **1991**, *32*, 1303.
[24] E.B.Zhulina, A.Halperin, *Macromolecules* **1992**, *25*, 5730.
[25] A.N.Semenov, A.V.Subbotin, Sov. Phys. *JETP* **1992**, *74*, 660.
[26] A.Subbotin, T.Klymko, G.ten Brinke, *Macromolecules* **2007**, *40*, 2915.
[27] T.A.Witten, L.Leibler, P.A.Pincus, *Macromolecules* **1990**, *23*, 824.
[28] Function $y = Ai(x)$ is one of the two linearly independent solutions of the differential equation $y'' - xy = 0$. The asymptotic behavior of the Airy function at $x \to +\infty$ is $Ai(x) \approx \frac{\exp\left(-\frac{2}{3}x^{3/2}\right)}{2\sqrt{\pi}x^{1/4}}$.
When x is positive, $Ai(x)$ is positive, convex and decreasing exponentially to zero.

Summary

This Thesis is devoted to a theoretical study of self-assembly in specific block-copolymer systems. The ability of block copolymer-based systems to organize at the nanoscale level depends on several parameters, such as volume fraction of the different components, their molar masses and the strength of the interactions. This work in its main part presents a theoretical analysis of two different classes of nanostructured systems: a lamellar self-assembled diblock copolymer/homopolymer blend where the homopolymer component interacts favorably with one of the blocks of the diblock copolymer, and lamellar-in-lamellar self-assembled linear binary and ternary two-length-scale multiblock copolymers. The lamellar-in-lamellar self-assembled states of the latter, are analysed in detail in this Thesis.

A literature overview of diblock copolymer/homopolymer blends and multiblock copolymers with two intrinsic length scales is given in the introductory part.

The main theoretical part of this Thesis starts from a theoretical analysis of the lamellar self-assembled state of blends of a diblock copolymer and a homopolymer where the homopolymer is assumed to interact favorably with one of the blocks of the diblock copolymer. Throughout the discussion a strong segregated lamellar morphology is assumed to be present, i.e. sharp interfaces, with the homopolymer dissolving exclusively in one of the two different layers. The essential parameter governing the incorporation of the homopolymer inside the corresponding lamellar domains turns out to be $k = (\pi\gamma\upsilon)/(4aN|\chi|^{3/2})$. Here γ is the interfacial tension, N - the block copolymer chain length and χ the Flory-Huggins parameter representing the favorable interaction between the homopolymer and the corresponding block. The homopolymer is assumed to have a chain length exceeding *N*. Furthermore, γ is assumed to be constant even if some homopolymer is present at the interface. The value of *k* determines whether the dissolved homopolymer will be able to reach the interface. If *k* is sufficiently small this will be possible, however, for the homopolymer to be actually present at the interface the amount of homopolymer still has to exceed some critical volume fraction. If that is the case, the homopolymer distribution is close to parabolic with its minimum at the interface and its maximum in the centre of lamellar microdomain, i.e. at the mid plane. If these requirements are not met, a “dead” zone will be present near the block copolymer interface where no homopolymer is present. Additionally, the maximal amount of homopolymer that can be incorporated may also be bounded. This property is, however, of less interest since for a large amount of homopolymer the assumption of a lamellar morphology will in general no longer hold. These predictions are based on calculations that assume the homopolymer conformational effects due to the inhomogeneous

distribution of homopolymer to be small. Such effects do, however, become important in the case of weakly favorable homopolymer-block copolymer interactions, i.e. $|\chi| << 1$. Since these conformational effects are unfavorable regarding the dissolution of the homopolymer into the lamellar domains, a critical value $|\chi|^{critical}$ exists such that for all $|\chi| \le |\chi|^{critical}$ the homopolymer will not dissolve.

The last three chapters of the manuscript are devoted to a theoretical study of the lamellar-in-lamellar self-assembled state of a specific class of two-length-scale linear multiblock copolymers. The main aim of this study is to relate the number of "short" blocks of the middle part of these multiblock copolymer to the number of "thin" internal layers.

We start our analysis from linear ternary multiblocks of the C-*b*-(B-*b*-A)$_m$-*b*-B-*b*-C type. In Chapter 5 the number *k* of "internal" layers for the lamellar self-assembled state of these C-*b*-(B-*b*-A)$_m$-*b*-B-*b*-C multiblock copolymers is determined as a function of *m* in the strong segregation limit. The outer C-blocks are assumed to be considerably longer than the 2*m*+1 blocks of equal length of the (B-*b*-A)$_m$-*b*-B middle multiblock. The self-assembled state is assumed to consist of *k* "thin" A- and B-layers sandwiched between "thick" C-layers. We demonstrate that to a large extent the domain formation is determined by the interplay between interfacial forces and elastic stretching of the individual blocks. The combinatorial contribution, corresponding to the number of different possibilities to create global loops or bridges, is taken into account in an approximate manner. This combinatorial effect becomes more pronounced for larger values of m. The theoretical predictions are in excellent agreement with the available experimental data. In order to investigate the influence of the block length and the Flory-Huggins interaction parameters χ_{AB} and χ_{BC}, on the number of internal layers in more detail we present an alternative analysis using the Alexander-de Gennes approach in Chapter 6. This simplified description allows us to get a clearer physical picture of the layers formation in these systems. We demonstrate that by increasing the unfavorable interactions between the B- and C-component we can achieve the "fully stretched", i.e. maximal number of internal layers, state of the multiblock copolymer. The opposite effect also occurs: increasing the unfavorable interactions between the A- and B-component we can get a structure with the minimal number of internal layers. Increasing the chain length of the end blocks also promotes structures with more internal domains. The theoretical predictions made in this chapter are corroborated by computer simulations results obtained by using the dissipative particle dynamics technique.

Physically the situation is fundamentally different for the two-length-scale linear binary A-*b*-(B-*b*-A)$_m$-*b*-B-*b*-A multiblock copolymers, discussed in Chapter 7. Compared to the ternary system, where all middle blocks are located in between the domains formed by the outer "long" end blocks, the binary system is considerably more complicated. Here the "short" A blocks of the (B-*b*-A)$_m$ middle multiblock can also be located inside the domains of the "long" A end blocks. This brings as an important new element in the analysis a conformational contribution associated with the "concentration" gradient in the outer A-domain due to the presence of "short" middle A-blocks. This gives an additional interfacial area depending contribution that turns out to be essential for the internal domain formation. Of course, similar conformational effects are present in the internal

domains of both the binary and ternary multiblock copolymer systems. However, these contributions are small compared to that of the outer domains in the binary multiblock copolymer system where we are dealing with “long” A end blocks together with loops formed by “short”A middle blocks. Without this additional interfacial contribution the final morphology would simply consist of alternating “thick” A-layers and “thin” B-layers. Because of this term, however, there is a strong tendency to form a “thin” 3 internal B-A-B layer, exactly as found in the only experimental study available.

Samenvatting

In dit proefschrift worden de resultaten gepresenteerd van een theoretische studie naar de zelf-assemblage in een drietal verschillende blokcopolymeersystemen. De aard van de spontane ordening op de nanometer lengteschaal in op blokcopolymeer gebaseerde smelten hangt af van verschillende parameters. De belangrijkste zijn de bloklengte, de samenstelling en de interactiesterkte. Hier beschouwen we de invloed van deze parameters op de zelf-assemblage in twee verschillende klassen van systemen, te weten **i**. mengsels van diblokcopolymeren met een homopolymeer dat een gunstige interactie heeft met één van de blokken en **ii**. lineaire binaire en ternaire multiblokcopolymeren met een moleculaire architectuur gekarakteriseerd door twee verschillende lengteschalen. In beide gevallen beperken we ons tot de lamelaire structuur waarbij er bij de multiblokcopolymeren sprake is van een dubbel gelaagde lamel-in-lamel structuur.

In het eerste deel van dit proefschrift wordt een overzicht gegeven van de relevante literatuur over bovengenoemde systemen.

Het theoretische deel van dit proefschrift begint met een analyse van de lamelaire toestand van mengsels van diblokcopolymeren met een homopolymeer dat een gunstige interactie heeft met één van de blokken van het diblokcopolymeer. We gaan uit van de sterk gesegregeerde situatie, i.e. scherpe grensvlakken, waarbij het homopolymeer uitsluitend in de lagen aanwezig is die gevormd worden door de blokken die een gunstige interactie met het homopolymeer hebben. In hoeverre het homopolymeer spontaan in deze lagen wordt opgenomen blijkt af te hangen van een specifieke combinatie van parameters $k = (\pi\gamma\upsilon)/(4aN|\chi|^{3/2})$. Hierbij is γ de grensvlakspanning, N de blokcopolymere ketenlengte en χ de Flory-Huggins interactieparameter die de gunstige interactie tussen homopolymeer en het betreffende blok van het copolymeer aangeeft. Er wordt aangenomen dat het homopolymeer een ketenlengte heeft die groter dan N is. We nemen verder aan dat γ constant is zelfs als enig homopolymeer tot aan het grensvlak is doorgedrongen. De waarde van k bepaalt of het opgeloste homopolymeer inderdaad tot aan het grensvlak reikt. Als k voldoende klein is kan deze vraag positief worden beantwoord mits de hoeveelheid toegevoegde homopolymeer voldoende groot is. In dat geval wordt een parabolisch samenstellingsprofiel gevonden met de minimum hoeveelheid homopolymeer bij het grensvlak en het maximum in het centrum van de laag, i.e. het middenvlak. Als er onvoldoende homopolymeer wordt toegevoegd is er sprake van een “dead” zone zijn in de buurt van het grensvlak waar geen homopolymeer aanwezig is. De maximale hoeveelheid homopolymeer dat in de lagen kan worden

"opgelost" blijkt ook begrensd, maar deze uitkomst is van weinig belang aangezien bij toevoeging van grote hoeveelheden homopolymeer de aanname van een gelaagde structuur niet langer geldig is. Deze resultaten zijn verkregen door aan te nemen dat de entropische (ongunstige) bijdrage tengevolge van de inhomogene homopolymeerdistributie kan worden verwaarloosd. Dit is het geval zolang de interactie voldoende sterk is. Deze factor wordt echter belangrijk als de interactie zwak is, i.e. $|\chi| << 1$. Omdat deze conformationele effecten ongunstig zijn met betrekking tot de incorporatie van het homopolymeer bestaat er een kritische waarde $|\chi|^{critical}$ zodanig dat het homopolymeer niet in de laag oplost voor $|\chi| \le |\chi|^{critical}$.

De laatste drie hoofdstukken zijn gewijd aan de lamel-in-lamel zelfgeassembleerde toestand van een specifieke klasse van multiblokcopolymeren. De kenmerkende eigenschap van de beschouwde multiblokcopolymeren is dat ze bestaan uit twee lange eindblokken waartussen zich een multiblokcopolymeer bevindt bestaande uit relatief korte symmetrische diblokcopolymeren. De eindblokken kunnen chemisch verschillen van deze diblokcopolymeren, ternaire multiblokcopolymeren, of chemisch gelijk zijn aan één van de blokken, binaire multiblokcopolymeren. De moleculaire architectuur wordt gekenmerkt door twee lengteschalen. Dit heeft tot gevolg dat zelf-assemblage aanleiding geeft tot hierarchische structuren. In dit proefschrift beschouwen we het simpelste geval van een lamel-in-lamel structuur. De belangrijkste vraag die we beantwoorden betreft het aantal "dunne" lagen dat binnen opeenvolgende "dikke" lagen aanwezig is.

We beginnen de analyse met lineaire ternaire C-*b*-(B-*b*-A)$_m$-*b*-B-*b*-C multiblokcopolymeren. In Hoofdstuk 5 bepalen we hiervoor hoe het aantal "interne" lagen k in de sterke segregatie limiet afhangt van het aantal diblokken m. Hierbij wordt aangenomen dat de C eindblokken aanzienlijk langer zijn dan de $2m+1$ blokken van gelijke lengte van het (B-*b*-A)$_m$-*b*-B midden . De zelfgeassembleerde toestand bestaat uit k "dunne" A- en B-lagen tussen opeenvolgende "dikke" C-lagen. De evenwichtsstructuur wordt grotendeels bepaald door de balans tussen de grensvlakspanning en de elastische vrije energie. Daarnaast is er de combinatoire bijdrage tengevolge van de verschillende manieren waarop de $2m+1$ midden blokken de k lagen kunnen vormen. Deze wordt belangrijker naarmate m groter is. De theoretische voorspelling komt goed overeen met de weinige beschikbare experimentele data. Om het effect van de bloklengte en de Flory-Huggins interactie parameters χ_{AB} en χ_{BC} in meer detail te onderzoeken presenteren we in Hoofdstuk 6 een alternatieve analyse die gebaseerd is op de vereenvoudigde Alexander-De Gennes benadering. Hiermee laten we zien dat een toename van de ongunstige interactie tussen de B- en C-komponent uiteindelijk leidt tot een "gestrekte" multiblokconformatie, i.e. het maximale aantal interne lagen: $k = 2m+1$. Het omgekeerde gebeurt ook. Als de ongunstige interactie tussen de A- en B-komponent toeneemt houden we uiteindelijk het minimum van 3 interne lagen over. De theoretische voorspellingen worden geïllustreerd aan de hand van computersimulaties gebaseerd op de zg. "dissipative particle dynamics" techniek .

De situatie is fundamenteel verschillend voor de overeenkomstige lineaire binaire A-*b*-(B-*b*-A)$_m$-*b*-B-*b*-A multiblokcopolymeren die in Hoofdstuk 7 aan de orde komen. Dit systeem is aanzienlijk complexer dan het ternaire systeem waar alle middenblokken

segregeren in de ruimte tussen de lagen gevormd door de eindblokken. In het binaire systeem kunnen de “korte” A-blokken van het (B-*b*-A)$_m$ midden multiblok ook in de lagen gevormd door de “lange” A-eindblokken zitten. Dat betekent dat in de “dikke” A-lagen een concentratiegradiënt aanwezig is geassocieerd met de aanwezige “korte” A-blokken en dientengevolge is er sprake van een extra conformatie-entropie term. Dergelijke gradiënten zijn in principe ook aanwezig in de “dunne” A- en B-lagen, maar de daarmee gepaard gaande bijdragen zijn klein en kunnen in eerste benadering verwaarloosd worden. Het blijkt dat het in rekening brengen van de bijdrage tengevolge van deze concentratiegradiënt in de “buitenste” A-lagen essentieel is om de experimentele resultaten te kunnen verklaren. Zonder deze bijdrage zou de uiteindelijke morfologie simpelweg bestaan uit “dikke” A-lagen afgewisseld met “dunne”B-lagen.

List of Publications

1. **Distribution of Homopolymer in Lamellar Self-Assembled Blends Involving Specific Interactions.**
   T. Klymko, A. Subbotin, G. ten Brinke.
   Macromolecules, 2007, 40, 2951.

2. **Lamellar-in-Lamellar Structure of A-b-(B-b-C)$_m$-b-B-b-A Multiblock Copolymers.**
   A. Subbotin, T. Klymko, G.ten Brinke.
   Macromolecules, 2007, 40, 2915.

3. **Lamellar-in-Lamellar Structure of Linear Binary Multiblock Copolymers**.
   T. Klymko, A.Subbotin, G. ten Brinke.
   Accepted to Journal of Chemical Physics.

4. **Lamellar-in-Lamellar Self-Assembly in Linear Ternary Multiblock Copolymers: Alexander-de Gennes Approach and Dissipative Particle Dynamics Simulations**.
   T. Klymko, V. Markov, A. Subbotin and G.ten Brinke.
   Submitted to Soft Matter.

Acknowledgements

This manuscript is the result of my research work over the past four years. But to the same extent the successful completion of this Thesis has become possible due to the efficient help of many people. It is my pleasure to acknowledge here all people who contributed to the successful realization of this Thesis.

Above all I wish to express my deep gratitude towards my promotor Prof. Dr. Gerrit ten Brinke for giving me the opportunity to perform interesting research in his group, for his guidance, for all attention and support he invested into this work, also for many helpful and interesting scientific discussions from which I have learned to see beyond the equations and which helped me to understand physical phenomena in polymers more deeply. It was very important not only for my professional but also personal growth. I also owe my appreciation to Gerrit for his help with articles and manuscript preparation.

I express my sincere gratitude to my copromotor Dr. Andrei Subbotin for all his ideas, patience and invaluable help during our collaboration, for his enormous contribution to this research. The successful realization of this project would hardly be possible without his constant assistance.

I would like to acknowledge the members of the reading committee, Prof. Dr. I.Ya.Erukhimovich, Prof. Dr. F.A.M.Leermakers and Prof. Dr. J.J.M.Slot for their careful reading.

My countless thanks go to all members of the Polymers Chemistry Department for nice and friendly working atmosphere, and especially to my present and former group-mates Yulia Smirnova, Vladimir Markov, Evgeny Polushkin, Sergei Ivanov, Sasa Bondzic,Wendy van Zoelen, Joost de Wit, Frans Roukes, Gerrit Gobius-du Sart, Thu Nguyen, Martin Faber, Johan de Jong, Nazar Sushko, Rikkert Nap. Yulia, my warmest thanks to you for being my friend. Your kind friendship and your support, especially in the beginning of my PhD, were very important for me. Thank you for your readiness to help every time I needed that. Vladimir, many thanks to you for being a good office-mate. Also thank you for our fruitful collaboration which resulted in the joint paper. Special thanks to Vladimir and Sergei for being my paranymphs. Wendy, thank you for your friendly help with translation of all sorts of Dutch documents.

I am thankful to Karin Woudstra for her help with plenty of administrative issues and for providing friendly and fun atmosphere in the Polymer Chemistry Department.

My hearty thanks are to Elena Kurbatova. All bad moments I had during these years I would never overcome without her help and advices. Lena, thank you for your

exceptional understanding and support. Also many warmest words to you and Ario for your kind hospitality and home atmosphere during my visits to your family in Tilburg.

Olenka Butriy, thank you for our conversations on all possible and impossible topics in the coffee-room, for all time we spent together not only in the Netherlands but also in Ukraine, and for all life lessons we got from each other.

Last but not least I thank my family. My dear parents and my dear brother, it is hardly possible to express in words how much I am grateful to you. This Thesis means to you as much as it means to me. I am immensely indebted to you for your unconditional love and encouragement, for your constant attention and understanding, for your belief in me and your vital support, for accepting my choice even sometimes it was not easy for you. Thank you for everything, my dearest.

It is impossible to name everyone who helped me during my research and my stay in Groningen. I express my sincere apologies and warmest thanks to those people whom I could not mention here.

09.08.2008 *Tanya.*
Groningen